7-28-2015

Tribological Study on Plasma Electrolytic Oxidation Treatment in Al-Si Alloys for Engine Application

Hoda Eiliat
University of Windsor

Tribological Study on Plasma Electrolytic Oxidation Treatment in Al-Si Alloys for Engine Application

By

Hoda Eiliat

A Dissertation
Submitted to the Faculty of Graduate Studies
through the Department of Mechanical, Automotive and Materials Engineering
in Partial Fulfillment of the Requirements for
the Degree of Doctor of Philosophy
at the University of Windsor

Windsor, Ontario, Canada

2015

Tribological Study on Plasma Electrolytic Oxidation Treatment in Al-Si Alloys for Engine Application

By

Hoda Eiliat

APPROVED BY:

_____
Dr. R.R. Chromik, External Examiner
Department of Mining and Materials Engineering, McGill University, Montréal, QC

_____
Dr. A. Fartaj, Outside Program Reader
Mechanical, Automotive and Materials Engineering, University of Windsor

_____
Dr. D. O. Northwood, Program Reader
Mechanical, Automotive and Materials Engineering, University of Windsor

_____
Dr. J. Sokolowski, Program Reader
Mechanical, Automotive and Materials Engineering, University of Windsor

_____
Dr. J. Villafuerte, Industrial Advisor
CenterLine Windsor Ltd., Windsor, ON

_____
Dr. X. Nie, Advisor
Mechanical, Automotive and Materials Engineering, University of Windsor

_____
Dr. J.S.Y. Tjong, Co-Advisor
Ford Motor Company, Windsor, ON

8 April, 2015

DECLARATION OF CO-AUTHORSHIP/ PREVIOUS PUBLICATION

I. Co-Authorship Declaration

I hereby declare that this dissertation incorporates material that is result of joint research, as follows:

Some of the presented results in chapter 4 are partially published. The methodology of the study was discussed with my advisers and the committee members. Major milestones of the research were discussed with Dr Nie and his guidance was used for the next steps of the research. Dr Vilafuerte has contributed to this study by providing feedbacks during the first and second PhD seminar sessions. Dr Tjong provided the under study piston rings and provided feedback on the progress of the research. In all other cases, the key ideas, primary contributions, experimental designs, data analysis and interpretation were performed by the author.

I am aware of the University of Windsor Senate Policy on Authorship and I certify that I have properly acknowledged the contribution of other researchers to my thesis, and have obtained written permission from each of the co-author(s) to include the above material(s) in my thesis.

I certify that, with the above qualification, this thesis, and the research to which it refers, is the product of my own work.

II. Declaration of Previous Publication

This thesis includes 4 original papers that have been previously published as follows:

Thesis chapter	Publication title/full citation	Publication status*
Chapter 4	Eiliat, H. and Nie, X., "Tribological Behavior of Plasma Electrolyte Oxidation Coating on Al 319 Aluminum Alloy," SAE Technical Paper 2012-01-0165, 2012, doi:10.4271/2012-01-0165.	Published
Chapter 4	Eiliat, H. (2012). Wear behavior of PEO coatings on AL319 aluminum alloy. In Society of Tribologists and Lubrication Engineers Annual Meeting and Exhibition 2012.	Published
Chapter 4	Eiliat, H. and Nie, X., (2013). Wear resistant coatings for engine application. In Materials Science and Technology Conference and Exhibition 2013, MS and T 2013.	Published
Chapter 4	Eiliat, H., Nie, X., Tjong, J., and Villafuerte, J., "Outside-Engine Wear Study of Ceramic Coated Cylinder Wall Tribo-System," SAE Technical Paper 2014-01-0958, 2014, doi:10.4271/2014-01-0958.	Published

I certify that I have obtained a written permission from the copyright owner(s) to include the above published material(s) in my thesis. I certify that the above material describes work completed during my registration as graduate student at the University of Windsor.

I declare that, to the best of my knowledge, my thesis does not infringe upon anyone’s copyright nor violate any proprietary rights and that any ideas, techniques,

quotations, or any other material from the work of other people included in my thesis, published or otherwise, are fully acknowledged in accordance with the standard referencing practices. Furthermore, to the extent that I have included copyrighted material that surpasses the bounds of fair dealing within the meaning of the Canada Copyright Act, I certify that I have obtained a written permission from the copyright owner(s) to include such material(s) in my thesis.

I declare that this is a true copy of my dissertation, including any final revisions, as approved by my thesis committee and the Graduate Studies office, and that this thesis has not been submitted for a higher degree to any other University or Institution.

ABSTRACT

Automotive industry strives to reach an optimum level of fuel economy. This can be achieved by overcoming two impacting factors on fuel consumption: weight and friction force. This research contributes to reduce both. The proposed surface treatment can replace cylinder liners of hypoeutectic aluminum silicon alloy engine blocks with a thin layer of ceramic oxide composed of alpha and gamma phases of Al_2O_3 and mullite. The coatings are achieved in an aqueous electrolytic bath with current densities of 0.1 to 0.2 A/cm2.

Coatings produced in silicate based solutions have shown good adaptability to the counter surface with an average 0.12 coefficient of friction. Coatings produced in phosphate and aluminate solution have shown signs of delamination, and excessive porosity and roughness respectively. Coatings produced under Bipolar Pulsed Direct Current mode has up to 12% higher hardness values compared to unipolar coatings. For each increment of 0.2 A/cm^2 current density, there is a 30% of increase in coating growth rate. Higher pH values of the solution creates faster growth rate up to 1.5 μ/min. These coatings are 20% more susceptible to wear. Samples treated in MoS_2 solution showed 22% lower average roughness values and 37% of reduction in coefficient of friction. Mild wear scars on the piston rings were detected for the optimized coatings.

DEDICATION

To My Grandparents:

Nezhat & Hassan

Robab & Omid

ACKNOWLEDGEMENTS

I would like to thank my Lead Advisor, Dr. Xueyuan Nie for sharing his wisdom and expertise with me throughout this research. His guidance and advisory method have helped me greatly to become an independent problem solver. I would also like to extend my gratitude to my Co-advisor, Dr. Jimi Tjong. Special thank goes to my Industrial Advisor, Dr. Julio Villafuerte for his great mentorship and involvement in progress of my work.

I would like to express my appreciation to my committee members: Dr. Derek Northwood who taught me the ethics of research and report writing, Dr. Jerry Sokolowski who inspired me to reach higher and look deeper and Dr. Amir Fartaj for his time and consideration.

I am thankful to CenterLine Windsor Limited Company, specifically Mr. Michael Beneteau for the abundant support and patience during this initiative. Special thank goes to Ford Motor Company for providing some of the piston rings for counter surface study of this research.

This has been an eventful experience during which I failed a lot, learned more and built priceless connections with gurus in the field of my studies. Dr. Ali Erdemir, Dr. Tibor Turi and Dr. Dimitry G. Sediako, I thank you for being great role models for me. I aspire to reach your level of knowledge and humbleness one day.

I also would like to thank Mrs. Sharon Lackie, SEM specialist and Mr. Mike Miller, CEO of Substrata Thin Film Solutions Inc. for sponsoring my AFM tests.

I thank my colleagues, friends and everyone who shared a part of their time and knowledge in completion of this dissertation.

I was six years old when I promised my father to pursue a PhD program. I am pleased that I kept my promise and made him proud. I could have never finished this task without the support and encouragements from my father, Reza, endless love from my mother, Mina and the happiness my sister, Hasti brings to my life.

Lastly, I would like to thank my soul mate, my husband, Mohammad whose ambition for progress has been contagious and influential in my decision to pursue my dreams and turn them into reality.

TABLE OF CONTENTS

LIST OF TABLES

LIST OF FIGURES

LIST OF ABBREVASIONS

AFM	Atomic Force Microscopy
APS	Atmospheric Plasma Spray
ASP	Anodic Spark Deposition
BMI	Bimetal Interlocks
BPDC	Bipolar Direct Current
CBN	Cubic Boron Nitride
COF	Coefficient of Friction
CVD	Chemical Vapor Deposition
DC	Direct Current
DI	Direct Inject
EDX	Energy-dispersive X-ray Spectroscopy
ESEM	Environmental Scanning Electron Microscopy
FRC	Fiber Reinforced Composites
HPDC	High Pressure Die Casting
HVOF	High Velocity Oxy-fuel Spray
LPDC	Low Pressure Die Casting
MAO	Micro-Arc Oxidation
MDO	Micro Arc Discharge Oxidation
MMC	Metal Matrix Composite
MPO	Micro Plasma Oxidation
NCC	Nickel-based Ceramic Coating

PEA	Plasma Electrolytic Anodization
PEO	Plasma Electrolytic Oxidation
PI^3	Plasma Immersion Ion Implantation
PTWA	Plasma Transferred Wire Arc Spray
PVD	Physical Vapor Deposition
SEM	Scanning Electron Microscopy
UPDC	Unipolar Direct Current
XRD	X-ray Diffraction

NOMENCLATURE

Å	Surface ratio
L	Surface profile measurement length
D_t	Duty cycle
F_f	Frictional force
A *Anode*	Surface areas of cathode
A *Cathode*	Surface areas of cathode
C	Surface tension
D	Coating thickness
h	Contact angle
h	Height of volume loss cap
h’	Lubricant film thickness
J	Current density
L	Lubricated condition
r	Radius of the steel ball
r’	Radius of circular plain of the wear scar
r°	Capillary radius
R_a	Arithmetic mean surface roughness
R_{ku}	Surface kurtosis
R_{sk}	Surface skewness
S	Starved condition
T	Treatment time
T_{off}	Period of pulse off

T_{on}	Period of pulse on
V	Voltage
V	Volts
wt%	Weight percent
Z(X)	Surface profile height function
Δa	Average slope of the surface profiles
Λ	Lambda ratio
ρ	Porosity
σ	Composite surface roughness of sliding pair
n	number of points on the surface profile
x	Horizontal coordinates of each point
y	Vertical coordinates of each point
ΔP	Pressure variation
θ	Slope of asperity
τ	Coating growth rate

CHAPTER 1. INTRODUCTION

Automotive industry is constantly searching for cleaner and greener cars with less emission and better fuel consumption. Recently, weight reduction has been a key process in automotive design. Studies have shown that every 10 per cent reduction of vehicle weight results in 6 to 8 per cent improvement in fuel economy [1]. These numbers are alluring enough for automakers and suppliers to redesign their processes and find adaptable technologies that can utilize lightweight materials such as aluminum alloys, magnesium and high-strength steel grades. Also non-metallic materials such as polyurethane, ceramics, composites and plastics are being used without compromising performance, durability and safety.

This chapter looks at the influence of material innovation in automotive industry on addressing global concerns such as fuel economy and environmental conscious processes in automotive manufacturing. It also reviews the processes used to-date on engine block surface treatment and modifications for weight reduction and improvement of wear resistance. Motivation and significance of this research is also presented in this chapter. Chapter 1 concludes with description of the objective of this dissertation.

Lightweight materials can enhance driving performance along with reducing the fuel consumption ratios. Specifically for the high-speed moving parts, the reduction in inertial mass enables the mass of supporting parts to be reduced [2].

Aluminum alloys has shown promising characteristics that make them a reliable substitute for steels. Also through development of advance metal matrix composites, it is

possible to tailor lightweight materials that demonstrate high specific strength and specific stiffness, high hardness and wear resistance, low coefficient of friction and thermal expansion, high thermal conductivity, high energy absorption ,and dampening capacity. Figure 1 illustrates a summary of the cylinder bore surface technologies for aluminum cylinder blocks.

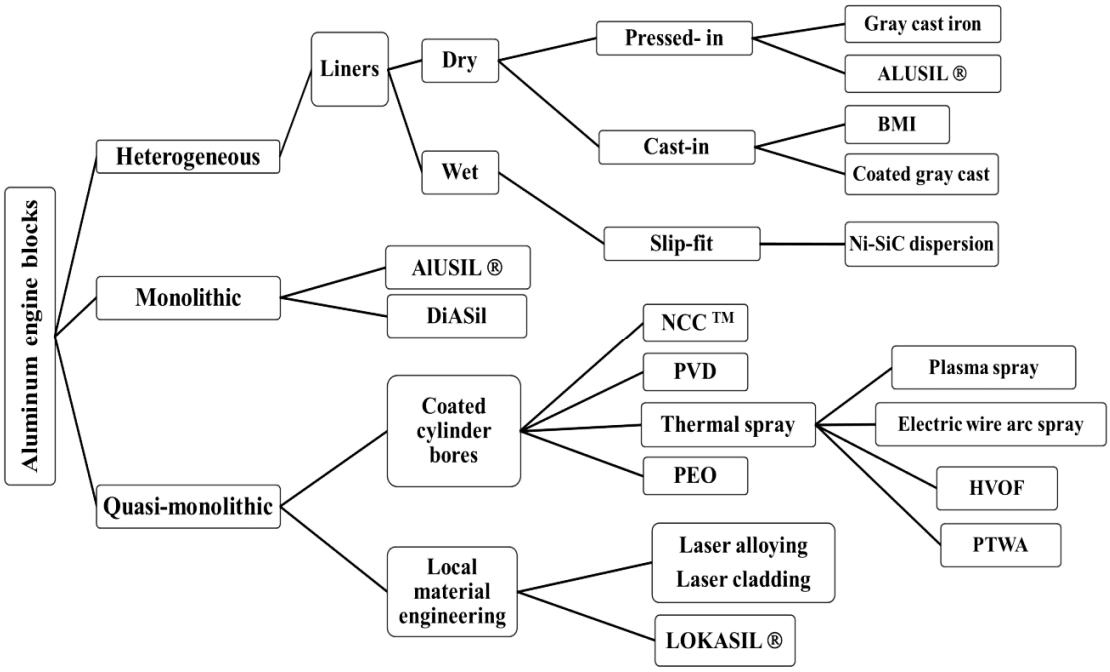

Figure 1. Cylinder bore surface technologies for production of aluminum engine cylinder blocks.

There are three methods of engine cylinder production: *Heterogeneous* concept, *Monolithic* concept and *Quasi-monolithic* concept [3]. Heterogeneous concept refers to the traditional cost-effective block and liner duo. Aside from higher weight, thermal conductivity between the cylinder wall and the liners is the main concern of this concept. Monolithic concept refers to production of cylinder blocks from a single cast and is

mainly bound to the low-pressure die casting process. In comparison to the other concepts, monolithic aluminum engine blocks are lighter in weight and have great thermal relief due to the casting method. Monolithic engine blocks have a very low tendency for distortion, vibration and piston noise. However, they are rarely being used for mass production of aluminum cylinder block production. Quasi-monolithic concept is designed to transfer the advantages of monolithic concept and improve the process for mass production either by local material engineering or coating the cylinder walls after the casting process. Each concept will be explained in detail in sections 1.1, 1.2 and 1.3.

1.1 Heterogeneous Concept for Cylinder Bore Surface Technology

Traditionally a gray cast iron of pearlitic structure was used for cylinder blocks and cylinder bore surface due to the low cost and formability [3], [4]. The first car with aluminum engine parts was made in 1901 by Karl Benz [5]. He presented this car for a prestigious car race in Nice, France.

By the end of World War II, aluminum became a more accessible material. Land Rover, a British company, launched its first aluminum V8 engine block. Later in 1961 Buick 215 is produced with an aluminum engine. The engine weighed about 114 Kg (318 lb.) which was a record breaker at that time and attracted many car race drivers due to its acceleration rate [6]. When in 1962 the legendary American racer Mickey Thompson drove a car with an engine made of the light-weight metal during the 'Indianapolis 500', the engine demonstrated great performance. In the course of time many companies improved this legendary engine to use it in mass-produced models and race cars, including in Formula-1 cars. In the late 1970s, European countries started using aluminum for gray cast-iron cylinder blocks of gasoline engines (SI) [3].

Aluminum found its way to luxury brand car engines in late 1980s and finally in the 1990s, aluminum cylinder blocks were mass-produced for standard-size and compact cars. It was around mid-1990s when the automakers have shifted their attention to aluminum diesel engines with direct injection (DI). By 2006, major share of engine blocks were equipped with aluminum cylinder blocks. Aluminum engine blocks typically need a cast iron lining inside each cylinder with a thickness of 1.5 to 3.5 mm [7]. These liners are needed due to poor wear resistant of aluminum. The accepted production method is a cost-effective high-pressure die casting technique with cast-in cylinder liners of gray cast iron which make a heterogeneous characteristic. This method would minimize the gap between the liners and the surrounding casting material and therefore would have similar thermal conductivity characteristic [2, 5]. This form of cylinder bore surface technology is known as heterogeneous concept.

There are two types of liners: wet and dry. A cylinder block with wet liners is equipped with cylinder walls that are entirely removable. These liners fit into the block by special gaskets. The term "*wet*" refers to the fact that the outer side of the liners is in direct contact with the engine's coolant. Dry liners on the other hand, are usually inserted into the block by either pressed-in or cast-in fitting methods. These sleeves remain dry and have only contact with the block material. In cast-in method, the outside cylindrical surface of the liner is machined to create parallel helical grooves from top to bottom of the liner. The liners are pre-heated above 400° K and then placed into the cylinder –block die casting. This will create a strong metallic bond between the two parts after solidification. High-pressure die casting technique is the best practice since shorter

solidification time is desired in order to prevent any fusion problems. However planar bond between the liner and the surrounding cast area is not sufficient [3].

In pressed-in fitting method, the liner is like a sleeve that is forced in or drawn out to fit in the cylinder block. The process needs precise interference fit and end-plate guide in order to ensure a perfect positioning.

Liners can also be made of aluminum materials. Coating the gray cast iron block and the aluminum liners with aluminum (a gray cast iron liner with outside aluminum coating is called hybrid) could in fact enhance the planar bonding however this would add to the cost of the production significantly [9]. To compensate for the weak bond between the block and the liners, bimetal interlocks (BMIs) were used [3]. Bimetal Interlock (BMIs) liners also known as "*rough liners*" were used to minimize the gap between liner and the surrounding casting material and enhance thermal conductivity. In this method the outer surface of the liner is grooved either by machining or by casting on a rough surface. Both techniques provide excellent heat transfer between the combustion and cylinder chamber due to the close attachment of the two surfaces [10]. The cost of this method is also distinctly higher than the traditional gray cast iron liners [3].

Slip-fit technique is used for wet liners where a cylindrical sleeve with a flanged top is pressed into the cylinder block. In this type of fit, there is less or no contact between the liner and the block and the outer side of the liner is exposed to the engine coolant. One example of this method is the high strength aluminum liners with an electro-plated nickel-silicon carbide dispersion layer (Ni-SiC).

Heterogeneous concept in cylinder bore surface technologies has been widely accepted due to low-cost and ease of manufacturing however it is not the optimum solution in terms of weight, thermal conductivity, differential thermal expansion and recyclability. For instance, the difference between thermal expansion coefficient of gray cast iron liners and the aluminum cylinder block can potentially cause deformation in liners [11], increase the friction force, deteriorate the lubrication conditions, influence the fuel and oil consumption ,and cause more emission. Therefore, other alternative technologies has been discovered and applied to overcome the shortcomings of this technology.

1.1.1. Hypoeutectic Aluminum Alloy Cylinder Blocks

In order to reduce the total weight and improve performance, one alternative is to cast the engine block out of hypereutectic aluminum silicon alloy instead of traditional hypoeutectic aluminum alloy. This way, the cast iron cylinder bore liners will be omitted and results in weight reduction. The term eutectic is derived from a Greek word, *eutectos* which means easily fused or melted [12]. Eutectic refers to the saturation point of silicon in aluminum matrix and is equal to 12.5 weight percent (wt%) in binary aluminum silicon alloys. At this point, a eutectic alloy solidifies at a constant temperature similar to a pure element [3]. Aluminum alloys with silicon saturation point below 12.5 weight percent (wt%) are called hypoeutectic.

In early 1950, hypoeutectic aluminum alloys such as A356 and A380 were die casted for cylinder production mainly due to the lower weight and good thermal conductivity, they offer. Cast-in steel cylinder liners were used to enhance the wear

resistance of the cylinder walls. Different methods were used to produce the liners and insert them into the cylinders. For instance, European automotive companies manufactured LM24 and LM26 aluminum-silicon cylinders with shrink-fitted liners in them [13]. The shrink-in method has the disadvantage of high cost and the main advantage of minimal cylinder distortion due to the tight fit between the liner and the cylinder wall which can facilitate the use of thin walled gray cast iron liners [3].

The cost issue of the heterogeneous concept creates a desire to eliminate the liners and move towards monolithic and quasi-monolithic concepts. Section 1.2 and 1.3 describe the two emerging concepts in detail.

1.2 Monolithic Concept for Cylinder Bore Surface Technology

Monolithic blocks are made with hypereutectic aluminum-silicon alloys without any coatings or liners. If the silicon percentage of the alumni alloy is above 12.5 wt%, it is known as hypereutectic. Some hypereutectic aluminum silicon alloys can have up to 30 wt% of silicon in their composition [14]. Higher content of silicon as the second hardest element known on earth, gives enough hardness to the structure to survive a high pressure environment like a combustion chamber. Silicon is precipitated once reaching the liquidus line, this phase is called primary phase and is directly related to the wear resistace of the alloy. The absence of silicon particles on the cylinder block surface causes quick wear of the cylinder wall by the piston rings and eventually premature failure of the engine system. Hence, a homogenous crystallization of the primary phase is desirable. It is also crucial to consider machinability. If the primary phase precipitates in a coarse structure, it will float to the surface of the casting during freezing. This is

called gravity segregation and it can inconvenience machinability [11,12]. To avoid mentioned problems, enhance a more uniform distribution of the primary phase, and refine the size of primary phase crystals; phosphorus (P) is added in part per million (ppm) amounts (0.05 wt %). Addition of magnesium improves the strength of the alloy in elevated temperature without increasing ductility. Copper also improves the castability characteristic by increasing the fluidity of the molten aluminum during the pouring process [15]. The casting method also needs specific conditions and treatments to guarantee a wear resistant surface on the cylinders. Casting techniques and alloying compositions are described below.

1.2.1. Hypereutectic Aluminum Alloy Cylinder Blocks

The use of hypereutectic aluminum-silicon alloy as a monolithic concept for bore surface technology was started in 1970s. There are many trade names and trademarks for hypereutectic Al-Si alloys used in cylinder blocks such as AlUSIL®and DiAsil (Die Cast Aluminum Silicon). The alloy ALUSIL® was manufactured in 1970s by KS Aluminium-Technologie AG (KS ATAG), a German leading manufacturer of hypereutectic Al-Si engine blocks. ALUSIL has (AA 390, AlSi17Cu4Mg) between 16 to 18 wt% of silicon which contributes to the superior wear behavior of this alloy. A casted engine block features lower weight, great thermal relief to dissipate heat, less likelihood of cylinder distortion and needs smaller clearance for the pistons due to minimum value of differential thermal expansion [3]. In 1971, Chevrolet produced its first liner-less hypereutectic automotive engine for the Vega [16]. The production initially started mainly by low-pressure die casting (LPDC). Due to high cost of LPDC that was a draw back since it would make it less desirable for mass production. However many

optimizations has been applied and high-pressure die casting (HPDC) is being replaced. Many automotive manufacturers are using hypereutectic Al-Si alloys, to name a few are BMW, Mercedes, Audi, Porsche, Volvo, Jaguar and Honda. Once the block is casted, cylinder walls are chemically etched. This surface treatment known as *exposure process*, exposes silicon and ensures that piston rings would be sliding on the primary phase of silicon particles and not the aluminum matrix [17].

The other well-known hypereutectic Al-Si alloy engine cylinder is DiASil (die cast aluminum silicon). This cylinder was manufactured by Yamaha Motor Company in 2002. With 20 wt% of silicon, this cylinder is casted under Yamaha CF Aluminum Die Casting Technology. This technology is developed for mass production and focuses on improving the fluidity of the molten alloy as it is poured into the die. Many factors are precisely controlled to satisfy the production and uniform distribution of primary hard silicon throughout the cast. Primary hard silicon is responsible for wear resistant behavior of the engine cylinder block. Another advantage of this technology is its low air intrusion rate (less than 20% of conventional die casting) which leads to a more uniform cast with minimum amount of cavities or air bubbles [18].

Most of the produced engines so far are European luxury brand cars with larger engines. Due to the production cost, expensive alloying elements such as magnesium and nickel and post-casting treatment, this method is yet to become attractive for the mass production of passenger cars.

1.3 Quasi-monolithic Concept for Cylinder Bore Surface Technology

The other approach is a quasi-monolithic concept that is intended to have the same benefits of monolithic concept such as ease of mass production at lower costs. Surface engineering and modification are usually used in Quasi-monolithic blocks replacing the liner in the cylinder block or treating the surface of the liner to achieve better tribological characteristics and to improve thermal distribution. Many surface engineering and coating methods as shown in Figure 1 have been used and more alternatives are on the rise. There are two major methods for enhancing the surface structure and properties of the cylinder bore without using a liner. One is to locally treat the bores in order to enrich the aluminum matrix with silicon particles. The engineered surface can therefore withstand the combustion environment of the engine. Laser alloying with silicon (see section 1.3.1) and particle or fiber reinforced aluminum alloy composites (see section 1.3.2) are well-known methods for locally engineering the engine cylinder surface. The other method is to coat the cylinder bores to enhance their wear and corrosion resistant properties. Many technologies have been developed in coating industry. Section 1.3.3 to 1.3.7 introduce and explains these technologies.

1.3.1 Laser Cladding and Laser Alloying

Both laser cladding and alloying are used to prepare a wear resistant coating on the internal surface of the Al-Si cylinder and/or liners. In Laser cladding, a powdered or wire feedstock material is melted and consolidated with the help of a laser beam. The dense deposited alloy usually has improved mechanical characteristics. The metallurgical bond between the alloy and the substrate guarantees great adhesion. The method has some drawbacks such as low deposition rate (1kg/h), narrow tracking width (less than 4

mm) and slow cladding speed (0.5 mm/min) [19]. Laser alloying is very similar to cladding but it has a higher alloying speed (up to 2.2 m/min). Once the molten pool deposited on the surface, the alloyed zone cools rapidly creates a track of solid metal with very fine dispersed hard phase of silicon particles [3]. Therefore an additional process, usually re-melting; is needed to further homogenize the aluminum matrix structure [19]. Also a chemical process is needed to finish the surface after honing [3].

1.3.2 Fiber or Particle Reinforced Aluminum Alloy Cylinder Blocks

This is an alternative replacement for cast iron lined aluminum blocks. A metal matrix composite (MMC) is usually composed of two constituents: the metal matrix and single or multiple reinforcements. The reinforcement material is added to the matrix, by a physical process and not by chemical bonding or alloying, to provide specific structural or functional properties to the compound beyond the individual constituents. Reinforcement material can be in form of fibers or particle and is embedded into the metal matrix. In the fiber reinforced composites (FRC), fibers are individual filaments of different materials such as alumina, boron carbide or silicon carbide and can be in the form of single crystal fibers known as whiskers, continuous lengthy fibers or discontinuous fibers usually shorter than 3 mm long [20]. Alumina and boron carbide fibers can improve the scuffing resistance and silicon carbide helps with the hardness and wear resistance. Graphite also has been used to provide self-lubricity and reduce the coefficient of friction considerably [21].

Honda used MMC in their Perlude model engine block in 1990 [4] and continued to use MMC in Acura NSX (1990-2005) and Honda S2000 (2000-2009). A pre-form consisting of α-Al_2O_3 and carbon fibers is first set into the die then using a medium-

pressure die casting the pre-form is enclosed into the aluminum block [22]. Also Toyota Motor Company used MMC liners [23] consisting of alumina-silica fibers and mullite for their Celica sport model (2000-2006). Mullite (with two stoichiometric forms of $2Al_2O_3SiO_2$ or $3Al_2O_3\,2SiO_2$) increases the mechanical strength of the composite material and also provides thermal shock resistance [24]. All the mentioned cars are compact sport cars with the capacity to operate at high revolution per minute. At higher engine speeds, a higher wear resistant fiber reinforced composite is needed.

KS ATAG patented an aluminum matrix composite with an aluminum alloy matrix and silicon reinforcement known as Lokasil®. The blocks are produced by placing a Lokasil® pre-form in the casting mold, pouring the molten aluminum alloy into the cast and allowing it to penetrate into the pre-form which creates a hardened silicon-reinforced cylinder bore surface [3]. Two types of Lokasil® are used. Lokasil I® with 5% volume alumina and 15% volume silicon and Lokasil II® with no alumina content and 25% volume of silicon. The main advantage of using Lokasil® is that the achieved finished surface needs no post-treatment such as chemical etching of the surface or honing. Lokasil® has been used in Porsche Boxster since 1996 and Porsche Carrera since 1997.

Problems can occur if the reinforcement material does not set properly in the matrix or if the reinforcement is a mismatch in the matrix. For instance if the reinforcement particle or fiber is too hard; it can permanently damage the piston ring, change the compression and cause engine failure. Also even distribution of reinforcement material is crucial. Aluminum matrix can be worn out in the absence of reinforcement particles or fibers. Finally, casting process is complicated and can be expensive. Metal

infiltration around the reinforcement fibers and post-casting machining are also complicated processes that need extra attention in order to achieve a casting and manufacturing process with near zero defect level of the cylinder bores [23].

1.3.3 Nickel Based Ceramic Coatings (NCC^{TM})

Nickel based ceramic coatings (NCC^{TM}) such as Ni-SiC was one of the primary state of the art in cylinder block surface treatment. It was first used in two-stroke engines of motorcycles produced by Suzuki Motor Co. in Japan around mid-1970s [25]. It was known for its hardness, wear resistant and self-lubrication thanks to nickel. During the process, a Ni layer is dispensed around SiC particles [4], [26] . The optimum results are gained on cylinder blocks with minimum porosity which is needed to be produced by LPDC [26], [27]. Initial problems and concerns about this process are disposal of nickel slurries and corrosion in cases of higher levels of sulfur in fuels [3]. Along with nickel, iron-based ceramic coatings were also studied and used for cylinder surface treatment however nickel has a better corrosion resistant specifically in withstanding high methanol fuels [25], [26]. Also cubic boron nitride (CBN) nickel based coatings were developed with lower coefficient of friction and better resistant to absence of lubrication. Often a small amount of phosphorus is added to the electrolyte to deliver age hardening [4]. NCC Coatings are applied either on the liner by dipping process of the liner and then inserting it into the cylinder or by flow-through process inside the cylinder bores. The associated cost of this process is estimated close to the traditional cast-in iron liners [25].

1.3.4 Physical Vapor Deposition (PVD)

Next method is physical vapor deposition (PVD) coating which creates a thin layer of titanium nitride (TiN) or titanium aluminum nitride (TiAlN) on a honed cylinder

bore surface by evaporating titanium under vacuum condition. Coatings are wear and scuff resistant. The method is not widely used due to the high cost and essential surface preparation and cleaning prior to the coating process [28].

1.3.5 Thermal Spray

Another coating method is thermal spray coatings. Thermal spraying is the process of melting or heat-softening materials in shape of wire, rod or powder and propelling the molten or semi-molten materials towards a surface through a jet of process gas. The particles are quenched upon impact with the surface and bond to form a thin anti-wear layer of coating. The method was initially used on two-stroke engines in 1973 by Kawasaki Heavy Industries [4]. Different thermal spray processes are developed and used to provide a wear resistant coating on the surface of cylinder bore or on the liners [29]–[31]. Thermal spray technology in general is a relatively new approach in surface treatment of engine blocks. Specific modifications are applied to the existing spray systems of thermal spraying for engine application. For instance the spray gun head should be modified to fit into the bore with a diameter of 60 to 100 millimeter and freely rotates coaxially in the bore. Usually the plasma generator or the combustion chamber is mounted at the bottom of a rotating spindle. Spraying distance is short and modifications should be applied to minimize heat transfer during spraying to avoid possible distortion of the bores. Four types of thermal spraying process have been considered for surface treatment of cylinder bores:

1.3.5.1 Plasma Spray

From all the developed technologies, plasma spray has reached high volume production due to a wide range of material selection. Plasma spray uses a plasma arc to

melt a variety of ceramics, cermets and super alloy powders and pass them through an inert gas which can be argon, nitrogen or hydrogen. The term plasma is used due to the significant quantity of heat that is produced in the gas by the arc. The flamed material is then propelled at the substrate and forms the coating. Depending on the cost of powders this process can be as economical as gray cast iron liner mass production or an expensive alternative which is usually only suitable for luxury brand car engines. If the coating is not applied properly, it can delaminate, cause premature wear of the bores and eventually failure of the engine.

1.3.5.2 Electric Wire Arc Spray

The other alternative is to use electric wire arc spraying. This technology uses two electrically charged wires that are fed into a torch and melted in contact with each other. An atomized gas of either air or nitrogen is dispensed through the center of the spray gun and deposited on the surface. Narrower choice of materials and reliability issue of the melting process are some of the shortcoming of this technology.

1.3.5.3 High Velocity Oxy-Fuel Spray (HVOF)

HVOF uses a high velocity flame which is produced by combining different gases and oxygen, injecting and igniting them in a combustion chamber of a torch. Finer powders are usually used for this process. The flame is released through an orifice in the torch nozzle. Coating material enters into the flame through a separate orifice; molten material is blasted towards the surface. This method provides lower temperature at a relative high velocity in comparison to Atmospheric Plasma Spray (APS) [32].

Compared to APS coating, this method creates better coating adhesion and lower porosity [3]. Inconsistency in coating properties occurs when the particles are splattered against the surface. This can generate pores in the coating and leads to cracks. The achieved morphology in this case is called splatter morphology. Also, high temperature and high velocity of the travelling particles in a short distance inside the cylinder can overheat and distort the block and possibly change the microstructure of the aluminum alloy substrate. Initial capital investment of the spraying equipment is high since many modifications should be applied to the existing production line of the plant.

1.3.5.4 Plasma Transferred Wire Arc Spray (PTWA)

Recently, Ford Motor Company in collaboration with Flame-Spray Industries implemented a thermal spray technology patented as plasma transferred wire arc process (PTWA) [11]. The technology was applied to 2009 Nissan GTR and Ford Mustang Shelby GT500. The coating reduces the friction force between the cylinder bore and the piston ring [29], [33]. This technology saves between 6 to 8.5 pounds of weight over the previous cast iron lined cylinder block. The process is similar to traditional electric wire arc spray process with the difference of using a plasma gas instead of normal gas. The arc is produced between a thorium-doped tungsten cathode and copper anode of the nozzle. DC power is transferred through these electrodes while the powder is passed through the arc to a negatively charged conductive path (pre-heated) which is usually a 1010 steel alloy wire. The plasma gas is fed through the center of the gun into the cathode and creates a vortex which adds to the speed of the molten material atomization. A high velocity gas including oxygen is then introduced to the molten droplets and creates a

form of iron oxide known as *wustite*. The composition of wustite is intermediate between pure iron monoxide (FeO) and magnetite (Fe_3O_4) and it adds to the coating hardness [34]. Also existence of hematite (Fe_2O_3) in the plasma mix increases the wear resistance of the coating [33]. Iron oxide particles are sprayed against the surface and rapidly solidify upon contact. An endurance test of 300 hour on full power in Ford Motor Company lab exhibited 50% less wear of the surface comparing to the cast iron lined cylinder. In general, PTWA coated engines had less oil and fuel consumption due to reduced friction (6.8% less than traditional cast-iron lined engines) [35].

1.3.6 Plasma Electrolytic Oxidation Coating

Electrochemical treatment processes has been considered for surface modification of cylinder walls. Plasma Electrolytic Oxidation (PEO) process is an electrochemical surface treatment that generates an oxide layer on the substrate. This layer has shown great wear and corrosion resistance [36], [37] which makes it a candidate for cylinder bore surface treatment. The reason is the formation of a ceramic layer of alumina (aluminum oxide) that acts as a barrier between the corrosive material and the substrate and also due to its high levels of hardness, it is resistant to abrasion. Furthermore, since the coating is oxidized rather than deposited, it has good adhesion to the substrate and delamination is rarely a concern. Additionally, the outer layer of the coating is porous and can retain lubricant in a similar way to the traditional cross-hatched honed cylinder bores. On top of all the advantages and desirable characteristic of this coating specifically in a corrosive, high temperature and high impact environment such as an engine, the process of creating the coating is considered environmental-friendly. This is due the fact that the electrolytes are generally alkaline water soluble based and easily recyclable. Plus during

the treatment process minimum amount of fumes and toxins is produced since the production does not require high processing temperatures. Moreover, it is much less noisy compared to other spraying methods.

Plasma electrolytic oxidation was commercialized for automotive application by a British company called Keronite in 2000. The company named the plasma electrolytic oxidation process, *Keronite process*. Keronite process is a self-regulatory treatment process in which a ceramic layer on the aluminum surface is fused with a uniform thickness and porosity [38]. The coating has shown high micro-hardness, superior wear and corrosion resistance, and good adhesion to the substrate. The mentioned features make this coating a great candidate for enhancing light materials' tribological capabilities. Hence, alloys of aluminum and magnesium have been considered for PEO treatment. Aside potential application for automotive industries, various range of industrial applications have been considered for PEO treatment such as biomedical [39], aerospace [40] [41] [42], marine [43] [44],and house hold appliance stoves and burners [45]. PEO process along with relevant literature will be described in detail in Chapter 2. The feasibility of using PEO treatment process in place of PTWA in terms of treatment time, energy consumption and cost analysis is studied in Appendix B of this dissertation.

1.4 Research Objective and Scientific Methodology

This dissertation aims to provide the research findings on tribological behavior of variety of PEO coatings under low to medium load wear mechanisms. Various types of PEO coating are achieved by changing different aspects of coating production such as electrolyte composition, current density, polarity of the input current, treatment time as well as acidity of the solution. The achieved coating is tested under different lubrication

conditions and results are compared in detail. The objective is to find optimum PEO coating for treatment of aluminum alloy cylinder walls. The desired coating should exhibit low coefficient of friction and illustrates best adaptability to the counter surface: piston rings.

In order to study a wide range of attributing factors in performance of the coatings, independent and dependent variables were defined. In studying the independent variables, all other variables are held constant so that the influence of the independent variable can be observable.

Along data analysis of wear results, coatings are observed under Scanning Electron Microscopy (SEM) for morphological observation. Atomic Force Microscopy (AFM) is used for topographical study and surface profile observation of wear scars and wear tracks. Roughness of the coatings are measured with a stylus device. Energy-dispersive X-ray spectroscopy (EDX) is also used to determine the phase structure of the coatings.

1.5 Dissertation Outline

This dissertation is a summary of the research and analysis results of PEO coatings. Chapter 2 reviews the background on plasma electrolytic oxidation process and its formation. A collection of significant studies done on mostly aluminum alloys is presented.

Chapter 3 presents the experimental apparatus, conditions and settings. Variables and parameters involved in fabrication, testing and analysis are defined and explained.

Chapter 4 gathers the results and discusses the effect of different variables on coefficient of friction and wear behavior of the coatings.

Chapter 5 investigates the counter surface behavior against the PEO coating by observing the wear scars and presenting the wear rate and volume loss values.

Chapter 6 highlights the contributions arising from the current research and summarizes the conclusions. Also the recent research trends and potential future work on PEO coatings are discussed.

Appendix A presents the documentation of copyright permission for published materials and Appendix B compares the two competing treatment processes of PEO and PTWA in terms of treatment methods, advantages and cost.

CHAPTER 2. PLASMA ELECTROLYTIC OXIDATION

Electrochemical processes have been used to alter the properties of different materials. This type of surface modification mainly is used to enhance the wear and corrosion resistance or fatigue and creep properties of the materials which have the potential for automotive, marine, refinery and, oil and gas industry applications. Plasma electrolytic oxidation (PEO) process is a recent electrochemical surface modification technology that has gained a lot of attention among researchers in industry and academia due to its great potential as an eco-friendly surface engineering solution for lightweight metals such as aluminum, magnesium and titanium. These metals and their alloys have high strength-to-weight ratio along with excellent physical and chemical properties however their wear and corrosion resistance should be enhanced by PEO technology. This chapter explains the origin and evolution of PEO coatings in section 2.1. Terminology that is used for PEO coatings are listed in section 2.2. There are times that PEO is mistaken with anodizing hence anodizing is described in detail in section 2.3. A summary of the literature is also given in section 2.4.

2.1 History and Emergence of PEO Technology

In 1880s, a Russian scientist, Sluginov discovered the discharge phenomenon [46] by observing a luminous light in an acidic aqueous solution with platinum electrodes connected to high current densities. The light or spark was a sign of discharge phenomena. Later in 1960s, McNale and Grass investigated micro arc oxidation (MAO) and its feasibility in synthesizing complex coatings produced by the chemical elements of the electrolyte on the surface of substrate [47]. Markov also studied the process of oxide

deposition on an aluminum anodic electrode by an arc discharge in 1970s [48]. During 1980s, MAO was considered for surface treatment studies on various metallic substrates for early industrial applications [49]. In 1999, Yerokhin et al [50], reviewed electrochemical treatment processes. They categorized PEO under plasma electrolytic deposition (PED). PEO is sub-categorized as an anodic oxidation method. Figure 2 shows the development timeline of PEO coating considering the major highlights of each decade. Since 1980s, a variety of PEO processes have been patented in different countries. Along with Keronite [51], proprietary versions of PEO technologies are developed by surface engineering industries. To name a few, Mofratech in France [52], Magoxid-Coat in Germany [53], Machaon in Russia, Tagnite [54], CeraFuse [55] and Microplasmic Corporation [56] in USA. Other patents have also been filed and granted in Canada [57] and USA [58] on method of formation and the process.

2.2 Terminology of PEO

Plasma electrolytic oxidation (PEO) is also called micro-arc oxidation (MAO) [48], micro plasma oxidation (MPO) [59], spark anodizing [60], anodic spark deposition (ASP)[61] , anodic spark oxidation [61] and micro arc discharge oxidation (MDO) [62]. Also plasma electrolytic anodization (PEA) [63] has been used for a process relatively close to PEO in terms of mechanism but closer to anodizing process. Therefore, PEA should not be used inter-changeably with PEO. Coating growth rate and thickness achieved in PEA is less than PEO process under the identical conditions [64].

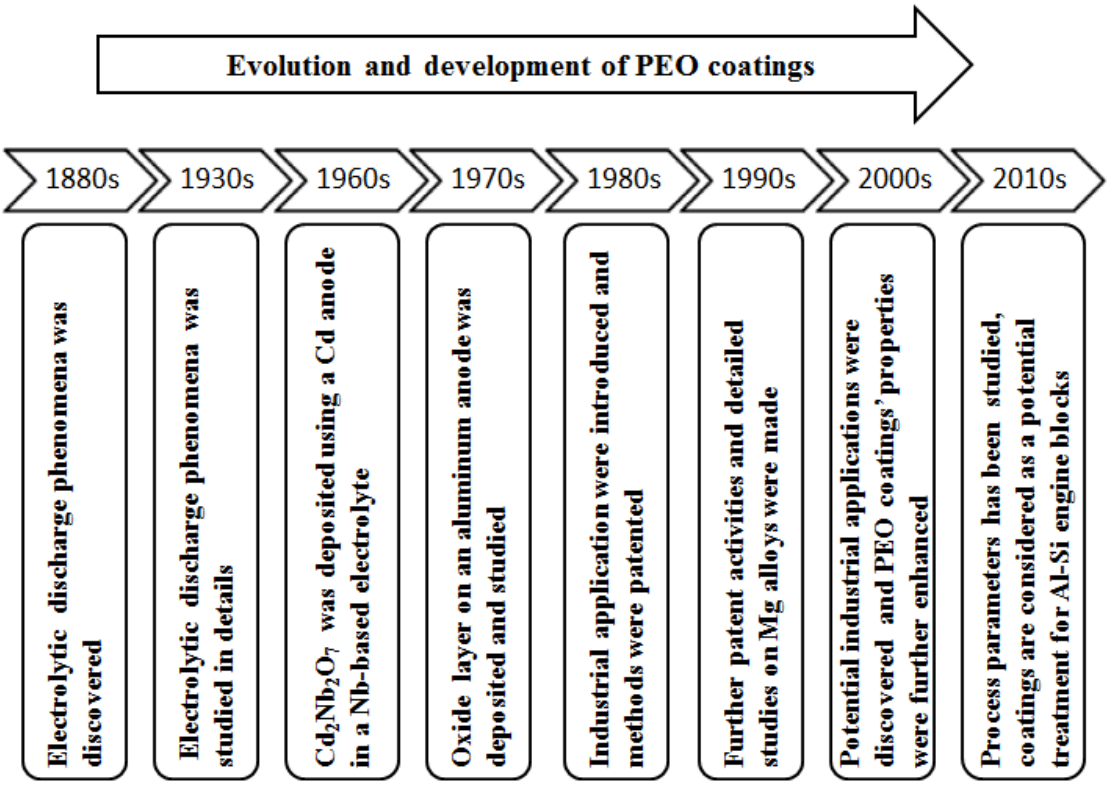

Figure 2. Development timeline of PEO coatings and treatment process.

2.3 Anodizing versus PEO

Anodizing is traditionally achieved using low-voltage direct current (DC) power source with 20 to 80 voltage input and current density of 0.01 to 1 A/cm^2, and an acidic electrolyte. The electrolyte is commonly sulfuric acid (H_2SO_4) however there are many cases that other acids such as oxalic ($H_2C_2O_4$), phosphoric (H_3PO_4), chromic (H_2CrO_4)and boric (H_3BO_3) acids are used instead [65].

Due to its components of process: electrolyte bath and power source, PEO was compared with anodizing process which is widely used in aluminum industry. However, there are many advantages of PEO in comparison to anodizing [64]. Firstly, PEO ensures

the production of a variety of materials with improved chemical and physical properties. Enhanced hardness, wear, corrosion and fatigue resistance are to name a few. Second, pre-treatment processes are minimal which makes it a time-efficient process for mass-production. Some other deposition methods need thorough surface preparation starting from etching and degreasing to washing [66], [67]. Etching process is mainly done to remove the natural aluminum oxide film on the substrate. Degreasing and cleaning is to remove the machining metal fluid such as lubricant or coolant [68]. Third, the process is eco-friendly due to its use of mostly alkaline aqueous non-toxic solutions which are less troublesome in recycling. Fourth, less toxic fumes are produced during the treatment. Finally, PEO can be used with higher voltage and current densities [69], also harder coatings with excellent adhesion can be achieved using PEO process compared to anodizing.

2.4 PEO Process Mechanism and Chemical Reaction Kinetics

PEO coating process has been studied by several researchers. One of the most cited paper in this field of study is written in 1999 by Yerokhin et al [50]. They described the process in detail according to current-voltage (I-V) characteristics of the electrochemical system involved in the plasma electrolytic oxidation process. The study was divided into two systems: on system that addresses the I-V characteristics around the electrode and another system in the dielectric film on the electrode surface (as shown in Figure 3).

During the initial stage, where the voltage are low, kinetic of the electrode process agrees with Faraday's law and the I-V characteristics of the cell agrees with Ohm's law. This stage corresponds with 0-U_1 near the electrode and 0-U_4 in the dielectric film.

Increase in voltage causes current oscillation and creates luminescence near the electrode. Increase in current is controlled by a partial shield of gas products such as O_2 and H_2, over the surface of the electrode. As the current density rises, local boiling of electrolyte happens around the electrode as seen in U_1-U_2 stage. Once U_2 value is reached, the electrode is completely covered by an envelope of gas vapor with low conductivity. This creates an electric field with 10^6 V/m strength that can initialize the ionization process. Scattered and rapid sparks are formed on the surface and creates further bubbling effects around the electrode. Sparks are then followed by a uniform glow that is distributed throughout the gas vapor which is now converted to an envelope of vapor plasma once U_3 stage is passed. Beyond this point, the uniform glow transforms into an arc. This stage is characterized by a low frequency acoustic feedback more like a whizzing sound.

Understanding the I-V system in the dielectric film is more complicated. The anodized passive film that was formed at U_4 stage starts to dissolve as the voltage increases and reached the corrosion potential of the substrate. A porous film in formed as the result of repassivation process from U_4 to U_5. The electric field strength continues to increase until it reaches a critical value of breaking the film at U_5. Tiny bright sparks surrounds the surface of the oxide film and assists the coating growth. At point U_6, thermal ionization process is started and creates larger arc discharge with longer intervals. In region U_6 to U_7, thermal ionization is interrupted by the bulk of now thickened oxide film. This would be the time that the micro-arcs form. Then the doping elements present in the electrolyte are fused into the oxide coating and thickens the oxide layer.

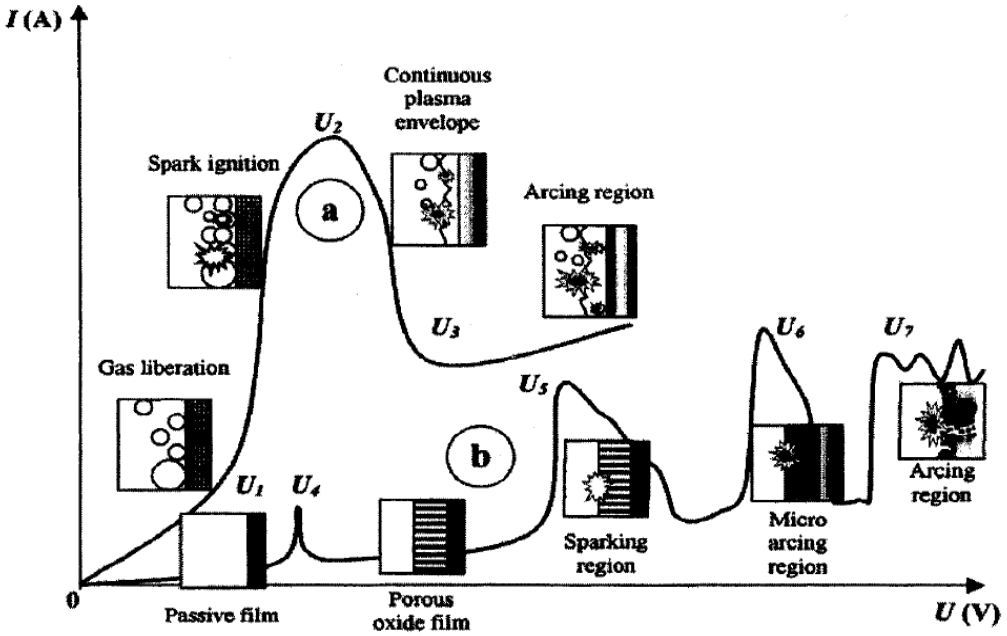

Figure 3. Current-voltage diagram of PEO process: a) around the electrode, b) inside the dielectric film on the electrode surface [50].

Yerokhin et al [50] also reviewed evolution and development of PEO coatings and proposed possible applications of PEO coatings in various industries. Other studies [64], [70] summarized the process into four sequential stages:

1. Anodization: this phase was also called electrolysis in some references
2. Spark Discharge
3. Microarc discharge
4. Arc discharge

During the anodization, a high porosity coating is formed as the anodic voltage increases across the working electrode. The main difference between the second and third stage is the intensity and size of the discharges. However the mechanism of discharge and coating growth process are the same for both stages. Stage four requires large enough

energy that can pass through the discharge channels and creates larger sparks not only on the surface of the substrate but also into the electrolyte.

Many reactions are involved during the process in the electrolyte tank as seen in Figure 4. For instance the coating growth on the anode due to the oxidation reaction is as follows [70]:

$$2\,Al + 3\,O^{-} \longrightarrow Al_2O_3 + 3\,e^{-} \qquad \textbf{Equation 1}$$

$$2\,Al + 3\,OH^{-} \longrightarrow Al_2O_3 + 3H + 3\,e^{-} \qquad \textbf{Equation 2}$$

$$2\,Al + 3\,H_2O \longrightarrow Al_2O_3 + 3\,H_2 \qquad \textbf{Equation 3}$$

Equation of the reaction 1 and 2 can be combined and simplified as [71]:

$$2\,Al + 3\,H_2\,O - 6e^{-} \longrightarrow Al_2O_3 + 6\,H^{+} \quad \text{(Anodic oxidation)} \qquad \textbf{Equation 4}$$

Surface oxidation results in vigorous escape of hydrogen that leads to cooling of the oxide film and the electrolyte absorbed into the pores. Due to the high anodic currents in PEO process, oxygen evolution occurs as represented in Equation 5:

$$2\,H_2\,O - 4e^- \longrightarrow O_2 + 4\,H^+$$ (Oxygen evolution) **Equation 5**

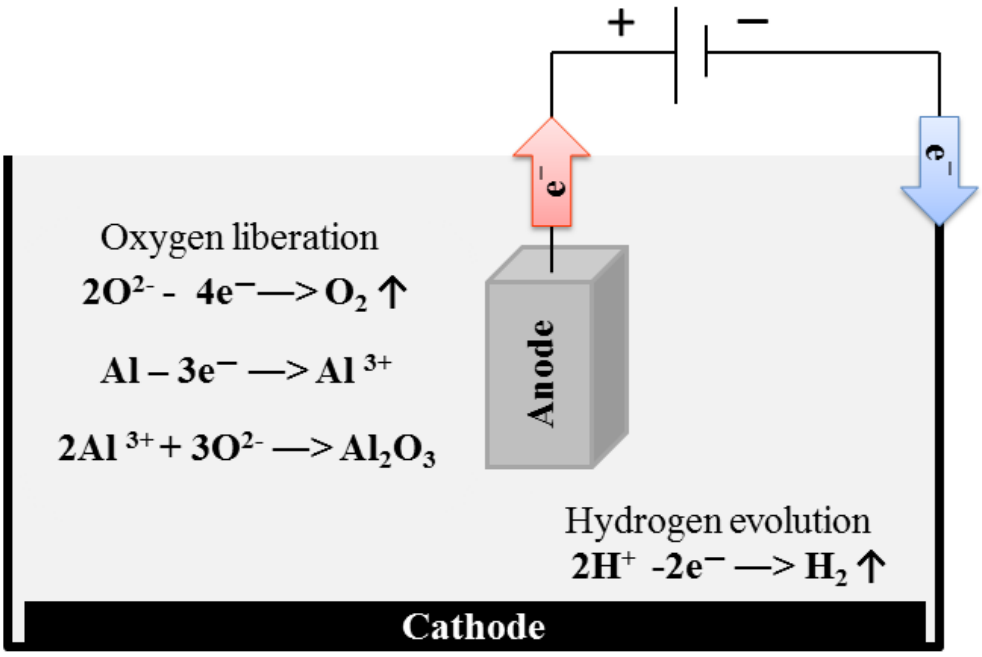

Figure 4. Electrode process in electrolyte tank.

Alumina chemical dissolution and oxidation of ejected Al obeys the following reaction (Equations 6, 7 and 8) if a hydroxide chemical is used in the electrolyte such as KOH [70]:

$$Al_2O_3 + 2(x-3)\,OH^- + 3\,H_2\,O - 6e^- \longrightarrow 2[Al\,(OH)_x]^{n-}$$ **Equation 6**

$$Al^{+3}_{ejected} + x\ \mathrm{OH}^- \longrightarrow [\mathrm{Al}\ (OH)_x]^{n-} \qquad \textbf{Equation 7}$$

$$[\mathrm{Al}\ (OH)_x]^{n-} \longrightarrow \mathrm{Al}\ (OH)_3 \downarrow + (x-3)\mathrm{OH}^- \qquad \textbf{Equation 8}$$

During the last stage of the process, direct injection of Al into the electrolyte occurs through discharge channels. The ejected Al is then hydrolysed (See Equation 7.) first and precipitated (See Equation 8.) as a hydroxide on the anode surface. Subsequent plasma discharges causes dehydration and recrystallization of deposits and results in further growth of the oxide coating. Most of the electrolyte solutions have a pH value of 13 since they are alkaline. Changes in the electrolyte pH during the PEO process happens only during the passage of charge through the system at the last stage: plasma discharge. Solution acidification is more evident at higher current density values. Snizhko et al [71], studied the acidification of electrolyte in silicate based solution mixed with different concentration of KOH. At 2 gr/lit of KOH concentration, no plasma discharge occurs and electrolyte pH remains almost the same (ΔpH= -0.02) however for less concentrations of 0.5, 1 and 1.5 gr/lit solution acidity changed with ΔpH of -0.6, -0.3 and -0.2 respectively. Also for the 1 gr/lit of KOH concentration, higher current density caused more change of solution pH.

2.5 PEO Coatings on Aluminum Alloy Substrates

As shown in Figure 2 during 1970s and 1980s PEO coatings were considered for aluminum substrates. Around 1990s there were series of patent activities and trademarks

on production of PEO coating as mentioned in section 2.1. The formation of oxide layers by PEO treatment has been studied widely on lightweight materials mostly Al, Mg and its alloys (for example in [72], [73], [74], [75], [76] and Ti and its alloys (for example in [77]–[79], [80], [81]). There are also studies on other metals such as zirconium and its alloys (for example in [82]–[84], [85]) and different grades of steels (for example in [86]–[88]). Since this dissertation is focused on Al 319, the literature survey is mostly focused on PEO coatings on aluminum alloy substrates.

Anodic process in PEO treatment was studied by Snizko et al [71] on aluminum alloy 6082 in potassium hydroxide electrolyte. In this study chemical dissolution of the substrate and anodic gas evolution were measured. The weight loss of the aluminum was measured after 40 minute of treatment. Following balance equation was used for partial processes of aluminum dissolution, oxide coating growth and gas liberation. The equation 9 is governed by Faraday's law:

$$\eta\,(Al_2O_3) + \eta\,(Al) + \eta\,(O_2) = 100\% \qquad \textbf{Equation 9}$$

where $\eta\,(Al_2O_3)$, $\eta\,(Al)$ and $\eta\,(O_2)$ are partial anodic products of alumina, dissolved aluminum and oxygen respectively. Specimens' weight loss was measured using an analytical balance. Coating growth mass was determined by cross sectional study of the coated samples under SEM assuming that the oxide density is around 3.1 gr/cm^3. A two liter glass vessel was connected to an inverted glass funnel above the electrolytic bath collecting all the evolution gases of the process. For 1 gr/lit concentration of KOH, oxide

formation as about 28.9 %, aluminum dissolution is 7.2 % and gas liberation is around 63.9% as Equation 9 implies. Higher concentration of KOH resulted in significantly less oxidation and higher dissolution; however the gas liberation percentage stayed the same. Collected gas was also analyzed using a residual gas analyzer. The anodic gas composition was consisted of predominantly oxygen (> 93%) and traces of nitrogen (< 4%) and hydrogen (2%). It was found that the increase in current density creates an increase in gas evolution. It was concluded that the amount of gas evolution is independent of electrolyte concentration and dependent on current density.

Many studies have been done on process parameters of the PEO coatings. For instance current mode and polarity of the coatings are studied in depth. Yerokhin et al [89] produced and studied the oxide coating using pulsed bipolar current mode for the first time. Optimum coating growth rate was achieved in pulsed frequency range of 1 to 3 kHz. A denser coating with 10 to 15 % of porosity was produced. Jaspard-Mecuson et al [90] studied the influence of bipolar current adjustment on 2214-T6 aluminum alloy. It is shown in their study that applying a higher negative charge setting compared to the positive charge can improve the homogeneity of the coating. Coatings had less large discharge channels in the final layer and were thicker.

Wei et al [91] studies the effect of distance between the cathode and anode plates on anodic current of the PEO process. A range of 5 to 25 cm distance matrix with 5 cm intervals was used. It is shown that less distance between the electrodes creates a higher anodic current. Also the current flowing through the front of the electrode is higher than the back. Front surface showed better resistant to wear and corrosion than the back surface. Corrosion resistance of PEO coatings is also studied. Potentio-dynamic

polarization curves were achieved in 3.5% NaCl solution. Corrosion current of the uncoated sample was 8.455×10^{-6} and 2.422×10^{-6} and 1.277×10^{-6} for the front and back side of the specimens respectively. The corrosion Potentials were also improved positively from -0.843 V for the uncoated case to -0.634 and -0.734 for the front and back surfaces of the coatings. The chemical stability of the coating compared to the substrate is a key reason for improvement of corrosion resistance. Also since the coatings on the front side of the specimens were thicker and denser, they resist better to the corrosion compared to the coatings on the back side of the specimens.

Thermal conductivity of PEO coatings was measured by Curran and Clyne [75] using a typical steady state method. Due to the smooth morphology with fine grains and the amorphous nature of the oxide layer, the thermal conductivity values were moderately low, mostly around 1.6 W/mK° for coating thickness of 100 μm. This is drastically lower than the thermal conductivity of the bulk material which is around 30 W/mK°. Discovered thermal properties of the coating, makes these coatings a great candidate for thermal barrier layer in electronics applications and etc. Coating density was also measured to be 3.61 (± 0.03) gr/cm^3 with up to 30% of amorphous phase. The relative low thermal conductivity of PEO coatings is due to high percentage of amorphous phase along with fine grain size. Later, Curran [92] discovered the effect of mullite phase on thermal conductivity of the coatings. Thickness of 200 μm coatings in silicate solution were produced and exhibited excellent resistant against spallation of thermal cycling and temperature alterations.

Khan et al [93] investigated the residual stress in DC PEO alumina coatings on thickness levels of 3 to 40 μm oxide layer produced on 6082 aluminum alloy in KOH

electrolytes. A range of current densities (0.5 to 2 A/cm2) were used as the electrical parameter variable. Increased current density tends to decrease the residual stresses of the coatings. The reason is that higher current density means higher plasma micro discharge which promotes stress relaxation by formation of micro cracks on the surface and also thermal annealing of the coating. The lowest stress value of (302 MPa) was measured for the 1.5 A/cm2 and the highest stress value (714 MPa) was measured for the lowest current density. They concluded that the internal stresses in PEO coatings are the result of a series of stress generation and stress relaxation processes. Stress generation processes are dependent of thermal and structural properties of the coatings and stress relaxation processes are the result of formation of a network of micro cracks within the morphology of the coatings. Denser coatings motivates the generation of micro cracks and porous coatings inhibits the formation of these networks.

PEO coatings have been considered for space application recently. Shrestha et al [42], examined a black finish coating produced on AA2219 aluminum alloy by the Keronite process. Coatings exhibited good adhesion and cohesion. Hardness values were measured to be around 1300 HV. Friction coefficient for the Keronite coatings against steel was measured to be around 0.5. These coatings were studied as an alternative to replace the black anodized aluminum with inorganic dyes (PSS-01-703). The solar absorbance of infrared emittance ratio for these coating was 1.2 which is less than the black anodized coatings and is desirable for space craft materials applications. Same results were achieved in another study [94] on aluminum alloy 7075. Coatings have shown no surface damage after torture testing against steel balls. In comparison anodized aluminum samples displayed severe chipping and extensive cracking under same wear

test conditions.

Matykina et al [95], researched on methods of optimization of PEO coatings. They combined the pre-anodizing technology with sequential treatments of PEO coatings on pure aluminum. This would promote the faster development of micro-arcs and increased the coating growth rate up to 10 μm/min. Monoclinic zirconium nanoparticles were incorporated into the PEO coating under AC current conditions in a phosphate-based solution and formed phases of tetragonal and cubic zirconia. Obtained coatings showed high microhardness (around 1700 $HV_{0.05}$) along with great capability to be used for thermal barrier applications. Matykina et al [96], earlier studied the formation of PEO coatings on pre-anodized aluminum prepared in sulfuric acid. Initial starting voltage for the pre-anodized coated substrate was much less than a non-pre-treated substrate and resulted in faster initiation of micro-arcs and accordingly less energy consumption. In a comparison study of coatings, the untreated and pre-anodized samples over 8 minutes of treatment time, energy consumption is reduced over 0.8 kWh m^{-2} μm^{-1}.Coatings were mainly consist of α-Al_2O_3 and ɤ-Al_2O_3 .Based on solution type, silicon sodium and potassium were located in the outer layer of the coatings were porosity is less dominant.

Tungsten particles were also incorporated into the PEO coatings produced on aluminum alloy 2024 in a mixture of sodium silicate and sodium tungstate solution. XRD analysis showed the presence of tungsten in the coating along with alumina and mullite [97].

The effect of SiO_2 concentration in the MMC of Al383 on tribological properties of PEO coating was studies by Zhang et al [98]. Volume content of 5 to 10% SiO_2 was

blended into molten Al383. Samples were treated in sodium silicate (Na_2SiO_3) solution to reach the thickness of 2 and 5 μm. Thicker coatings showed better wear resistant properties with higher COF and volume loss of the counterface. Specimen with higher percentage of SiO_2 content exhibited less wear and volume loss of the counterface and lower COF values for the thinner coatings. For the thicker coatings, higher SiO_2 content is beneficial to the wear resistant properties of the PEO layer. Nie et al [62], investigated the influence of coating thickness on tribological behavior of aluminum alloy BS Al-6082 in sodium silicate solution. Thicker coatings (100 μm) appeared to perform better in sliding and scratch tests while thinner coatings (20 μm) are effective in low-load sliding wear. Medium thickness coatings are performed relatively poor in wear tests. Wang and Nie [99], later studied the effect of silicon on formation of PEO coatings produced on Al319 and Al390 in sodium silicate (Na_2SiO_3) solution. Coatings were mostly thinner than 10 μm. Higher content of silicon in the MMC resulted in rougher surface therefore Al390 coated specimen were rougher than Al319 coated specimen. They also anticipated that the effect of silicon on surface roughness for thicker coatings (>50 μm) are insignificant.

Effect of graphite as a lubricant on tribological behavior of the PEO coatings was explored by Nie et al [100] on eutectic (12.0 %Si) Al-Si alloy. A single layer of PEO coating was formed in a sodium silicate (Na_2SiO_3) electrolyte, in the next step an oxide/graphite composite was deposited as the top layer. During treatment, a graphite rod was rubbed against the surface in 1 minute intervals to ensure the incorporation of the graphite in between the layers. The coatings with the graphite interface showed better compatibility with the steel ball counterface, other coatings caused severe wear scar on

the steel counterface. Further research on the effect of graphite on microstructure and corrosion resistance of alumina PEO coatings was studied by Lv et al [101]. Samples of pure aluminum were coated in a mixture of sodium silicate (Na_2SiO_3), sodium hydroxide (NaOH) and graphite grains with the average diameters of 10, 30 and 70 μm mixture for 30 minutes. They discovered that the size of graphite grains have a great impact on morphological structure of the coating. Finer grains of the graphite were absorbed in the pores of the coatings. The embedded graphite created a denser coating with less porosity that exhibited better corrosion resistance in a 3.5 wt. % NaCl solution. Tong et al [102], also added nano-powders of iron (Fe) to the electrolyte. Similar tribological improvement was achieved in the coatings.

Hussein et al [103] studied the PEO process under pulsed unipolar and bipolar DC current modes. The effect of current frequency and other current parameters such as duration of positive and negative pulses and resting time between the positive and negative pulses on coating formation was investigated. For pulsed unipolar DC mode, duty cycle is measured using Equation 10:

$$D_t = \frac{T_{on}}{T_{on} + T_{off}} \qquad \textbf{Equation 10}$$

where D_t is the duty cycle, T_{on} is the period of pulse-on and T_{off} is the period of pulse-off. A common duty cycle for unipolar current mode is 80%. For bipolar current mode, positive and negative pulses are involved. Process parameters such as operating frequency (f = 1/T), duration of each pulse and the resting pause between the pulses are

represented in Figure 5. T_{on}^{+} and T_{on}^{-} are periods of pulse-on for the positive and negative pulse ,and T_{off}^{+} and T_{off}^{-} are periods of pulse-off for the positive and negative pulse.

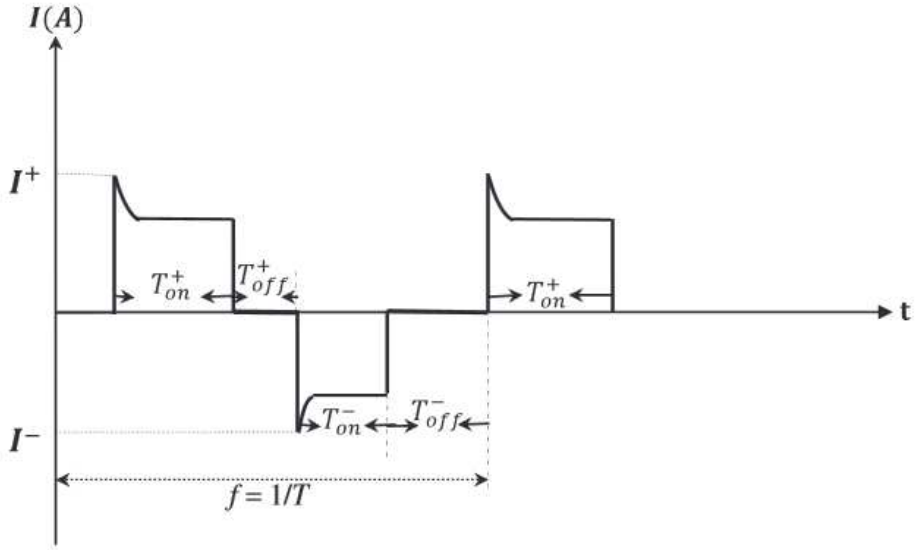

Figure 5. Schematic of a pulsed unipolar current wave [103].

Also plasma temperature was characterized and analyzed against process time. Plasma temperature spikes were caused by the strongest plasma discharges initiated in the dielectric oxide region between the coating and the substrate. It was shown that the pulsed unipolar DC mode created more temperature spikes. Morphological structures of the coatings under pulsed unipolar and bipolar DC mode were compared. Bipolar coatings showed an improvement in quality and density of the coatings. However the study lacks the tribological investigation of the achieved coatings in order to determine the coatings performance.

Many studies were conducted on tribological behavior of PEO coatings [104-106] along with characterization of the coatings [107]. Improved wear and reduced coefficient of friction are two desirable factors that each researcher is after. Trevino et al. [104]

studied the effect of load amount on coefficient of friction using 10N to 40N for coating thicknesses of 100, 125 and 150 μm on aluminum alloy 6061. The weight loss on the PEO coatings increased as the applied load increased. Thinner coatings resisted marginally better against the load increase. Under 30N and 40N load, all samples demonstrated a severe metallic wear that resulted in loss of the coating on the substrate.. Khan et al [106] studied the effect of current density on coating thickness and growth. They also investigated the effect of KOH on coating properties and structure. They found that coating thickness increases with the increased current density. Also addition of KOH has a reverse influence on coating thickness. Coatings prepared at the same current density in a solution with 0.5 gr/lit KOH were thinner than the ones prepared in a solution with 2.0 gr/lit of KOH. Guo et al [107] investigated the effect of voltage and treatment time on coating thickness and phase structure of alumina which can be a factor in wear and corrosion resistant of these coatings

This dissertation aims to present research findings on coating parameters that could reduce the coefficient of friction of the coatings and affects the wear rate. Adaptability of each coating with the counterface is also examined by measuring the wear scar on the counterface and investigating the wear grooves on the coating. The oil analysis and also material transfer from the tribo-pair in contact is also presented.

CHAPTER 3. EXPERIMENTAL APPROACH

3.1 Experimental Apparatus

Typical equipment unit consists of three major parts: power supply, electrolyte, and the electrodes. Figure 6 shows the schematic of the treatment equipment and the major parts. These parts with their components are explained in detail below:

3.1.1 Electrolyte tank

Electrolyte is kept in a tank made out of stainless steel base and polymeric transparent sidings which is connected to the negative pole of the generator. The tank is insulated and the bath is grounded, also the whole tank is confined to a frame that is earthed for safety reasons. The stainless steel plate on the base of the tank acts as the counter electrode in the process. In order to prevent localized high temperature and non-homogeneous distribution of solution particles, some form of agitation is required. This can be achieved by using a simple mixer for small specimen applications or a pump to circulate the solution. In some cases a gas exhaust arrangement [70] is also used for further investigation of the byproducts of the reaction.

3.1.2 Power equipment (Power supply and pulse generator)

Power source can be DC or AC. This study uses DC power supply with a pulse wave generator. Pulse generator provides controlling options for intensity, polarity and process continuity/ interruption settings for the arc process. Process parameters can be adjusted as needed. For the unipolar current mode, $t_{on}^{+} = 400\,\mu s$ and $t_{off}^{+} = 100\,\mu s$

with duty cycle of 80% (using Equation 10) were used and for the bipolar current mode, also $t_{on}^{+} = 400\,\mu s$, $t_{off}^{+} = 100\,\mu s$, $t_{on}^{-} = 400\,\mu s$, $t_{off}^{-} = 100\,\mu s$ were used. According to Yuming Tang *et al* [108] higher duty cycle, increases the bonding strength of the substrate to the PEO coating. Duty cycle of 80% is chosen based on a trial and error. Duty cycle can have an effect on coating porosity and also coating thickness. Power supply comes with different options such as constant current control, constant voltage control, adjustable ramping, end-of-cycle timers/signals and emergency shut-offs button

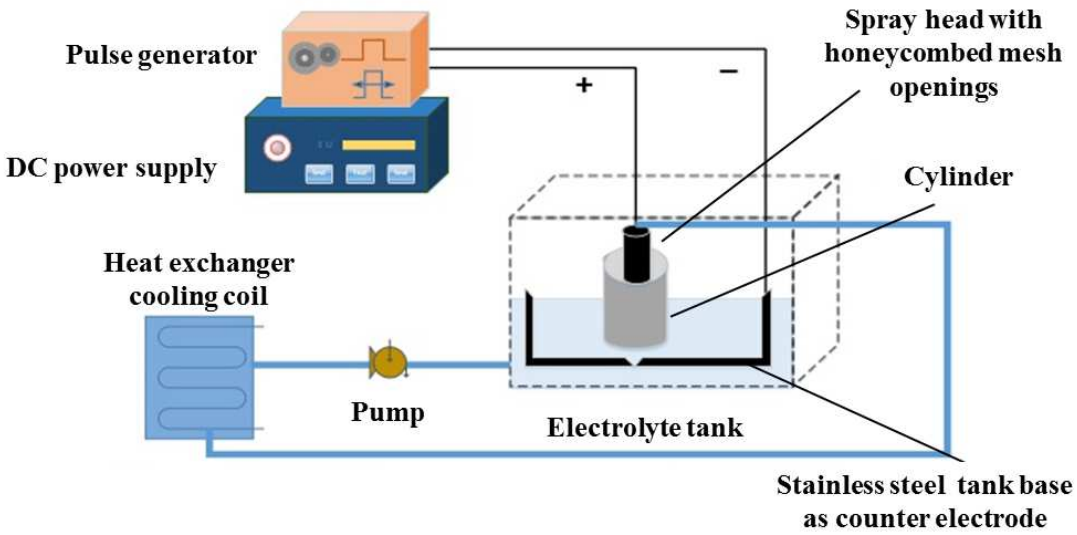

Figure 6. Schematic of the PEO equipment and its major parts for cylinder treatment process.

3.1.3 Specimen holder

The specimen holder configuration can be different based on the specimen size and shape. In case of a small specimen, a sample holder with a hinge or claw can be used and then dipped into the solution tank. In case of a whole engine block being treated, the

engine will be bolted down to the base of the tank and a vertical spray head with symmetrical honey comb mesh nozzles situated around the spray head is used. One spray head was available for engine application process. For industrial mass application, there should be enough spray heads to treat all the cylinders at the same time, For instance 8 spray heads are needed to treat a V8 engine block. The spray heads rotate 360 ° in the cylinder to ensure uniform formation of oxide coating. The spray head is connected to an inlet and electrolyte flows through the inlet into the spray and the mesh nozzles. Extreme caution should be applied to make sure there is an optimum distance between the cylinder walls and the spray head. Any type of touching will cause shortening and damaging the generator system.

3.1.4 Heat exchanger

Based on treatment time and current density, output voltage and also solution temperature can vary. It is however desirable to keep the temperature of the electrolyte less than 60 °C [70]. Longer treatment times (≈ 1 hour) can cause evaporation of the electrolyte and temperature variance through the tank. Although the solution pump can circulate and ensure a more homogenous distribution of heat through the tank, a heat exchanger is beneficial to control the processing temperature. A cooling coil made out of copper in dimensions close to the bottom of the tank (counter electrode surface area) is used and placed underneath the tank and is connected to a heat exchanger filled with cold water.

3.2 Coating Preparation

Before the treatment process there are specific steps taken to ensure achieving of high quality coatings with good adhesion. Following the treatment also a routine cleaning is performed before any tribological tests or morphological observations.

3.2.1 Pre-treatment

Surface preparation prior to the treatment is essential. Rectangular coupons of aluminum alloys Al319 (20×15×5 mm^3) was used as the substrate for the coating deposition; the nominal composition of Al319 is ≤ 7.7% Si, 3.8% Fe, 3.38% Cu, 0.27 % Mg, 0.23 %, 0.12 % Ti, 0.08 % Zn and Al balance (weight %). Coupons were sanded with 4000 and 2500 grit of silicon carbide sanding paper and finally polished to a semi-mirror finish with roughness of Ra= 0.1 ± 0.01 μm using 0.1 and 0.05 micron alumina suspension. Samples were then washed and sprayed with acetone and blow dried before each coating to ensure elimination of dirt or polishing material residue. Same process of surface preparation is necessary in case of the engine treatment.

3.2.2 PEO Treatment – Solution preparation

Once the specimens are ready to be treated, electrolyte is prepared. A series of different solutions is used to see the influence of doping elements on wear properties of the coatings. Doping elements are the elements that are incorporated into the coating. Electrolyte composition and concentrations used in this study are gathered in Table 3, section 4.3.

Most of these solutions are alkaline electrolytes made of salts, metal passivaters and electrolyte conductivity enhancers. These salts should be dissolved in purified and deionized water with electrical conductivity around 11Ms/cm and total dissolved solid elements of 7 to 10 mg/liter.

Samples were dipped into the electrolyte right before the treatment in order to prevent any surface corrosion or etching. Treatment time range of 3 to 10 minute are considered for this study.

3.2.3 Post Treatment

After treatment of the specimens, they were removed from the electrolyte, brushed with a soft bristled brush, flushed with distilled water and blow dried under a hot stream of air. This is to make sure to detach loose particles that might be sitting on the surface of the coating. Based on the experiment, samples are then sanded with silicon carbide sanding papers and polished using alumina suspension solution at 0.1 and 0.05 micron.

3.3 Roughness Measurement

Arithmetic mean surface roughness (Ra) usually called as average roughness of the coatings is measured by a Mitutoyo SJ-201P stylus surface profiler with ± 0.01 to 0.04 μm uncertainty. Ra is the average of the absolute values of the profile height (peaks and values) deviations from the mean line, collected within the measurement length. Equation 11 shows the calculation equation of Ra:

$$Ra = \frac{1}{L}\int_0^L |Z(X)|\, dX$$ **Equation 11**

where L is the measurement length, Z(X) is the profile height function. Figure 7 shows the roughness terminology and the relation between the profile height at each point and the Ra.

In order to compare the coatings achieved under different conditions such as different current density or solution composition, surface of the coatings are sanded and polished into similar roughness values. Roughness values of 1, 0.8 and 0.4 μm were chosen for the tribo-test experiments. Figure 8 shows the profiles of the coatings achieved at different stages of polishing. A surface profile of the polished and ready-to-be treated specimen is also shown.

Roughness plays a role in wear behavior and coefficient of friction (COF) values of the coatings. Results of the influence of roughness on performance of PEO coatings are presented in Chapter 4.

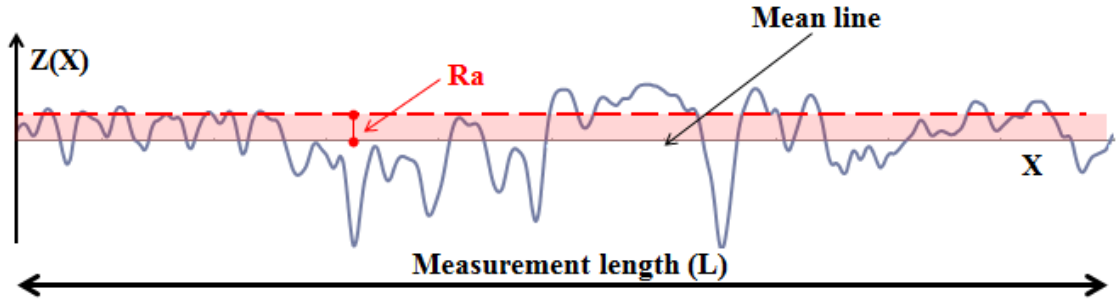

Figure 7. Arithmetic mean surface roughness (Ra) in relation with the surface height profile of the coatings

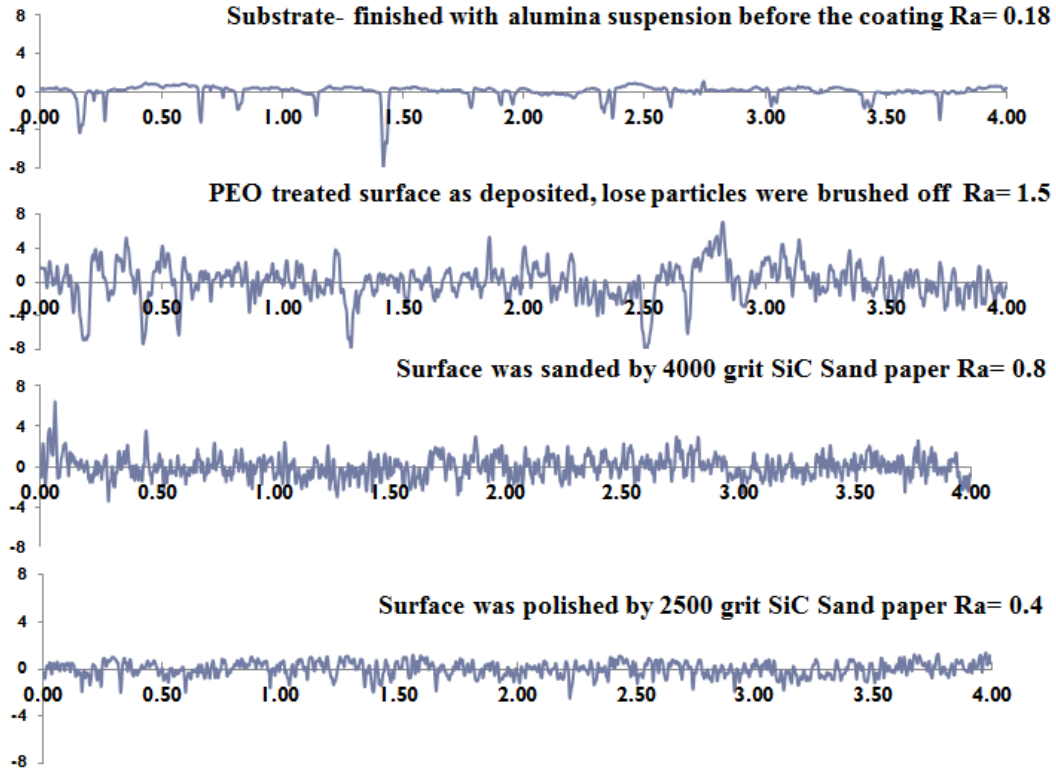

Figure 8. Surface roughness profiles of pre-treatment substrate and post treatment coatings at different stages of polishing.

3.4 Coating Thickness Measurement

Coatings thickness was measured by two different methods. An electromagnetic Induction gauge (PosiTector 6000 N Series) equipped with eddy current measurement setting with ±1% measurement uncertainty was used. Eddy current setting was selected due to non-magnetic and non- ferrous nature of the substrate and the ceramic oxide coatings developed by PEO process. Since the measurements with this device is very sensitive to coating roughness and porosity, cross sectional Scanning Electron

Microscopy (SEM) measurements were also conducted to confirm the acquired values. Figure 9 illustrates the coating thickness of a PEO coated cross-sectioned sample under 0.1 μm/A^2 current density over 3 minutes of treatment time.

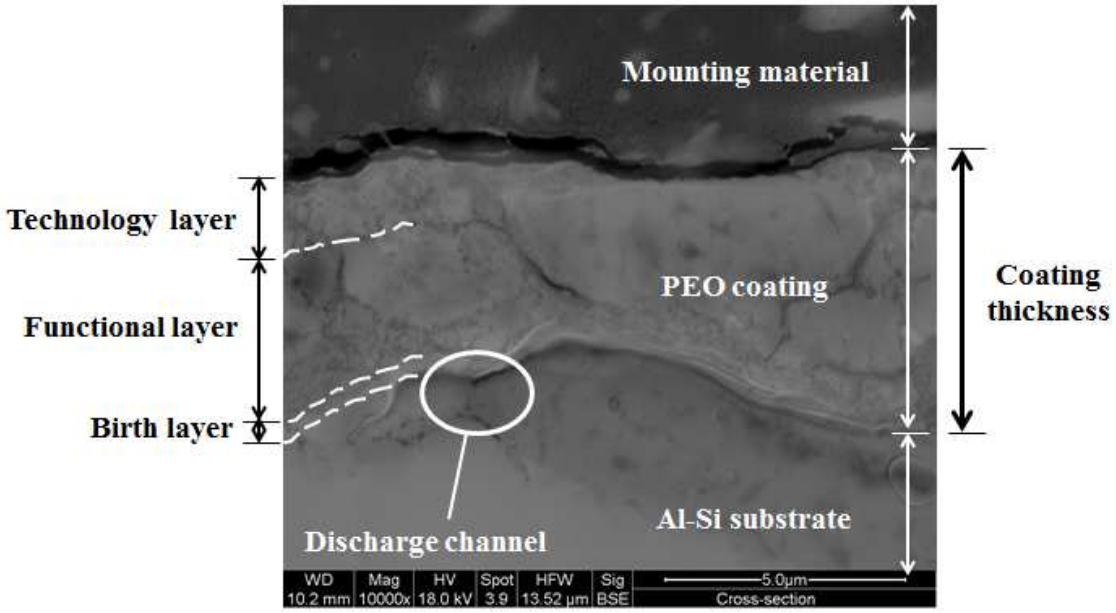

Figure 9. Cross sectional structure of a coated Al319 sample under 0.1 μm/A^2 current density over 3 minutes of treatment time.

3.5 Morphological Observation

Coatings developed in different solutions have different characteristics: tribologically and morphologically. Some of the morphological differences such as coating texture or uniformity were apparent by naked eye. The difference in surface finish was also observed and at times was noticeable to the touch. Post treatment processes as discussed in section 3.2.3 were applied to the surface of the coatings to prepare them for SEM observation.

3.5.1 Coating Surface Observations

Surface morphology and composition of the coatings are characterized using a JOEL 2100 Scanning Electron Microscopy (SEM), operating at 15 Kv. Figure 10 shows a typical PEO-treated coating of Al319 with a network of micro-cracks.

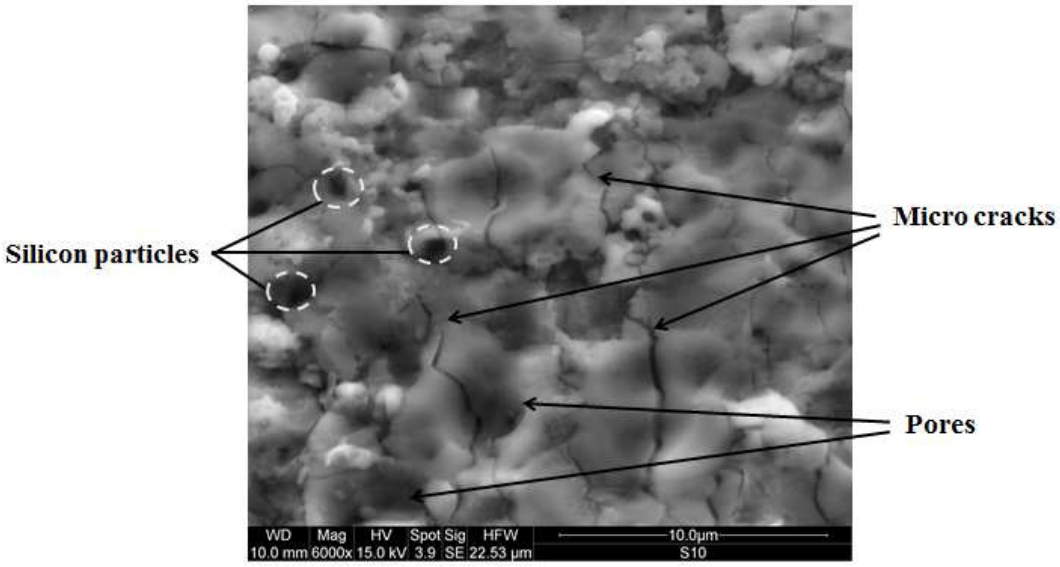

Figure 10. A typical PEO coating with network of micro cracks.

Formation of the coating on the eutectic and dendritic structure of Al319 is shown in Figure 11. Sample is sliced vertically and mounted on a holder stub with a 45° angle. The SEM stub used for this image analysis is shown in Figure 11 as well. This position will permit a better view of surface topography of the coatings by showing the top surface of the coating (on top side of the images) along with the surface of the substrate (the bottom part of the images). Intersection of the two planes of coating surface and substrate is the coating layer thickness. If the same mounting condition is used for the sample, it will be mentioned in the figure caption as: *specimen was mounted on an angle of 45° under SEM.*

As shown in figure 10 and 11, coatings usually have a uniform cauliflower-like structure with apparent volcano-shaped opening throughout the surface. These openings are called discharge channel. Molten alumina is ejected out of these channels and quenched into dense structure around the opening. Also a network of micro cracks can be observed on a typical PEO coating. Pores (voids) are a common feature in this type of coating.

3.5.2 Cross-sectional Observation

Cross-sectional studies are considered to measure the coating thickness and understand the regional structure of the coatings (see Figure 9). Metallographic process on the samples is composed of sectioning, cleaning, mounting, grinding (SiC 400), sanding (SiC 800, 1200, 2400) and polishing (Alumina suspension 0.01μ). Once a mirror finished surface is achieved, it is helpful to sputter the surface with a thin layer of gold to prevent charging under SEM and promote better image resolution.

According to literature [50], [70], there are distinct regions in the PEO coatings produced on Al-alloys: outer region with a porous external layer of the coating. This layer is X-ray amorphous and should be polished off for nano-indentation and micro hardness analysis. Outer layer is the result of outward growth of the coating and is called “Technology” layer [70]. Technology layer is a foam-like layer consolidated as nodular deposits on top of a denser layer called “Functional” layer. Second region is a dense inner region which is formed with higher temperature variation and is responsible for load bearing and hardness characteristics of the coating. There is a thin layer between the substrate and the dense layer which I call “*Birth*” layer due to formation of discharge

channels on this layer. This layer has complex phases of the alloying elements. Refer to Figure 9 for an illustration of cross-sectional images of the total coating thickness with all three regions.

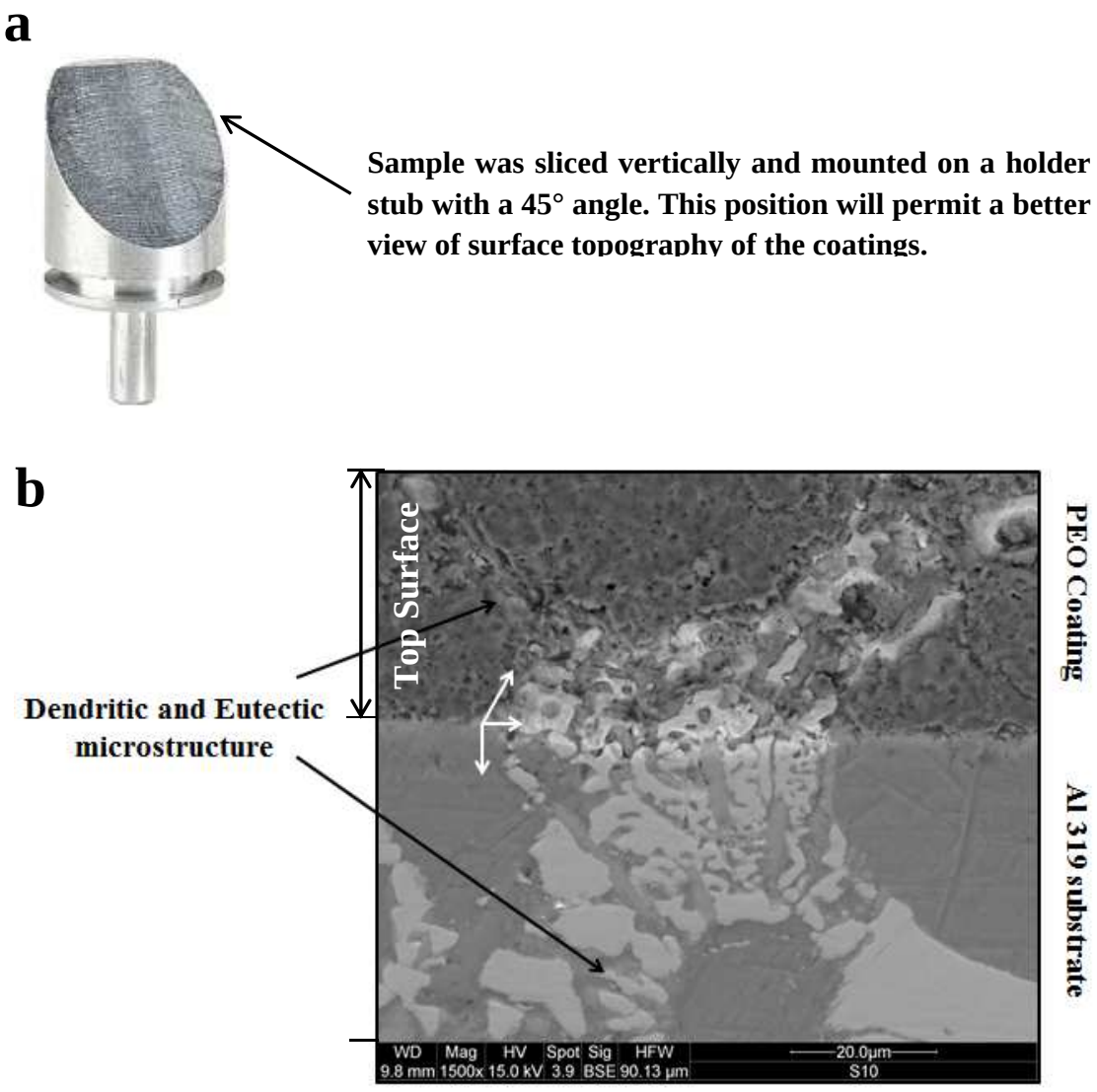

Figure 11. a) sample holder with a 45°angle: b) Aluminum Alloy 319 metal matrix with eutectic and dendritic microstructure and the PEO coating developed in a silicate based solution under 0.1 A/cm^2 current density over 3 minutes of treatment time. Note: The top part of the image is showing the top surface of the coating and the bottom part of the image is the surface of the substrate. Intersection of the two planes of coating surface and substrate is the coating thickness layer.

3.6 Porosity Measurement

PEO coatings are categorized with an amorphous phase with a distribution of fine scale pores. Porosity inside the cylinder blocks is desirable. The reason is that oil can be retained in these voids and reduce the friction between the piston rings and the cylinder wall especially during the Stop-start system or anytime that the engine is started after a long period of inactivity (Start-up). Gravity makes the oil to be drained down into the oil pan at the bottom of the cylinder block. Insufficient lubrication on the cylinder wall can cause more friction between the rubbing surfaces and could shorten the life of the engine. The function of the reservoirs on PEO treated surface is similar to the cross-hatched patterns that are honed on the cylinder walls as a surface finishing process. In typical engine blocks the surface of the cylinder liners are honed in a cross-hatched pattern to ensure optimal lubrication and good seal between the ring and cylinder walls. The oxide layer achieved after PEO treatment is a ceramic coating consists of high concentration of alumina. As for any ceramic materials, porosity is inevitable and can influence the performance and coating properties. The porosity network is formed as the result of oxygen entrapment in molten alumina in the vicinity of local electrical discharge [109]. Also the vigorous escape of hydrogen during the anodic oxidation stage of PEO process can lead to formation of pores on the oxide film. Curran and Clyne [109] used different techniques to measure and analyze the pore size and distribution of PEO coatings. They used Keronite treated 6082 aluminum alloy samples and measured the density of the coatings using the proportions of the phases present in the XRD analysis. In their analysis, they measured mass and physical dimensions of the samples and calculated bulk density of 3 ± 0.3 gr/cm^3. Phases of α-Al_2O_3 and γ-Al_2O_3 counted for

35% of the volume each and the rest was assumed as the amorphous phase of Al_2O_3 [75] .The estimated theoretical density of the PEO coatings is 3.63 ± 0.2 gr/cm^3. The wide range of error is due to the uncertainty in phase determination using XRD. The difference between the calculated bulk density and the estimated theoretical is 17% ± 12% which suggests the approximate total porosity of the coating. They also suggest that the porosity is largely surface-connected. Figure 12 illustrates a schematic representation of pore types. Cross-linked pores and blind pores are the main types of the pores in this study.

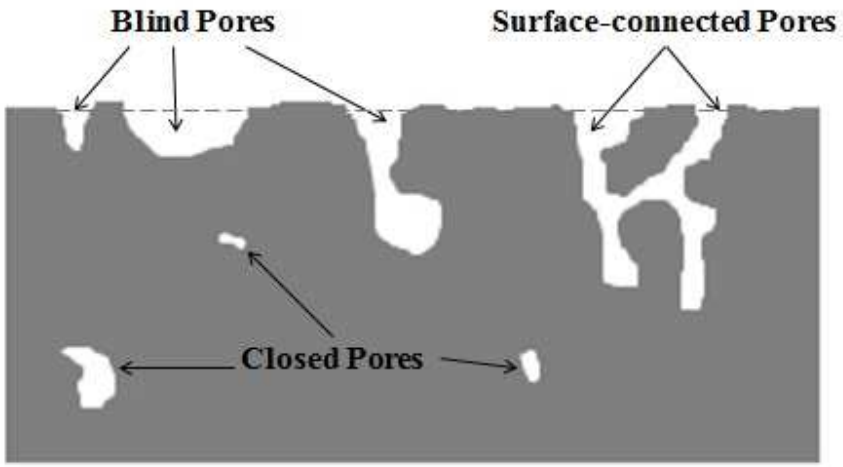

Figure 12. Schematic representation of pore types. Recreated curtesy of Herbert Giesche **[110].**

In the same study, Curran and Clyne [109] researched the pore size distribution of the coatings. They used mercury porosimetry to evaluate the pore size distribution along with pore geometry and also the total volume of the surface-connected porosity network. The apparatus consists of a chamber, a pressure transducer, an air pump and mercury tank. Once the sample is located in the device, the chamber is evacuated of air and then filled with mercury. Mercury is a non-wetting liquid which does not penetrate into pores on its own. Therefore an external pressure is applied into the chamber. The pressure can

go up to 100 Mpa. The required pressure has an inverse relation with the pore size [110] as shown in Equation 12.

$$\Delta P = \frac{2c\cos(h)}{r^{\circ}} \qquad \textbf{Equation 12}$$

where ΔP is the pressure variation, c is the surface tension of the mercury taken as 0.485 N/m, h is the contact angle which is usually assumed at 130 °and r° is the capillary radius. Surface tension of a liquid is the cohesive force of the surface of the liquid towards the external forces. Surface tension is measured by the amount of energy required to increase the surface area of the liquid by a unit of area. The behavior of a liquid towards a solid is determined by the amount of attraction force between a liquid and a solid (adhesive force) and the surface tension of the liquid (cohesive force). Mercury does not wet the sample due to the stronger cohesive forces within the drops of mercury than the adhesive forces between the drops and the sample. Once the pressure is applied, liquid mercury is sucked into the pores; its surface has a convex shape because the cohesive forces in liquid mercury tend to draw it into a drop. The penetration volume is then monitored by measurements of capillary radius and height. Pore size and pore volume is then obtained. It is concluded that the average pore size is of the order of 30 nm and most pores are in the range of 5nm and 1 μm. Value of 20% was consistently obtained as the overall volume of porosity [109]. Closed pores cannot be measured for obvious reasons since the mercury cannot enter these pores.

Porosity can affect other characteristics and properties of the coatings such as hardness, thermal conductivity and permeability. According to McColm [111] 20% of porosity can reduce the hardness from the fully dense value by up to 70%. Thermal conductivity of PEO coatings is considered one order of magnitude lower than the bulk alumina due to the presence of fine grain size, amorphous phase and pore network [109]. Also during the XRD analysis, the X-ray penetration into the coatings was much deeper than the bulk alumina. This is again due to porosity. Permeability is important since it can predict the behavior of the coating in contact with lubricants. In fact, impregnation of the surface by Teflon, dry lubricants and graphite has shown remarkable results on wear behavior of the coatings only due to good permeability of the PEO coating surface. Combination of oil retention and linked pores of the coatings make them desirable for cylinder wall application. The adverse effect would be in the presence of corrosive materials that can penetrate into the pores and cause corrosive attacks on the substrate. However the permeability advantage of the PEO coatings makes them a good candidate for sealants or anti-corrosive sealing materials. These can be applied on the treated surface as a post-treatment/finishing layer.

Before the tribo-tests in comparison studies, coatings were polished into a similar roughness values and then were tested for wear behavior. When the coatings were polished, the pores' geometry would change. We call these re-shaped openings, "*reservoirs*". In order to measure the porosity of the coatings, the SEM-obtained surface profiles of the coatings were digitized using a digital image analyzing software. Figure 13 shows the different stages of the surface digitizing process. Digital image analysis

methods have been widely used due to their versatility and simplicity for analysis and characterization of the coated substrates [112].

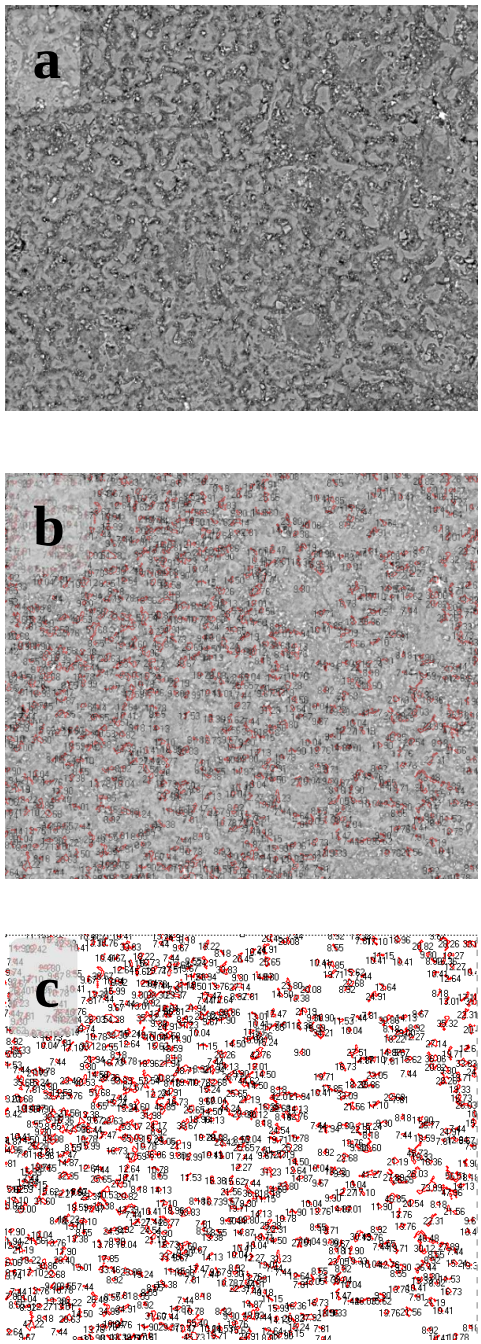

Figure 13. Different stages of digitizing process for porosity measuring process: a) SEM image of a polished sample with Ra = 0.8 μm, b) identified surface oil reservoirs, c) analyzed values of digitized surface. Porosity percentage for this sample is 17%.

Porosity is an average value; therefore different fields of views from the same sample are taken and analyzed by the software. Also several small domains (30 X 30 μm^2) from each image are chosen, analyzed and averaged. Pore size (ρ) varied from very small openings of (ρ< 0.5 μm), usually in round shapes to larger openings of (3 μm< ρ <5 μm). Figure 14 shows the percentage of porosity of the coatings versus average roughness values. Most PEO coatings in this study have the porosity range of 17 to 25%. Highest porosity was achieved for the samples that were treated in silicate based solution for 3 minutes. Also coatings treated under pulsed bipolar direct current condition tend to have higher porosity compared to coatings treated under pulsed unipolar current condition. Average porosity was calculated around 19.93% for unipolar coatings and 21.13% for bipolar coatings. It can be concluded that rougher surfaces seem to have more porosity.

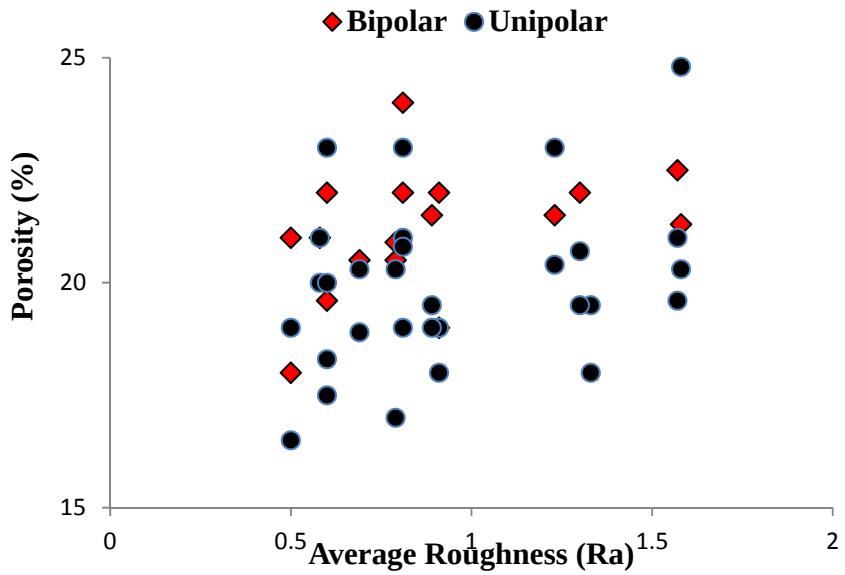

Figure 14. Average roughness versus porosity in percentage for bipolar and unipolar coatings.

3.7 Crystal Phase Structure and Elemental Analysis

In order to determine the atomic structure of the PEO coatings, a series of x-ray crystallography were conducted. The phase structures of the PEO coatings were studied using x-ray diffraction analysis. Figure 15 shows the results of XRD analysis for three type of coatings: aluminate, silicate and phosphate based coatings treated for 5 minutes. X-ray radiation of Cu Kα with a wavelength of 0.154 nm in the rage of 20° to 80° with the intervals of 0.02° was used. There was no distinct difference observed between the phase structure of PEO coatings produced in silicate, aluminate and phosphate solutions.

XRD analysis of the coatings indicates the formation of stable α- Al_2O_3 and meta-stable γ- Al_2O_3 along with mullite phase of $Al_2O_3.nSiO_2$. Larger peaks of aluminum are detected due to porous nature of the coating and the thin oxide film which cause the penetration of X-ray beam into the substrate. During the formation of coating, molten γ-Al_2O_3 is injected to the electrolyte through the discharging channels that are formed between the substrate and the surface of growing film once the sparks are produced. Meta-stable γ- Al_2O_3 is quenched rapidly because of temperature difference between the growing layer and the electrolyte solution and creates stable α- Al_2O_3. Formation of mullite phase is important specifically for coatings on engine cylinder bores since this ceramic phase has a dominating effect on thermal stability of the coating [113].

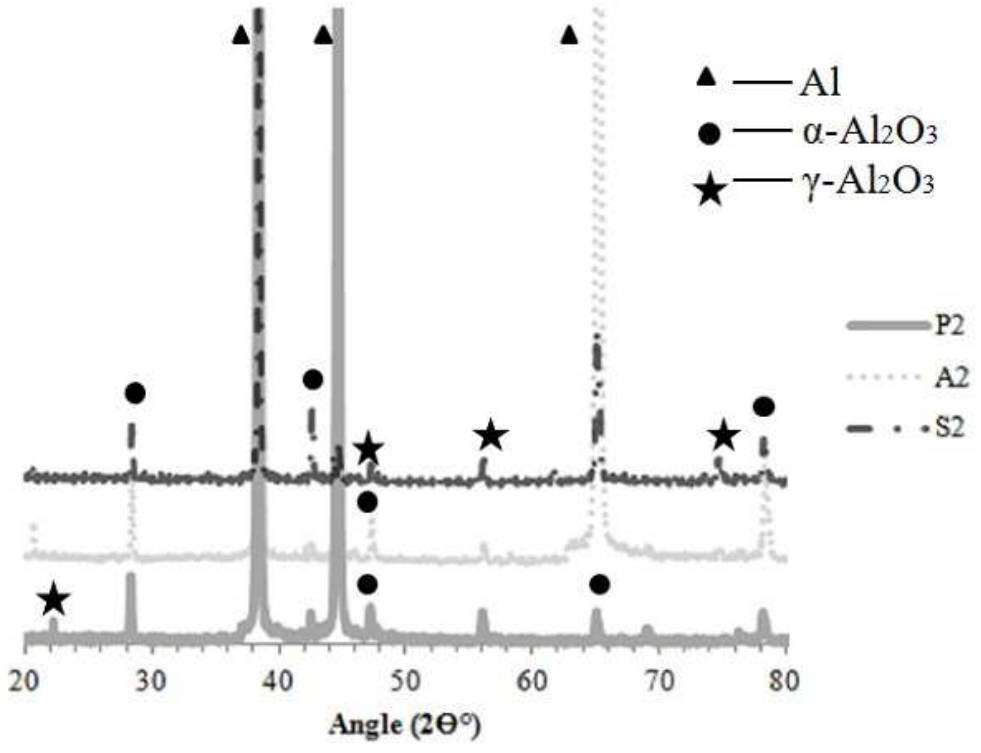

Figure 15. XRD patterns of PEO coatings prepared in different solutions: P (phosphate), Al (aluminate) and S (silicate).

Wang [114] found that in silicate electrolytes, SiO_3^{-2} transforms to SiO_2 on the growing layer or the interface between the substrate and the electrolyte. Once the γ-Al_2O_3 is ejected out of the discharge channel at a temperature close to 3000 °C, it will combine with SiO_2 and solidifies to the mullite phase. This phase due to its thermal stability does not quench as fast as α- Al_2O_3 and accumulates around the break-through of the discharge channel in a circular form. Once the coating is cooled the discharge channel can create a pore with the accumulated mullite and quenched α- Al_2O_3 all around it just like an opening of a volcano [113].

EDX (Energy Dispersive X-ray Spectroscopy) analysis is also a good indicator of the component and chemical characteristics of the coatings and is used in comparison study of the PEO coatings achieved in various solution compositions. The quantitative analysis of main elements of aluminum, silicon and oxygen can be a good indicator of chemical structure of the coating. Element count was gathered over 10 kilo electron volt (KeV) of electron beam energy. Figure 16 gathers the EDX elemental analysis of the coatings. Main parts of the coatings consist of aluminum oxide (alumina). Silicon particles are visible as black points under SEM. Silica and alumina also sintered together during the coating process and can be seen as more platelet shapes under the SEM.

3.8 Tribological Study

Tribology involves the study of friction, lubrication and wear therefore it is essential to research the influence of each of the components of tribological system in order to understand the behavior of the materials in contact.

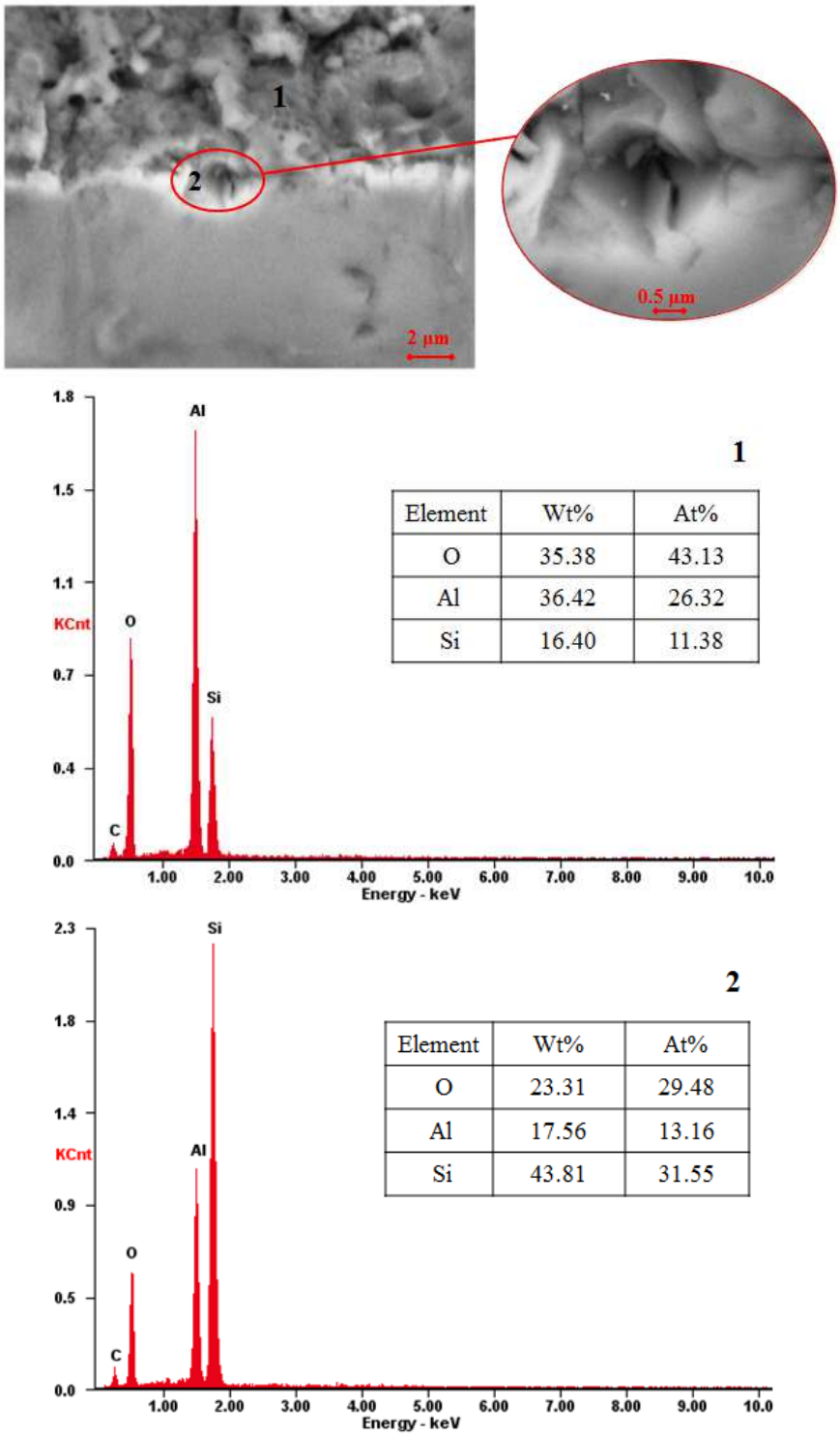

Figure 16. EDX spectra and analysis of a PEO coated sample collected at the pore (1) and on the surface (2). The coating is produced in a mixture of aluminate and silicate solution over 5 minutes of treatment time. Specimen was mounted on an angle of 45° under SEM.

3.8.1 Tribo-system

Two types of wear test machines were used in this study. Initial tests were done on a reciprocating pin-on–disk tribo tester. Reciprocating mode is used to mimic the movement of the pistons in the cylinders of an engine and since most of the sliding surfaces of an engine operate within a lubricated environment, engine oils were mostly present during the tests. Later a modification was made to the existing tribo tester machine by designing a piston ring holder. We called this modified set-up ring-on-disk tribo testing. Figure 17 illustrates both holders in relation to the substrate.

A tribo-system consists of two major parts: tribo pair and an auxiliary sub system. Tribo pair was the coated PEO samples of Al319 alloy as the cylinder wall and counter surface of steel alloy E52100 testing balls for the case of ball-on-disk tribo testing. In the ring-on-disk condition, moly coated piston rings and steel coated steel rings were used as the counter surface. The auxiliary sub system is the lubrication sub system and the testing conditions that are responsible for controlling and monitoring the system.

Tribo pair's behavior is influenced by various elements such as materials, contact geometry, loading, motion type and speed, and environmental factors. Environmental factors such as humidity (average 45%), testing room temperature, air pressure and vibration are considered constant for all the tests. In principle, all the tribo test parameters and conditions of an out-side engine study should correspond to the practical conditions of an engine however they were limitations during our tests such as temperature variations. The results will be presented and discussed in Chapter 4.

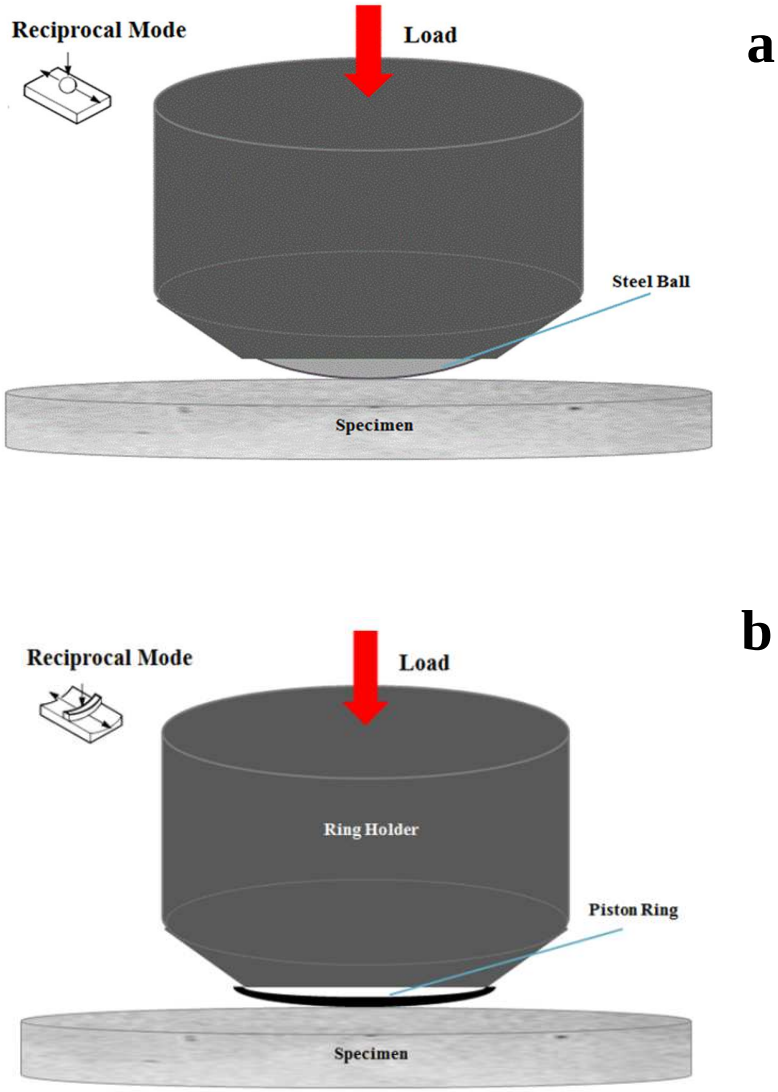

Figure 17. Reciprocating tribo pair: a) ball-on-disk tribo-test, b) ring-on-disk tribo-test.

CHAPTER 4. RESULTS AND DISCUSSIONS

This chapter gathers all the findings of this research based on effects of various variables, parameters and conditions on performance of the coatings and their influence on wear behavior of the coated surface and also the counter surface. Figure 18 illustrates the research path that was followed along with a summary of studied parameters and variables during this research. As shown the effect of current mode, current density, solution type and acidity on morphological behavior of the coatings are studied. Surface roughness, porosity and coating thickness of different samples were compared and analyzed. In terms of tribological behavior, main subsystems were investigated: coating surface behavior and counter surface behavior. Indicators of the wear behavior: coefficient of friction and wear rate are presented for each variable.

4.1 Effect of Electrical Parameter on Morphological Structure and Tribological Behavior of PEO

Properties of the PEO coatings and their resistant to wear are related to electrical parameters used during the treatment time. These parameters are: current polarity, current density, current frequency, anodic and cathodic voltage, and duty cycles. Of the mentioned parameters, current polarity and current density are studied in this research in details. This section contains a series of coatings that are produced in three major types of electrolytes: aluminate, silicate and phosphate. The experiment matrix along with finishing voltage and hardness values of each sample are gathered in Table 1.

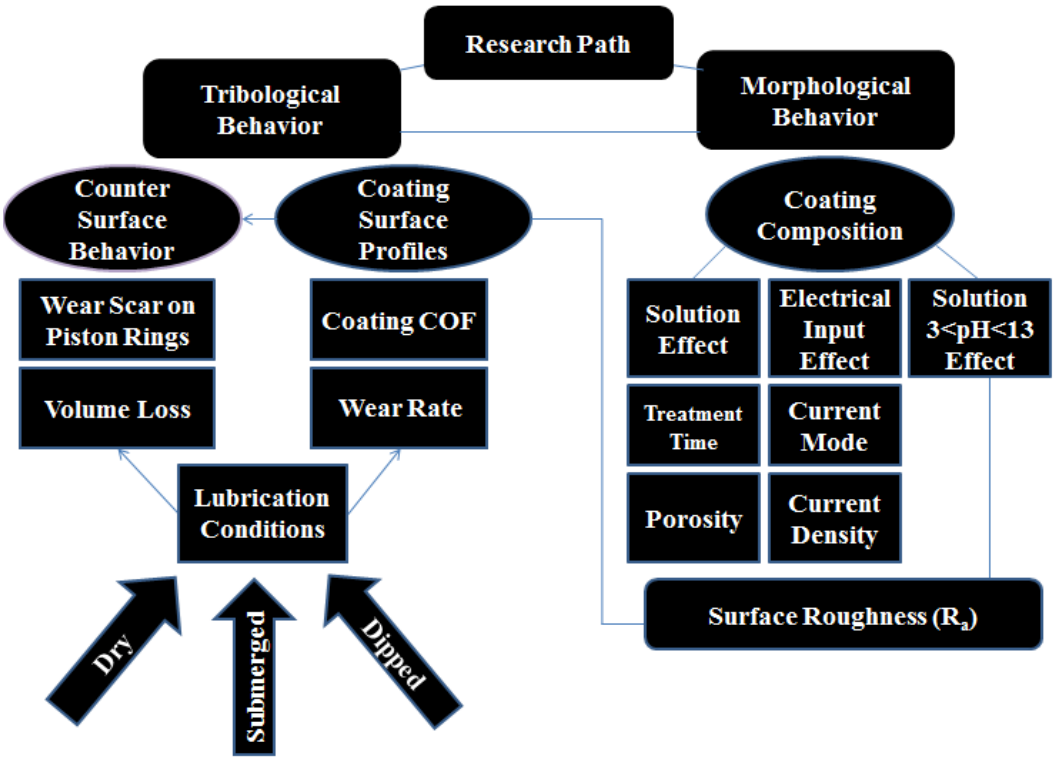

Figure 18. Research path taken for this study with all the elements under investigation.

Table 1. Experiment Matrix for Aluminate, Silicate and Phosphate based solutions.

Sample	Polarity	Solution Composition	Output Voltage (v)	Average Vickers Hardness ($HV_{0.2}$)
A1	Unipolar	8gr/lit Al_2O_3 + Fe_2O_3 + Na_2O	387	345
A2	Bipolar	8gr/lit Al_2O_3 + Fe_2O_3 + Na_2O	401	350
S1	Unipolar	8gr/lit Na_2SiO_4	398	325
S2	Bipolar	8gr/lit Na_2SiO_4	411	370
H1	Unipolar	8gr/lit Na_2HPO_4	320	245
H2	Bipolar	8gr/lit Na_2HPO_4	348	270

4.1.1. Current Polarity

Current polarity can affect the coating growth and morphology distribution. The coatings under investigation in this research are produced using direct current at moderately low voltages (< 500 V) with unipolar and bipolar pulsed settings. Polarity can be set through a power supply enhanced with a power modulator controlled by an external step waveform generator. Polarity of the current in a unipolar pulsed DC is either positive or negative. A bipolar current is one with cycles of positive and negative current. These cycles will have different types of discharge effects on the coating formation phases. Dynamic of the cycle loading dictates the discharge levels of each cycle and has a significant influence on homogeneity of the coatings [115].

In unipolar operation mode, the pulsed DC voltage is applied to the substrate which acts as a cathode and the walls of the electrolyte bath serve as the anode (as seen in Figure 4). In bipolar operation mode, there are two cycles of positive and negative "*pulse*". During the positive pulse, the substrate is the anode and the electrolyte bath container is the cathode, these positions are changed during the negative pulse.

There are three sets of discharge time: T^{+}_{on}, T^{-}_{on} and T_{off}. During T^{+}_{on} and T^{-}_{on}, a short high voltage pulsed wavelength creates additional discharge on the substrate, this causes dielectric breakdown of the electric field around the substrate and creates discharge channels from which molten aluminum is ejected onto the coating surface, oxidized and solidified rapidly due to the extreme temperature difference between the plasma blanket (also called envelope) and the electrolyte. T_{off} represents the pausing time or absence of positive or negative pulse. During T_{off} localized molten oxide cools down and the cycle continues by initiation of another pulse. Duration time of the positive and

negative pluses can be programmed through the waveform generator. Through a series of trial and error, cycle loading of 80% was chosen for the bipolar direct current mode at operating frequency of 2 kHz. Shorter T_{on} time in general is desirable since this would create highly ionized plasmas. During the positive pulse, the surface ratio (å) of the cathode to anode is increased, therefore higher discharge current and also plasma power densities are present. Surface ratio (å) is defined by Equation 13:

$$å = \frac{A_{Cathode}}{A_{Anode}} \qquad \textbf{Equation 13}$$

where $A_{Cathode}$ and A_{Anode} are surface areas of cathode and anode respectively.

During T_{off}, the electrolyte still has remaining charge from the previous pulse and once the negative pulse begins, a higher density of charge is initiated. Higher density means more sparks, faster breakage of dielectric discharge, more exposure of the surface to the discharge and eventually illuminating the whole surface of the specimen once the discharge current saturation point is reached.

Coating Morphology

Morphological characteristic of the coated samples can have a great impact on the way the coated surface responds to friction. Since plasma temperature spikes change with different current mode, the achieved coatings are different in quality. Bipolar current mode results in a balance in average plasma temperature of the process and can create a

more uniform distribution of the porosity on the surface and improve the quality of the coating in terms of surface morphology.

In general, coatings produced under bipolar pulsed direct current (BPDC) mode exhibits a significantly more porous morphology with higher surface roughness values (Ra) mostly in longer treatment times. Coatings achieved under both conditions (UPDC and BPDC) have large network of micro-cracks. Non-homogenous deposition on the surface and inclusions were also observed on UPDC coatings. Coatings achieved using bipolar pulsed direct current mode (BPDC) are mostly more dense with smaller pore sizes and less porosity in the inner layer. More randomized agglomerates of alumina (defects) deposited on the surface can be seen in unipolar coatings. Quality of bipolar and unipolar coating can be controlled by setting the on and off or positive to negative pulse current ratio of the pulse in an optimal range. An optimal range can guarantee elimination of sudden high impulses of high discharge with very high temperature differences. Occurrence of high temperature surges during the process can create fast quenching and generally creates a non-uniform surface with randomized agglomerations of alumina (α and γ phases) on the substrate. According to Hussein et al [103] unipolar condition is capable of creating a dense coating morphology if only positive to negative ratio of pulse current is determined properly. Appropriate controlling conditions results in elimination of high temperature spikes and strong troublesome plasma discharges. Solution composition has a significant effect on coatings' morphology. Three types of solutions: sodium aluminate, sodium silicate and sodium phosphate (8 gr/lit) are used for a comparison study on the effect of solution and current polarity on morphology and coefficient of friction of the coatings. Figure 19 to 24 show the coatings produced by

UPDC and BPDC for 3 minutes of treatment time. SEM (FEI Quanta 200 FEG) operating at 15 kV, with an energy-dispersive x-ray spectroscopy (EDS) analyzer was used to observe and analyze the specimen. Observations were made under low vacuum conditions with assistance of back scattering electron imaging. Degaussing was applied to avoid and eliminate surface charging. Each specimen was sliced vertically after coating, mounted on the uncoated exposed side and polished. Samples were then fixed on a 45-degree tilted sample holder. All figures (19 to 24) represented in this section show two surface plains of the specimen. Upper part of each figure is the PEO coating surface and lower part is the polished substrate.

As seen, coatings are different in texture, porosity size and their network of micro cracks. One reason can be the dissimilar patterns of micro-sparks and discharge formation during the treatment. For instance, more intense sparks can create a rougher surface or multiple numbers of sparks can create more porosity on the surface. As the oxide layer thickens during the process, surface gets rougher and agglomerates become bigger in size and coarser in texture [116], [117]. Ghasemi et al [118] described that in a thicker layer of the coating, a higher current is needed to pass through the coating. Therefore it is easier for the current to pass through weaker parts of the coating. If the coating is developing uniformly with less weak points, then the number of the discharges/sparks would decrease. If the layer is getting thick the number of the discharge remain the same but its intensity grows. In another word, coating layer acts like a dielectric material. If the coating is uniform without any surface defects the process would be terminated [109]. Pores provide a possible path for the discharge to penetrate into the coating. Creation of discharge around the opening and inside the tubular path of a

pore creates formation of the oxide layer. These paths are usually called *discharge channels*. These channels are continuously formed and filled throughout the process [117]. The process can be seen as a recovery process to heal the defect and cover it with another layer of coating which might have further defects. So long these defects appear on the surface, electrolyte has a way to penetrate into the coating, discharge/sparks are created and a new layer is formed. Coating grows both inward and outward on top of the previous layer. Inward growth fills in the discharge channel and outward growth creates more pores and tubular channels.

Coating roughness and thickness of the bipolar and unipolar coatings vary as well as their surface structure and distribution of pores and micro-cracks on the surface. Of all three solutions, silicon based solution created the roughest surface with larger pores as shown in Figure 20 and 23. The reason is the effect of SiO_3^{2-} anions in comparison to the aluminate and phosphate anions. Meta-silicate (SiO_3^{2-}) anions also promote higher growth rate of the PEO coatings [89]. This can be again explained by the ease of penetration of the electrolyte into the discharge channels through the larger pores on the surface of the coating. However as described before these holes and channels will be sealed during the process therefore cross section of a silicate coating shows not much porosity or defects.

Coatings can be compared based on their growth rate as well. Coating growth rate is the achieved thickness of the coating over the treatment time of the PEO process as shown in Equation 14.

$$\tau = \frac{D}{T}$$ **Equation 14**

where τ is the coating growth rate in μm per minute, D is the thickness of the coating in μm and T is the duration of treatment time in minutes.

Roughness and growth rate of the coatings are compared in Figure 25. Silicate coatings have 1.25 μm/min of coating growth in unipolar condition. Coating growth decreases to 1.03 μm/min for bipolar condition. Cross sectional observation of silicate coatings shows a dense, uniform and compact layer of coating. Aluminate coatings have the lowest growth rate compared to silicate and phosphate. They show finer porosity on the surface of unipolar coatings. Phosphate coatings have very fine porous structure both on the surface and cross section along with defects. This is due to the less possibility for the electrolyte to penetrate into the discharge channel through small pores. Therefore coating growth is slower.

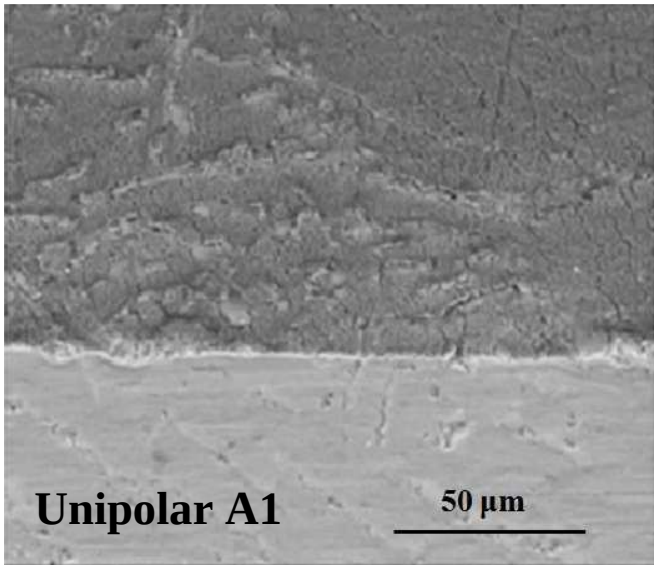

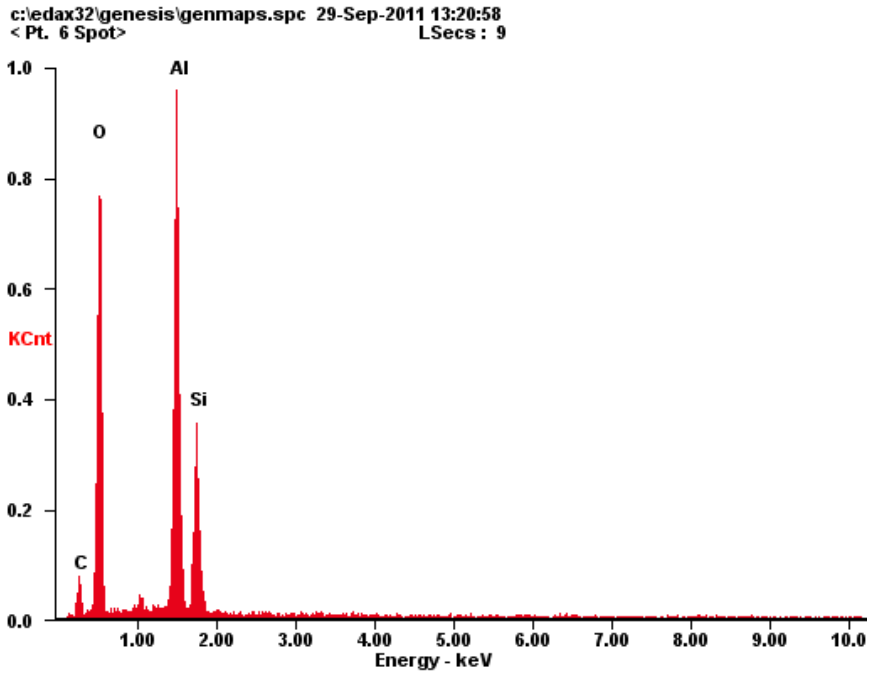

Elements	Wt%	At%
Al	28.26	18.89
O	43.06	48.54
Si	12.22	7.85

Figure 19. Morphological observation of Coating produced under UPDC condition in 8 gr/lit of sodium aluminate (A1) during 3 minute treatment time along with EDX analysis results on the coating with corresponding elemental contributors. Specimen was mounted on an angle of 45° under SEM.

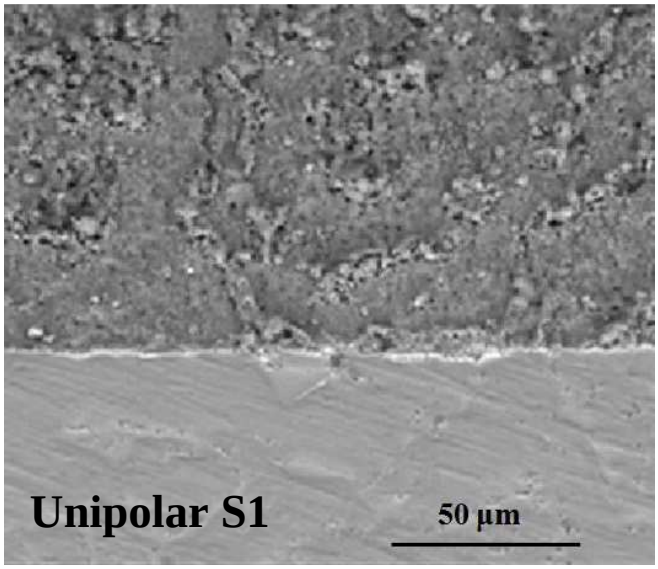

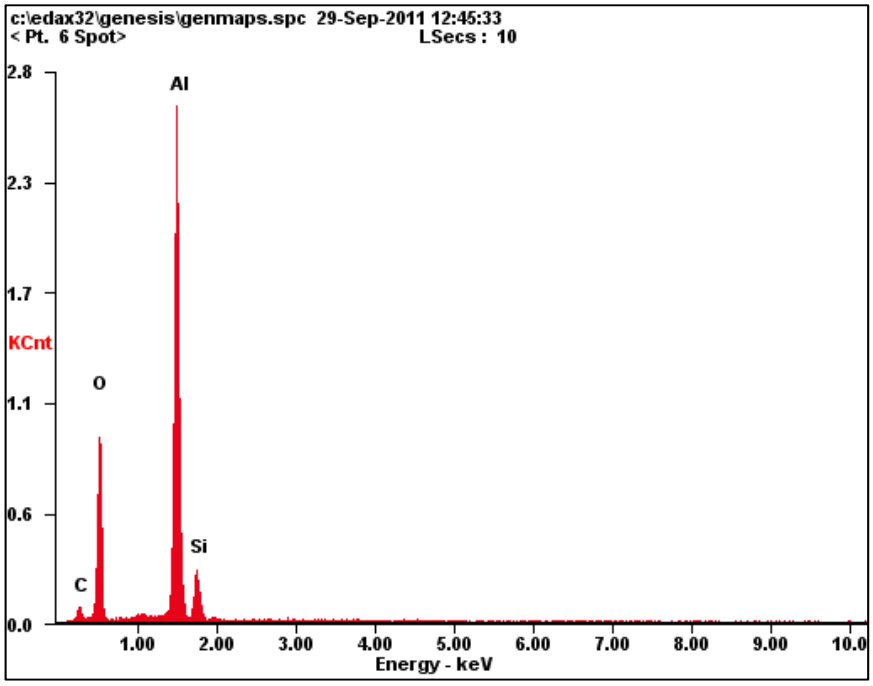

Element	Wt%	At%
O	39.72	44.84
Al	37.65	25.21
Si	4.73	03.04

Figure 20. Morphological observation of Coating produced under UPDC condition in 8 gr/lit of sodium silicate (S1) during 3 minute treatment time along with EDX analysis results on the coating with corresponding elemental contributors. Specimen was mounted on an angle of 45° under SEM.

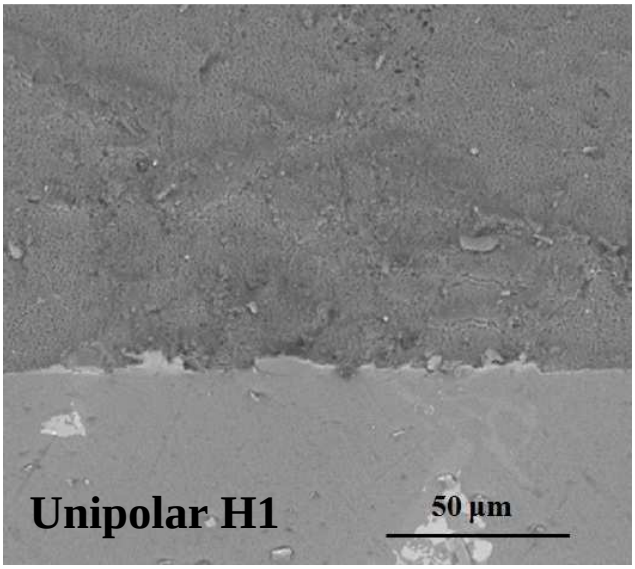

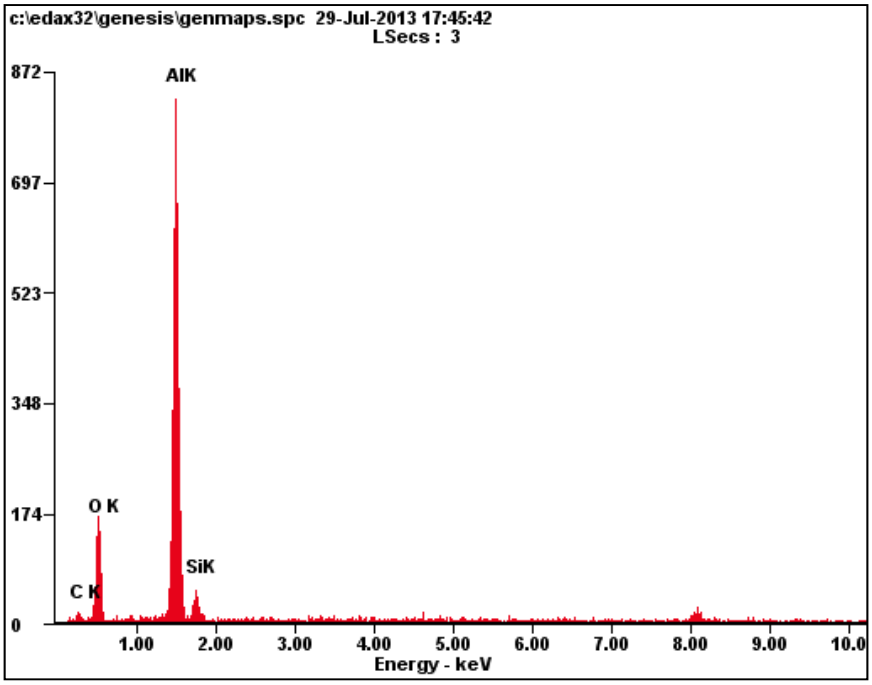

Elements	Wt%	At%
Al	35.28	23.72
O	40.40	48.50
Si	7.23	4.67

Figure 21. Morphological observation of Coating produced under UPDC condition in 8 gr/lit of sodium phosphate (H1) during 3 minute treatment time along with EDX analysis results on the coating with corresponding elemental contributors. Specimen was mounted on an angle of 45° under SEM.

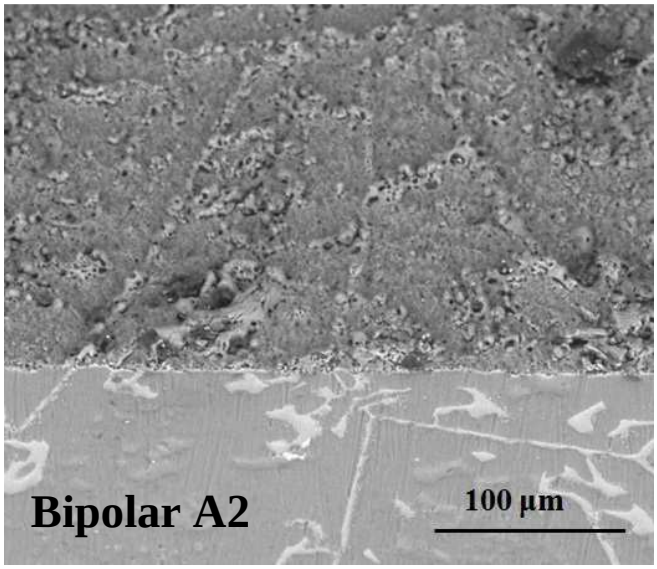

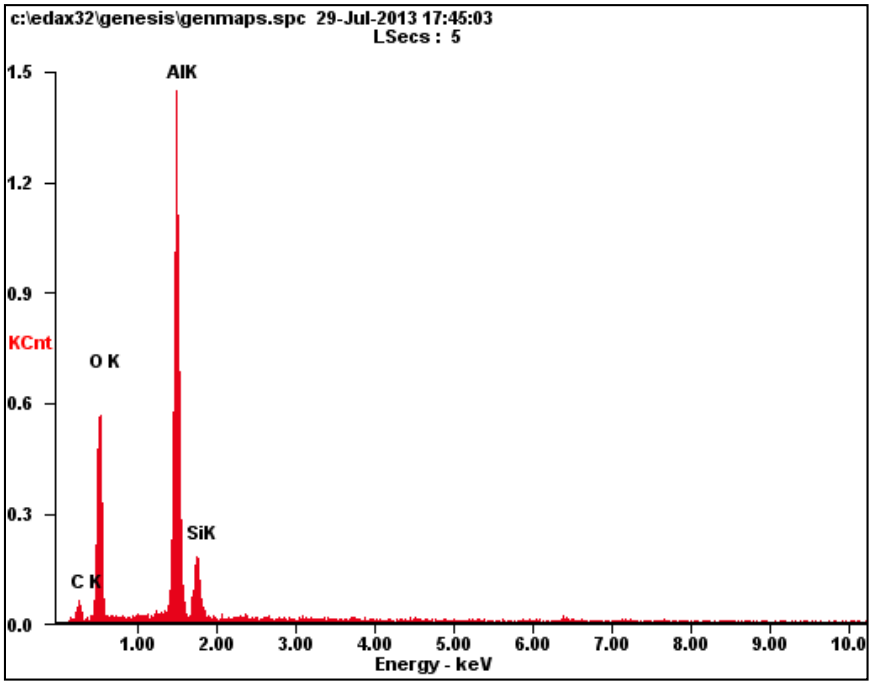

Elements	Wt%	At%
Al	52.49	38.63
O	29.36	36.44
Si	5.34	3.78

Figure 22. Morphological observation of Coating produced under BPDC condition in 8 gr/lit of sodium aluminate (A2) during 3 minute treatment time along with EDX analysis results on the coating with corresponding elemental contributors. Specimen was mounted on an angle of 45° under SEM.

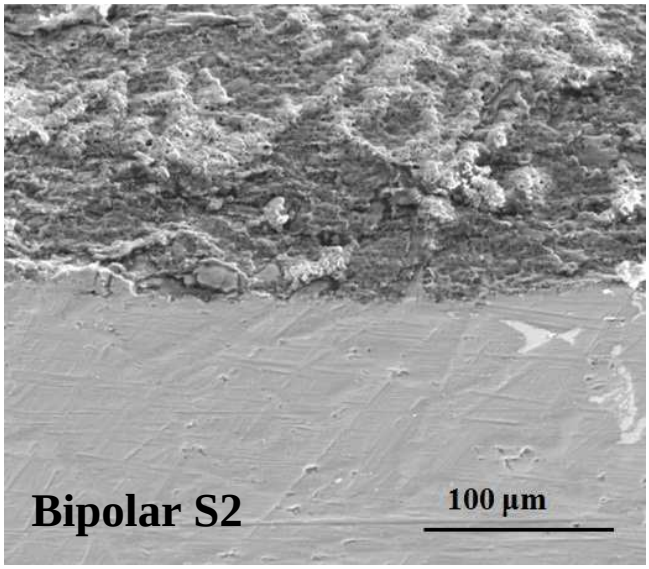

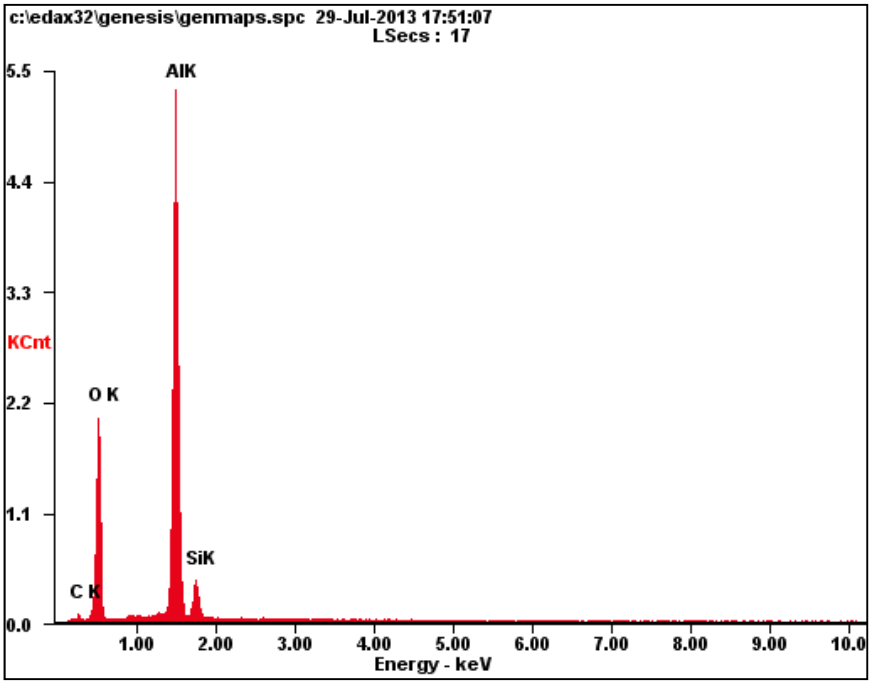

Elements	Wt%	At%
Al	35.28	23.72
O	40.40	48.50
Si	7.23	4.67

Figure 23. Morphological observation of Coating produced under BPDC condition in 8 gr/lit of sodium silicate (S2) during 3 minute treatment time along with EDX analysis results on the coating with corresponding elemental contributors. Specimen was mounted on an angle of 45° under SEM.

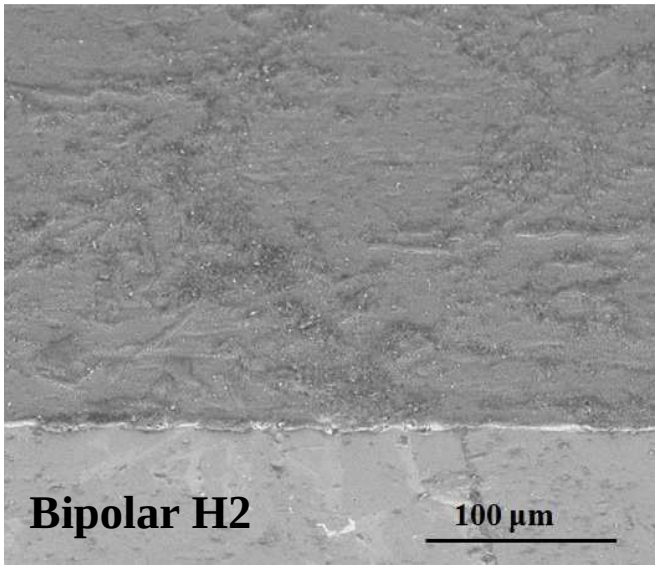

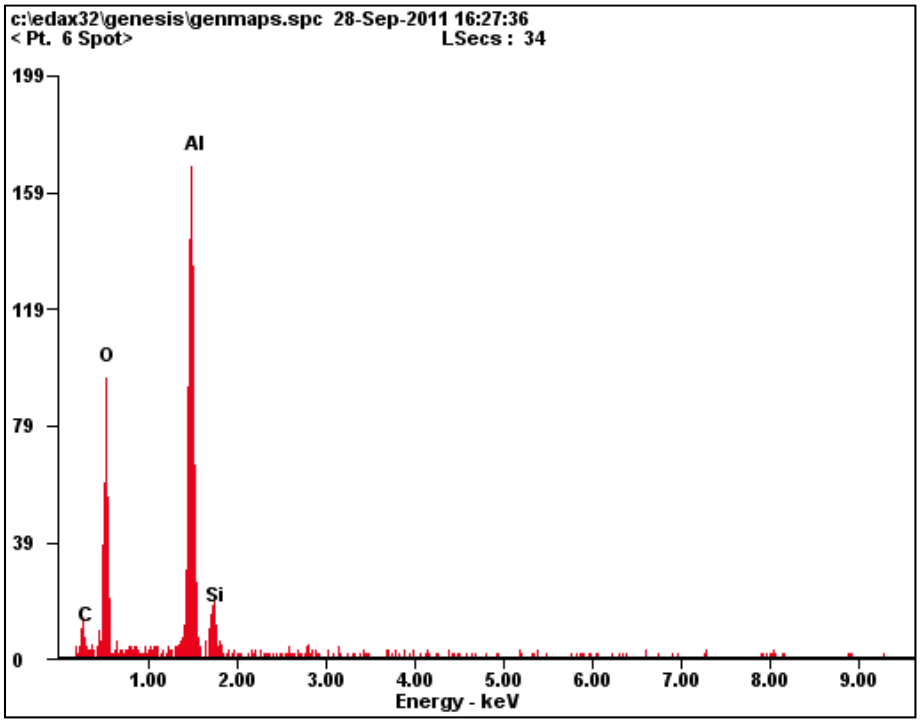

Elements	Wt%	At%
Al	37.65	25.21
O	39.72	44.84
Si	4.73	3.04

Figure 24. Morphological observation of Coating produced under BPDC condition in 8 gr/lit of sodium phosphate (H2) during 3 minute treatment time along with EDX analysis results on the coating with corresponding elemental contributors. Specimen was mounted on an angle of 45° under SEM.

Another way to explain the fact that silicate coating grows faster than aluminate and phosphate is by looking at the coatings structure. Coatings can be divided into major layers: an inner barrier layer and an outer porous layer. Both of these layers interact with the electrolyte during the process. As mentioned, electrolyte composition and anions type in the solution have a great impact on the formation of coatings [114], [119]. Barrier layer forms when the metal ions of the substrate (Al^{+3}) and the anions present in the electrolyte react. The reaction is an anodic dissolution as shown in Figure 4. Anodic dissolution provides metal ions to react with the anions such as SiO_3^{2-} to form the oxide layer. According to Ghasemi et al [118] the rate of anodic dissolution and coating formation are related reversely to the coating growth and thickness. Snizhko et al [71] proved that coating growth is initiated once the rate of coating formation is faster than the rate of anodic dissolution of the substrate. Also since the SiO_3^{2-} demonstrates a more stable passive layer on the metal surface compared to aluminate or HPO_4^{-}, it can prevent further anodic dissolution which means faster growth rate and thicker coatings.

Another indicator is the final output voltage of the PEO process. Generally thicker coatings show a larger value for the finishing voltage. According to the output voltage values in Table 1, during the bipolar process, there is up to 8% of increase in the final voltage of the process compared to unipolar process.

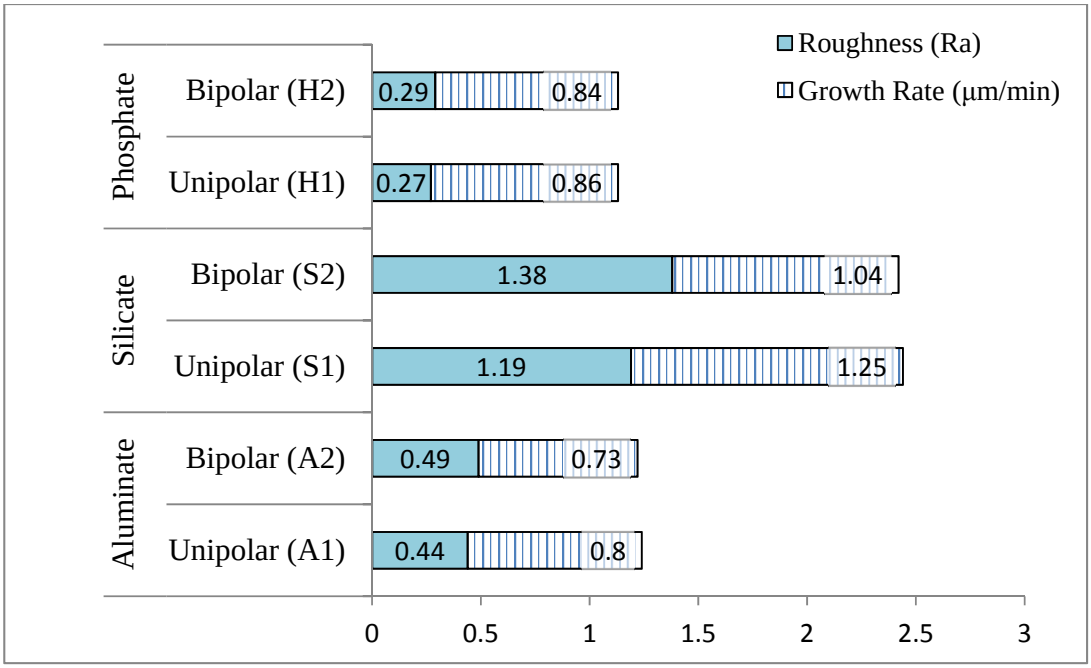

Figure 25. Roughness (± 0.01 μm) and growth rate values for coated specimens under UBDC and BPDC for 8 gr/lit of sodium aluminate, sodium silicate and sodium phosphate solutions measured after 3 minutes of treatment time.

Tribological Behavior

At the initiation stage of this research, tribo-tests were conducted in both modes of reciprocal and rotational and it was determined that the reciprocating mode is a better mimic to the actual engine block and piston movement. Figure 26, shows the COF values of PEO coatings achieved in different solutions under BPDC and UPDC conditions. As shown, unipolar coatings have generally a higher value of coefficient of friction compared to bipolar.

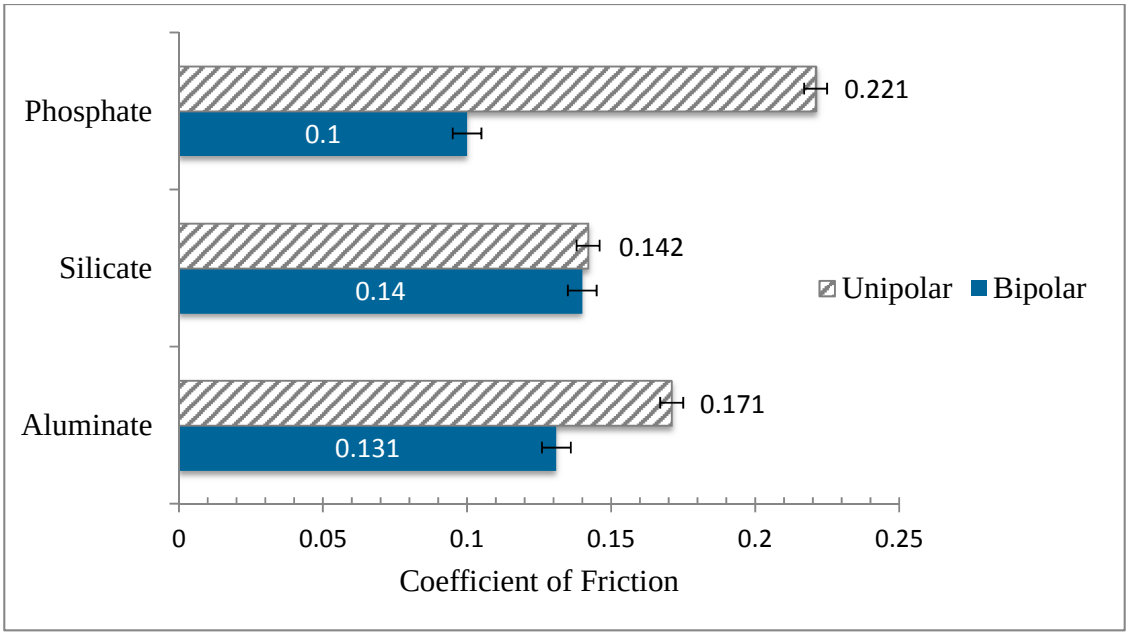

Figure 26. Effect of current polarity on COF for three samples coated in 8 gr/lit solutions of phosphate, silicate and aluminate over 5 minutes of treatment and tested under 2N load over 1 km of sliding distance.

Phosphate coatings for instance showed a 45% difference between the coefficient of friction values of unipolar and bipolar coatings. In fact, unipolar coatings that are produced in phosphate electrolyte showed a very smooth surface after treatment with very little porosity (refer to Figure 21). Under the same wear test condition, unipolar phosphate coatings have less adhesion to the substrate and were peeled off midway through the test. Figure 27 shows the result of weak adhesion of PEO coating to the substrate of a phosphate treated coating. This is the result of rotational tribo-test. As shown, parts of the coatings were flaked off. Weak adhesion properties cause detachment of particles. These particles can act as abrasions on the surface and creates micro-cuts on the coating which eventually cause further detachment and results in coating failure. Also on the wear track marks on the coating surface a dark almost spherical particle can be observed. This is a protruded silicon particle that is revealed due to wear.

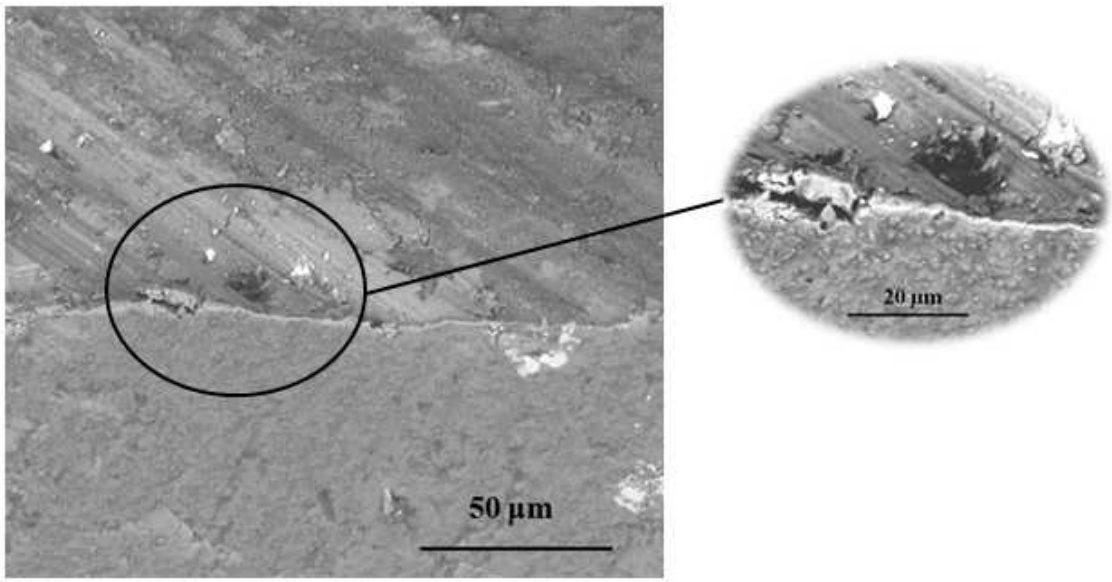

Figure 27. Weak adhesion of a PEO treated sample in phosphate solution under UPDC condition which leads to flaking and peeling off the coating. The sample is cut and mantled under SEM at 45 degree of angle. The top part of the image is the coating surface with apparent wear track marks and the lower part of the image is the substrate surface.

Another fact is that bipolar coatings show better corrosion resistance than unipolar coatings [76] and this can be due to the coating density and permeability of the coating. However based on the electrolyte composition unipolar coatings and bipolar coatings could behave the same. For instance using silicate solution will usually eliminate the effect of current polarity on coatings tribological behavior. The finishing output voltage of the bipolar coatings is up to 8% higher than the unipolar coatings. Hardness values of the bipolar coatings are up to 12% more than unipolar coatings. Industrial application of PEO coatings would be feasible if coating synthesis can compete with the existing technologies on mistake-proofed application, ease of pre and post treatment, eco-friendliness, optimal energy consumption and process treatment time. Coating growth rate is important to automotive industry since production time is of essence for mass

production. Based on all the beneficial factors mentioned in this section, unipolar condition can be desirable if other variables such as solution type and current density are chosen carefully. Coatings under study in this research are achieved under UPDC condition unless mentioned otherwise.

4.1.2. Current Density

Another electrical parameter that affects the coating properties is current density. Current density (J) is defined as electric current per unit area of cross section and is expressed in ampere per centimeter cubic. Coating thickness increases in PEO treatments with higher current densities. Figure 28 shows the effect of current density on coating growth rate for three different coatings of aluminate, silicate and phosphate. Aluminate coatings respond more rapidly to the changes of the current density compared to silicate or phosphate. Average coating growth for aluminate coatings is 0.95 μm/min. Phosphate coating growth rate is almost independent of changes in current density. The average coating growth rate for phosphate coatings is around 0.88 μm/min. Silicate coatings have the highest coating growth rate of 1.32 μm/min and grow with a rate of 30% per each increment of 0.2-0.3 A/cm^2 increase in current density.

Coatings produced with higher current densities are thicker and mostly rougher. Figure 29 shows a silicate coated sample under J= 0.1, 0.15 and 0.2 μm/min current densities. As shown higher current density have an influence on coating structure. For instance, coatings produced under 0.1 A/cm^2 current density; has a uniform structure with more discharge channels and smaller sized pores. On the other side of the extreme, coatings formed under 0.2 A/cm^2 current density, have more bulky plate-like agglomerates with fewer numbers of discharge channel. Parts of the coating have a

densely packed structure mostly around the discharge channel. Also micro cracks on these coatings are continuous and have longer arms with fewer nodes.

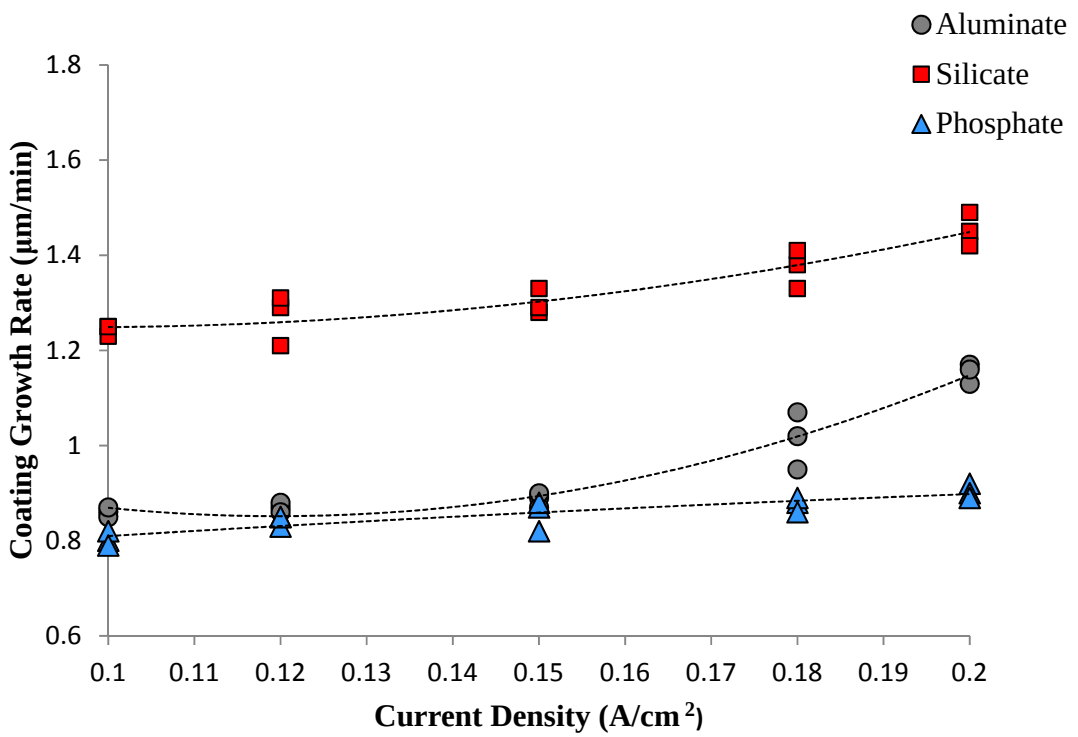

Figure 28. Effect of current density on coating growth of aluminate, silicate and phosphate coatings produced under UPDC mode over 3, 5 and 8 minutes of treatment time.

Khan et al. [106] studied the effect of current density on residual stresses during the plasma micro discharge phase. According to their study increased current density results in a decrease in residual stresses in alumina coatings. The reason is that higher current densities create a larger plasma micro-discharge field. In this field, a network of micro cracks is formed on the surface of the coatings which contributes to stress relaxation. Also Larger micro-discharge field means larger temperature spikes. Larger temperature spikes creates a higher range of temperature difference between the surface and the surrounding which create thermal annealing on the coatings.

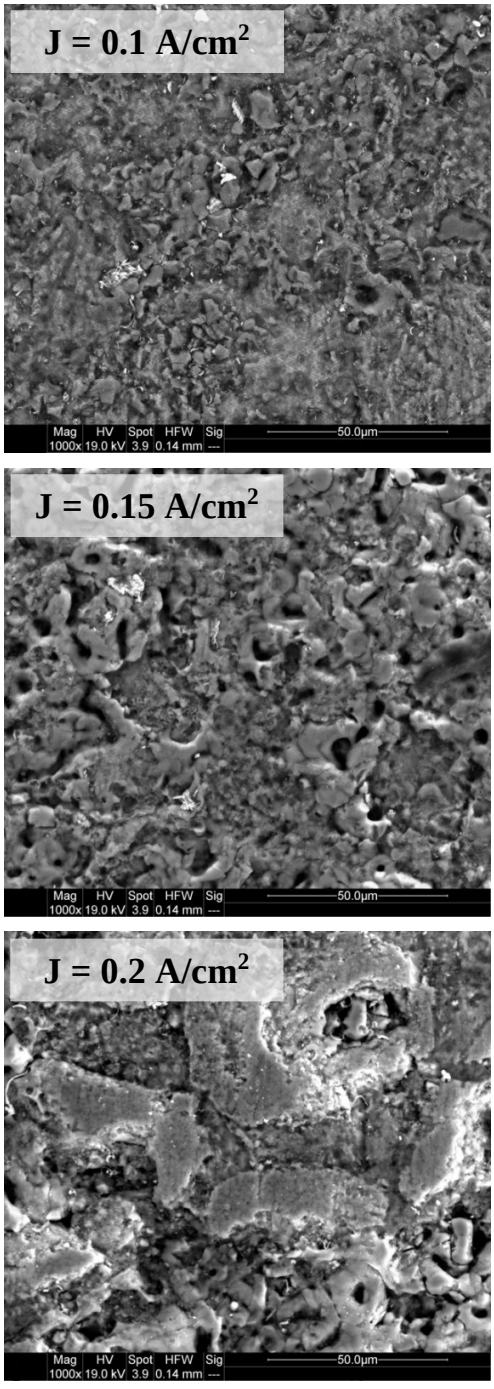

Figure 29. SEM micrographs of the top surface of the PEO coating treated in silicate solution under UPDC condition at 0.1, 0.15 and 0.2 A/cm^2 current densities over 5 minutes of treatment time.

Coating Morphology

Higher current densities, usually lead to faster growth rate and thicker coatings however this does not indicate a better performance of the coating. Higher current densities could create rougher surface with more microstructural defects such as cracks and accumulation of deposited material on the surface. This will create a non-homogenous surface with high roughness values ($Ra > 1.2\ \mu m$) and porosities above 20% (see Figure 29).

Coating Defects

Coating structure in general has a direct effect on the coating behavior against wear. Defects such as non-homogenous coating structure usually create positively skewed surface profiles. This means more distribution of peaks and sharp points which translates into more wear on the counter surface. A treated sample with non-homogenous morphology in silicate solution with 8 gr/lit concentrations is shown in Figure 30 treated over 5 minutes at 1.5 A/cm^2 current density. As seen there is a variety of different sizes of alumina deposits on the surface from large plate like deposits to smaller droplet.

Also excessive porosity ($\rho > 35\%$) can be problematic since it can affect the surface hardness of the coating along with its tolerance level against contact pressure. Figure 31 shows a sample with excessive porosity which was produced in a phosphate solution with concentration of 8 gr/lit over 5 minutes of treatment time at 1.2 A/cm^2 current density.

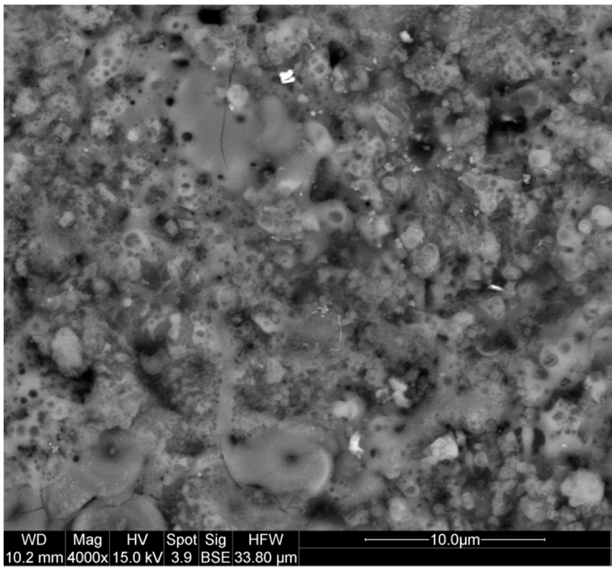

Figure 30. Top view of non-homogeneity: Surface defect on a PEO coated sample in sodium silicate solution (8 gr/lit) over 5 minutes of treatment time at 1.5 A/cm^2 current density and BPDC mode.

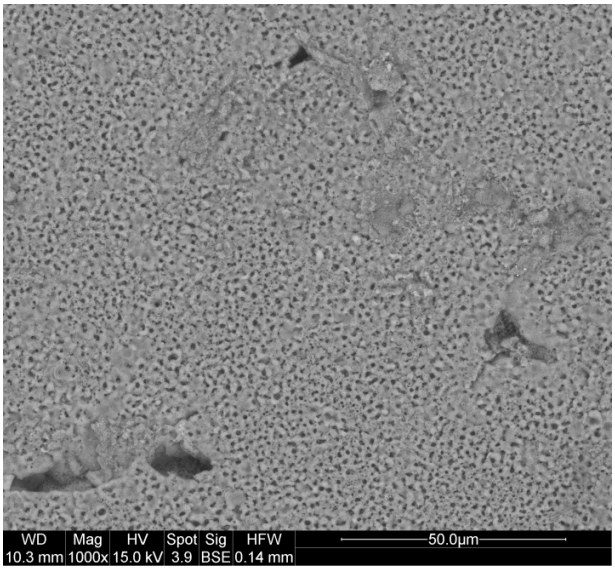

Figure 31. Top view of excessive porosity observed on a sample treated in phosphate solution (8gr/lit) over 5 minutes of treatment time at 1.2 A/cm^2 current density and BPDC mode.

Micro cracks can propagate into larger cracks across the coating surface and also transmits into deeper valleys into the coating thickness. Propagation of cracks can

drastically transform the structure and the dynamic of the tribo-system. Propagation of micro cracks on the PEO coating produced in aluminate (6 gr/lit) and silicate (2gr/lit) solution over 5 minute of treatment time can be observed in Figure 32. Also after the treatment, loosely deposited particles can be seen on some coatings. Loose deposits usually have a very weak bond to the surface and can be detached with minimum contact force. This type of flaw is usually observed when salts of aluminate are being used as the passivation agent in the solution at higher current densities. Other causes of these loose deposits can be water impurities or/and mineral residues on the solution tank walls. The troubleshooting is immediate since the particles can be removed by either brushing the samples, water flushing or lightly sanding the surface.

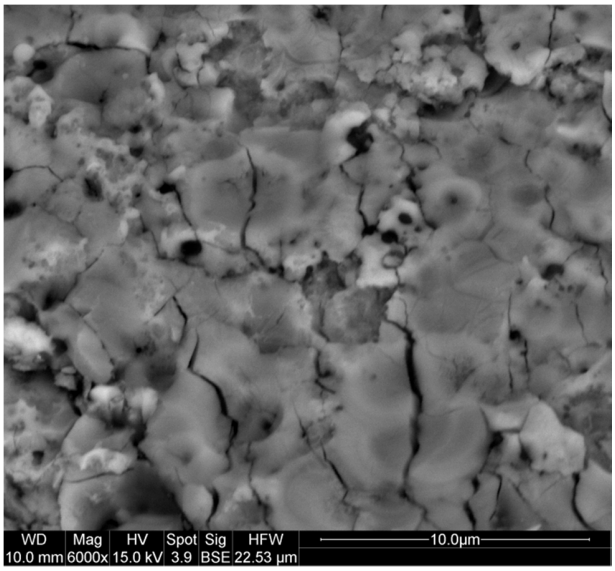

Figure 32. Top view of micro-cracks propagation observed on aluminate (6 gr/lit) and silicate (2 gr/lit) solution treated over 5 minutes.

All other mentioned defects: non-homogeneity, excessive porosity and propagation of micro cracks are not desirable and have to be prevented during the coating synthesis since they can jeopardize the coating performance. Table 2 gathers a simple root-cause analysis of each defect with some suggestions on trouble shooting techniques

to prevent these defects. The root-cause analysis is the result of treating sixty samples with a sampling matrix of (3×5×2×2) produced in three categories of solutions: aluminate, silicate and phosphate at five different current densities (0.1, 0.12, 0.15, 0.18 and 0.2 A/cm^2) with UPDC and BPDC and treatment time of 3 and 5 minutes.

Table 2. Root cause analysis of coating defects along with relevant troubleshooting techniques.

Defects	Root Cause	Troubleshoot
Non-homogeneity	• Bipolar Direct Current mode • Overuse of Silicate salts	• Switch to Unipolar Direct Current • Adjust the concentration ratio of Silicate salts
Excessive Porosity	• Contamination (oil, debris, polishing residue and etc.) • Over use of Phosphate salts	• Clean the surface prior to treatment • Adjust the concentration ratio of Phosphate salts • Avoid contamination when making the solution
Micro-cracks Propagation	• High current density • Over use of Aluminate salts	• Adjust the current density • Adjust the concentration ratio of Aluminate salts
Loose Deposits	• Water impurities • Low current density	• Use higher purity water • Adjust the current density

4.2 Effect of Surface Roughness on Tribological behavior of PEO

Surface roughness affects the performance of PEO coatings and influences the coefficient of friction. Many studies have shown that the behavior of surfaces in contact and their friction during sliding depends on the degree of roughness. According to roughness theory [120] and [121], the frictional force (F_f) is the force required to climb

up the asperity of slope θ and as seen in Equation 15, can be mentioned as the tangent value of the slope:

$$F_f = \tan\theta \qquad \textbf{Equation 15}$$

There are a variety of roughness components that can be looked at when analyzing a surface such as average roughness (R_a), kurtosis (R_{ku}) and skewness (R_{sk}). Throughout this research, terms “roughness” or “surface roughness” refers to average roughness. Some studies were selective on what parameters to include when looking at the effect of roughness on coefficient of friction. For instance, average roughness (Ra) is mostly related to the coating performance due to a simpler demonstration of variance in surface asperities. Other parameters such as kurtosis and skewness were investigated widely in recent years [122], [123] and [124]. Surface skewness (R_{sk}) is an indicator of symmetry of a distribution. For instance if $R_{sk}=0$, this means that the data distribution is symmetrical on the left and right side of the center point of data. If a surface is *negative skewed* ($R_{sk} < 0$), more valleys and pores are on the surface and in contrast a positive skewed ($R_{sk} > 0$) surface have more peaks and asperities and less valleys. Generally, a negative skewed surface is more desirable in tribology since it will have good lubrication properties.

Surface kurtosis as the Greek name implies (kurtosis means curved and arched) is a measure of the peakedness or flatness of the surface relative to normal distribution of

surface profile data. High kurtosis of a surface profile ($R_{ku} > 3$) is called *Leptokurtic* which means slender. This indicates topography with sharp peaks near the mean that drops sharply into both sides. Surface profile would be a more centrally distributed surface with an acute peak and fatter tails on the sides of the distribution. *Platykurtic* surface is a surface with lower kurtosis values ($R_{ku} < 3$). Surface profile is broad with a wider peak near the mean with thinner tails on the sides of the distribution. A normal distribution would have a kurtosis value of 3. Measurement on the surface skewness of the silicate coatings indicate the fact that the rougher surface is negatively skewed therefore it could reserve the lubricant better and minimize the wear rate. Su *et al*. [37] studied the effect of surface skewness and surface kurtosis on wear behavior of PEO coating

Koura and Omar [121] emphasized the effect of average slope of the asperities as the single best correlated parameter for predicting the surface behavior. Also Terrance [122] reported that the average slope can be a good predicting factor for boundary friction. He concluded that the asperity slope of the harder surface of the tribo-pair determine the coefficient of friction behavior. If the asperity slope of the harder surface decreases, coefficient of friction will also decrease. Menezes *et al*. ([125] and [126]) did a comparative analysis on correlation coefficient of varieties of surface parameters. They did the analysis on a wide selection of materials such as aluminum alloys (Al-4Mg and Al-8Mg) and pure metals of Al, Mg, Zn, Cu and Pb. All the wear tests were conducted under lubricated conditions. According to their study average roughness and average slope of the surface profile have the best correlation with coefficient of friction. They also pointed out that the average value of the coefficient of friction is strongly dependent

on the average or mean slope values and is independent of surface texture of the materials investigated.

Average or mean slope of a surface profile is defined as the mean profile of the slope over the assessment length. This value is calculated by finding the slope between each consecutive points of the surface profile and averaging them [127]. The equation 16 is used for calculation of the average slope of the surface profiles [125]:

$$\Delta a = \left| \frac{1}{n} \sum_{i=1}^{n-1} \frac{\delta y_i}{\delta x_i} \right| \qquad \textbf{Equation 16}$$

where n is the number of points on the surface profile. Parameters x and y are the coordinates of the each point. It is worth noting that the value of Δa is always considered absolute.

In this research, a series of PEO coatings produced in a variety of electrolytes over 5 minutes of treatment time, are used to discover the correlation coefficient between all four mentioned roughness parameters (Ra, R_{sk}, R_{ku} and Δa) and coefficient of friction. Wear tests are conducted under lubricated conditions over 1 km of sliding distance. Figure 33 illustrates the correlation coefficient between coefficient of friction with average roughness parameter (Ra). As shown and represented by the trendline, there is a good positive correlation between coefficient of friction and Ra. This behavior is in good agreement with results from Menezes *et al.* 2008 [125] study.

Under lubricated condition, skewness and coefficient of friction are negatively correlated. This means coefficient of friction tends to decrease when skewness increases. As seen in Figure 34, samples with skewness of -0.5< Rsk <1, tend to have lower values of coefficient of friction and higher values of coefficient of friction can be mainly seen in samples with surfaces with Rsk <-0.5. This can be explained by the fact that in a surface which has more peaks, under lubricated condition the areas between the peaks are filled with oil, the liquid pressure from the oil can impose an upward force to the counter face upon contact. This will create a negative force and decrease the force resultant. The acquired result of the analyzed data points are in agreement with Menezes *et al.* [126].

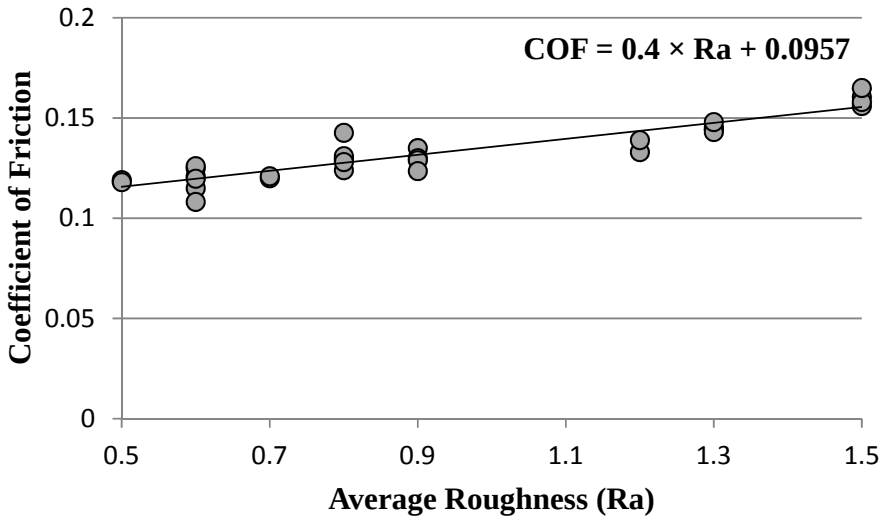

Figure 33. Correlation coefficient between coefficient of friction with average roughness parameter (Ra) for PEO samples treated over 5 minute in a variety of electrolytes.

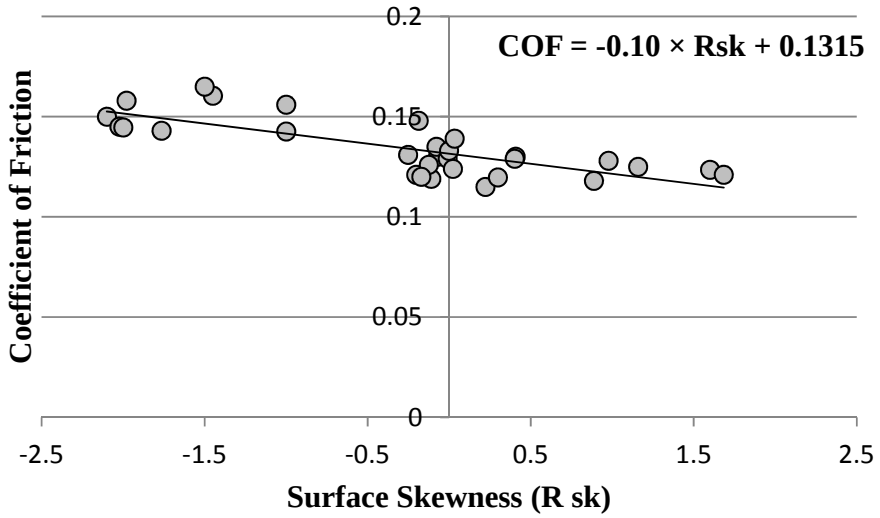

Figure 34. Correlation coefficient between coefficient of friction with surface skewness (Rsk) parameter for PEO samples treated over 5 minute in a variety of electrolytes.

Kurtosis is also another characteristic of the surface profile. Rku < 3 demonstrates surfaces with low peaks and low valleys. The under investigated data as shown in Figure 35 is in the range of Rsk = [-2.5, 2]. This makes sense since all these samples were sanded under the same condition. The only difference would be the starting average roughness of the samples. Lower coefficient of friction samples can be found in surface profiles with kurtosis range of Rku = [0, 1.5]. On the other hand negative kurtosis shows higher coefficient of friction. The correlation coefficient is negative which means as the surface kurtosis increases, coefficient of friction decreases. The negative correlation between coefficient of friction and surface kurtosis is in agreement with the comparison analysis on roughness parameters conducted by Menenzes *et al.* [126] and Sedlacek *et al.*[123].

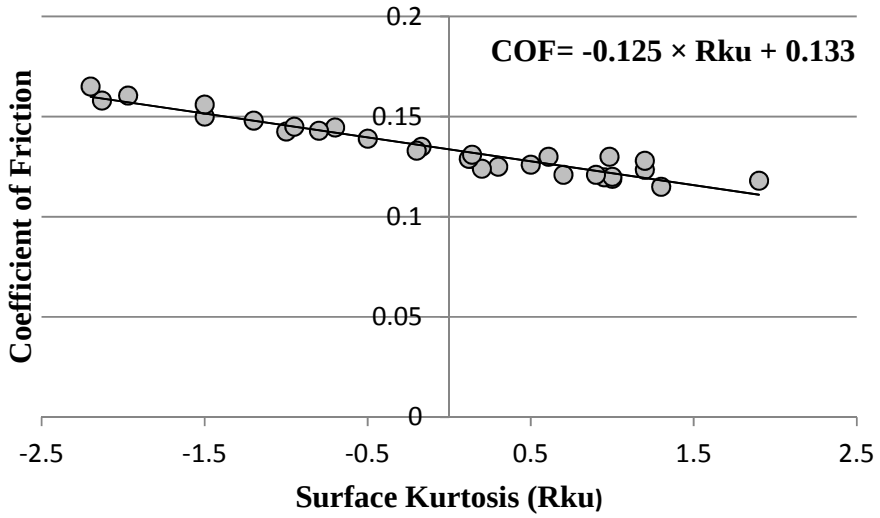

Figure 35. Correlation coefficient between coefficient of friction with surface kurtosis (Rku) parameter for PEO samples treated over 5 minute in a variety of electrolytes.

As mentioned before, average slope can be a good indicator of the coefficient of friction trend. Average slope of each sample is calculated using Equation 15 and results are plotted against coefficient of friction in Figure 36. A stronger correlation is deduced compared to surface skewness and kurtosis. Coefficient of friction is correlated positively with average slope of the surface profile. Lower average slope is more desirable as shown in Figure 36 since most of the lower values of coefficient of friction represent lower values of average slope. The plotted results are in agreement with results published by Menezes *et al.*[126].

The correlation coefficient between coefficient of friction and roughness parameters used in this research under lubricated condition are gathered in Figure 37. Average roughness and average slope show a stronger correlation with coefficient of friction compared to skewness and kurtosis.

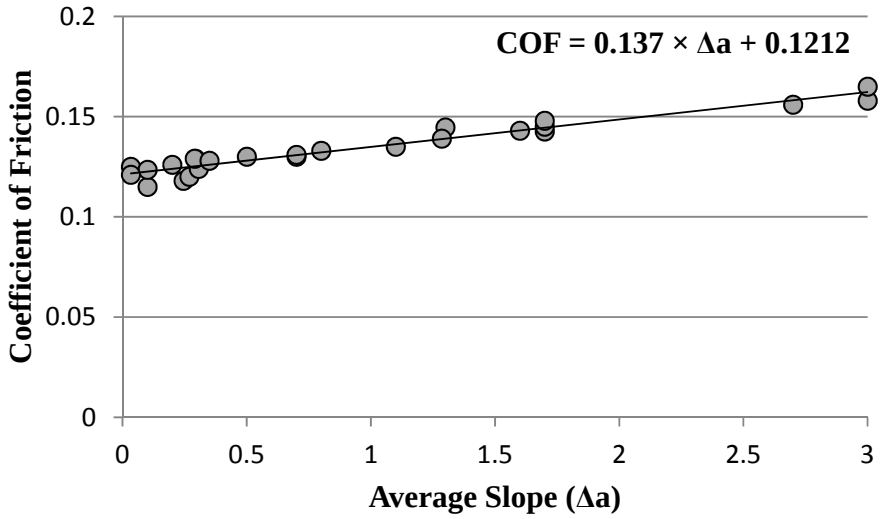

Figure 36. Correlation coefficient between coefficient of friction with average slope (Δa) for PEO samples treated over 5 minute in a variety of electrolyte.

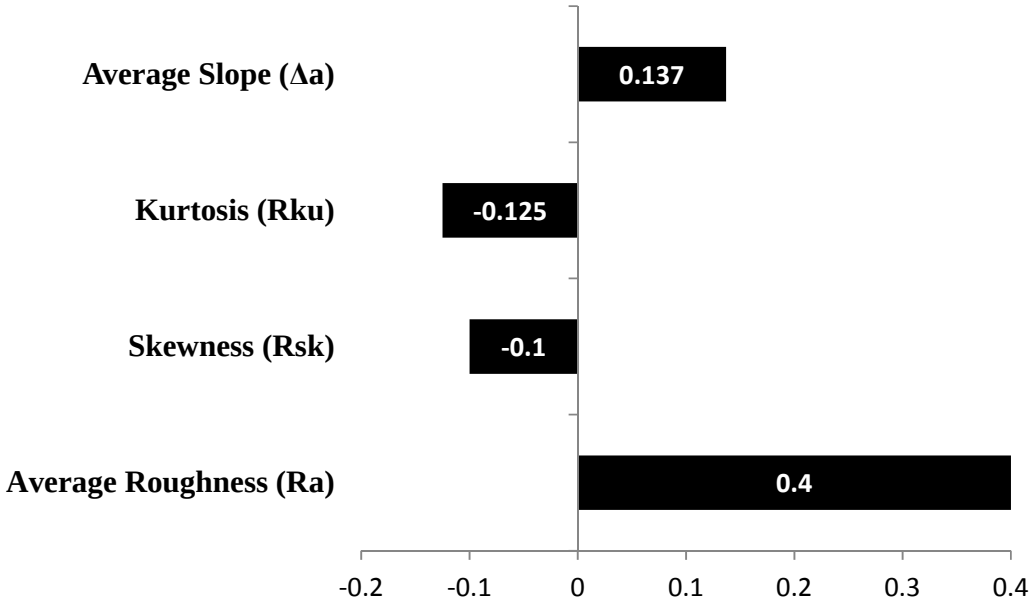

Figure 37. Correlation coefficients between coefficient of friction with roughness parameters under lubricated condition.

4.3 Effect of Solution Composition on Tribological Behavior of PEO

The composition of the electrolyte has a great influence on properties of the achieved coating. Growth rate, morphology and phase composition can change by using different electrolytes. There are four main categories of electrolytes that can be utilized in production of PEO coatings [128], [129].

1. Electrolytes that provide fast dissolution of metal such as salts like NaOH
2. Electrolytes that provide slow metal dissolution such as H_2SO_4 and Na_2SO_4
3. Electrolytes that promote slight passivation of the metal
4. Electrolytes that promote strong metal passivation such as H_3PO_4

When group 1 and 2 of the solution categories is used, it is crucial to start the process as soon as the substrate is dipped in the solution otherwise, the substrate would have residues of the immediate corrosion or etching effect which can influence the adhesion of the coatings. Once the process is started, it takes longer time for these solutions to provide an environment for the spark generation. Group 3 and 4 on the other hand reach the sparking voltage in a shorter time. Another classification of the electrolyte coatings is to divide them into acidic and alkaline solutions. Most of the alkaline solutions include one or a mixture of the followings [69]:

1. Hydroxide based electrolytes (Sodium and Potassium)
2. Silicate based electrolytes
3. Phosphate based electrolytes
4. Aluminate based electrolytes

Also according to literature most frequent electrolytic composition for PEO

coatings on an aluminum alloy substrate are aluminate-based [130], [114] silicate-based [85], [118] and phosphate based [131]. List of the various electrolytes used in this research can be found in Table 3.

Coatings on the substrate are formed in different type of solutions and are compared in terms of morphological appearance, roughness values (average roughness is used since it has the best correlation with coefficient of friction) and growth rate. These coatings are also compared for their tribological performance and wear rates.

Figure 38 shows the roughness values of PEO coating after 5 minutes of treatment time under 0.1 A/cm^2 current density. As shown silicate has a great impact on average surface roughness of the coatings and phosphate tends to act as a smoothing agent in the coating. In other words, phosphate solution produces the smoothest coating and silicate solution produces the roughest. When they get mixed together, phosphate reduces the roughness value of the achieved coating. Potassium hydroxide tends to increase the intensity of the breakdown dielectric discharge and adds to the coating thickness and also roughness of the coating. It is desirable to achieve coatings with less roughness, adequate porosity for oil retention, good hardness properties, and also lower coefficient of friction values. Silicate based unipolar coatings showed lower roughness values when mixed with Potassium hydroxide and also showed almost the same roughness values when mixed with phosphate salts.

Table 3. Various electrolytes used in this study.

Solution Composition	Solution Chemical Formula
Aluminate	50-56% Al_2O_3 + 0.05% Fe_2O_3 + 40-45% Na_2O
Silicate	Na_2SiO_4
Phosphate	Na_2HPO_4
Aluminate and Silicate	(Al_2O_3 + Fe_2O_3 + Na_2O) + Na_2SiO_3
Silicate and Phosphate	Na_2SiO_4 + Na_2HPO_4
Silicate and Potassium Hydroxide	Na_2SiO_4 + KOH
Silicate, Potassium Hydroxide and Citric Acid	Na_2SiO_4 + KOH + $C_6H_8O_7$
Silicate, Potassium Hydroxide and Molybdenum Disulfide	Na_2SiO_4 + KOH +MoS_2

In order to compare the coatings behavior and coefficient of friction, a series of samples were chosen from production of PEO coatings in the mentioned electrolyte solutions. All samples were chosen with average surface roughness values between 0.5 and 0.7 μm in order to minimize the effect of surface roughness for our comparison study. Tribological properties of the samples were evaluated using a reciprocating sliding tribo-tester under a normal load of 2N for 1 km of sliding distance. The maximum Hertz contact stress is estimated at 980 MPa. Sliding stroke and frequency were 10 mm and 4 Hz, respectively.

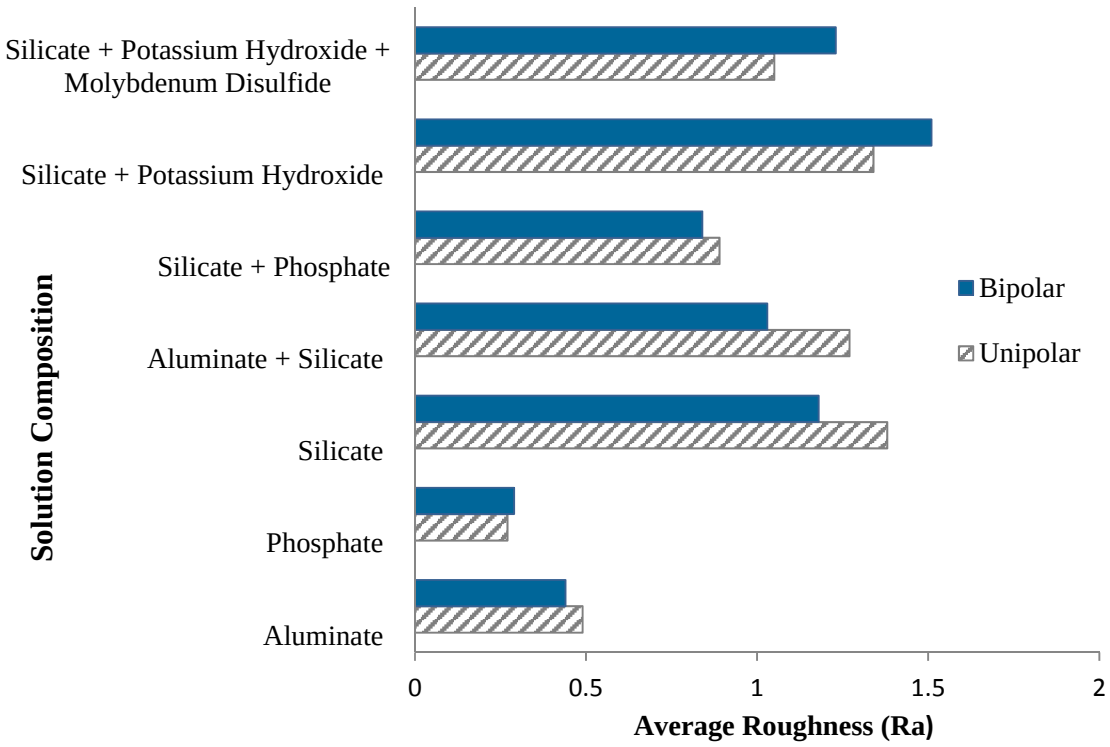

Figure 38. Roughness values in relation with the solution composition for 5 minutes of treatment time. Six samples were treated in each solution type: 3 under bipolar and 3 under unipolar pulsed direct current mode. Roughness of each sample was measured 5 times at 5 different directions on the surface and then averaged.

Samples were tested under lubricated condition with the use of 5 ml of 5W30 engine oil. A preliminary test has shown no difference in the results of coefficient of friction using 5W20 engine oil. The main difference between 5W20 and 5W30 is the oil viscosity/thickness which determines the resistance of the oil against heat. 5W30 stays thicker when heated and is more desirable for higher performance engines. Same tribo-test condition was used for the tribological evaluation of this study unless mentioned otherwise. A result of this comparison is shown in Figure 39.

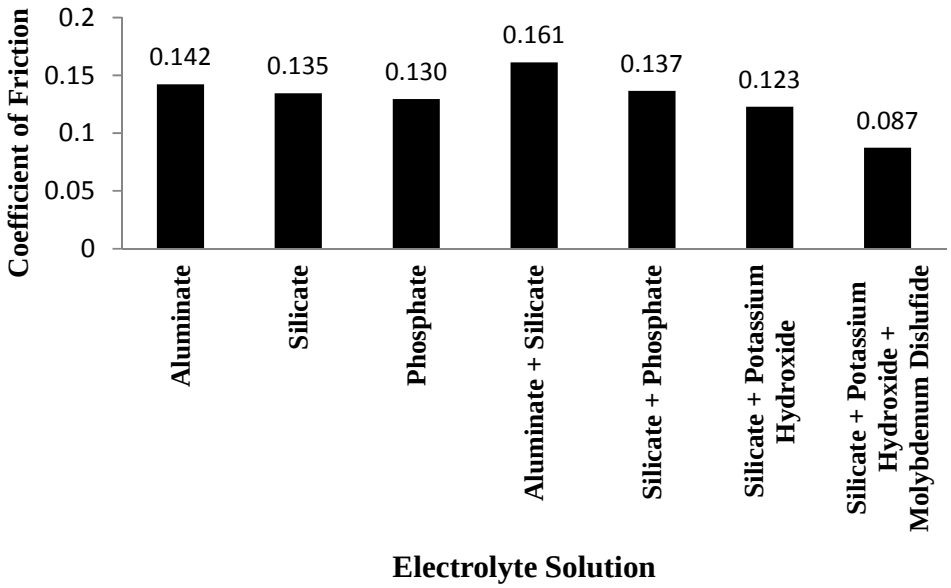

Figure 39. Coefficient of friction of PEO coatings produced in variety of electrolyte solutions. Samples were tested over 1 km of sliding distance under lubricated condition against the moly piston rings. (SD= ± 0.01)

The highest coefficient of friction is achieved using a combination of silicate and aluminate solution. Among aluminate, silicate and phosphate based coatings, phosphate shows the lowest coefficient of friction however the coating is softer in terms of hardness and tends to delaminate over longer sliding distance (see Figure 27). Phosphate coatings also tend to have more porosity which sometimes exceeds the optimum limit of efficiency (17-25%). Jun Liang *et al.* [116] also investigated the effect of silicate and phosphate coatings on wear performance of the PEO coatings and demonstrated that the coatings formed in silicate solution have a higher coefficient of friction but exhibit a better wear performance compared to the coatings prepared in phosphate solution, aluminate solution compared to silicate and phosphate solution produce coatings with higher coefficient of friction. Of the three typical solutions (aluminate, silicate and phosphate), silicate solutions tend to create coatings with good coefficient of friction,

shallow wear tracks on the coating surface and minimum of wear loss on the counter surface. Therefore more emphasis was made on silicate and silicate mixture solutions. Addition of phosphate to silicate solution decreases wear loss on the counter surface and has not improved the coefficient of friction values for the better. Addition of potassium hydroxide to the silicate solution shows an 8.75 % improvement on coefficient of friction values and also 20% less wear loss on the counter surface. Further investigation on tribological behavior of the coatings produced in silicate and potassium hydroxide solution at different pH levels is presented in section 4.4. As shown in Figures 39, addition of molybdenum disulfide has helped with the coefficient of friction. Figure 40, gathers the results of volume loss on the counter surface of steel balls and as shown, wear loss on the counter surface against the coatings produced in the solution mixed with molybdenum disulfide is 8% less than the same solution without the use of molybdenum disulfide. Tribological influence of addition of molybdenum disulfide to silicate and potassium hydroxide mixture can be found in section 4.7.

4.4 Effect of Solution Acidity Level on Tribological behavior of PEO

Acidic solution has not been explored as much as alkaline solutions due to their environmental effects. Although using environmental-friendly alkaline solutions are one of the main advantages of PEO treatment, it is good to see the effect of an acidic solution on PEO process. Therefore a series of tests has been conducted under a variation of electrolyte acidity starting from the most alkaline solution with pH=13 to neutral solution with pH=7 and finally reaching a high acidic solution with pH= 3.

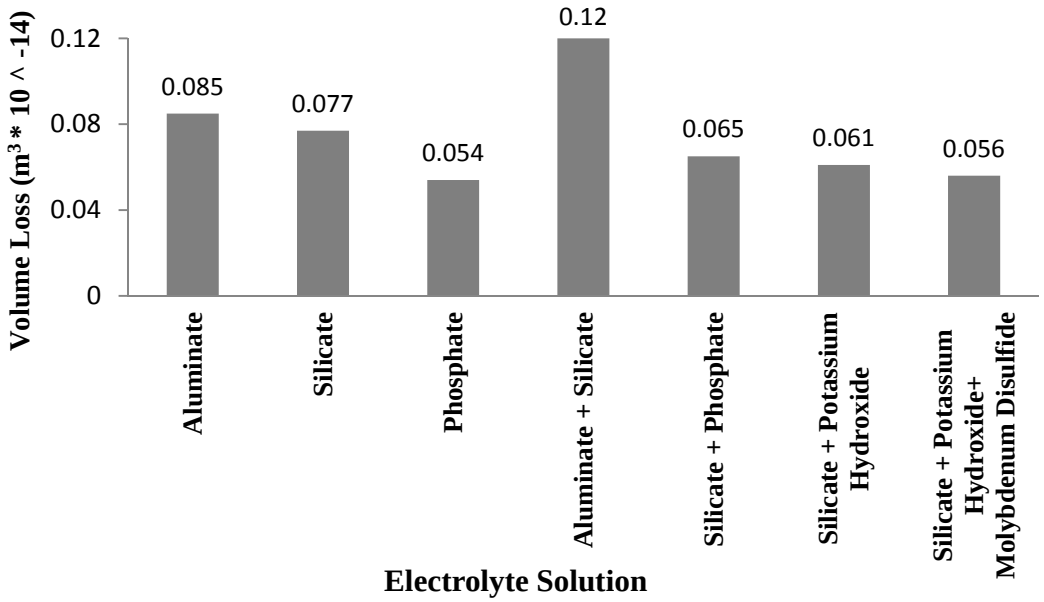

Figure 40. Wear loss on the E52100 steel balls against a variety of PEO coated samples. Samples were tested over 1 km of sliding distance under lubricated condition (SD= ±0.001).

Acidity of the solution has an impact on coating thickness and also morphology and roughness of the oxide layer. As shown in Figure 41, a series of coatings were achieved in a mixture of silicate and potassium hydroxide solution with the addition of citric acid. As shown, the more acidic the solution is, the faster it grows. Coating growth rate is under 1 μm/min for the solutions with pH= 13 and it increases to 1.5 μm/min for the solution with pH=3.

Coatings formed in the solution with pH=10 showed the roughest surface. Data points are fitted using a 3rd polynomial fitting curve and represent a strong correlation between the pH values and surface roughness.

Table 4 shows the test matrix of the samples. Since roughness has a great impact on behavior of the coating in contact with the counter surface, it is essential to design a matrix of samples that can be compared to each other. Therefore, achieved coatings were sanded and polished to different values of roughness. At first achieved coatings were brushed before the first round of tribotest and were tested. These samples were called *As-deposited* samples. At the next stage, samples were sanded and polished lightly to reach average roughness value of Ra= 0.8 µm and finally samples were polished further to reach Ra= 0.4 µm. After each polishing session, samples were washed with water, cleaned with acetone and dried completely. Prepared coatings were tested under 2N load at lubricated condition. Figures 42 shows the coefficient of friction curves for the coatings produced in solutions with variety of pH levels at different roughness values.

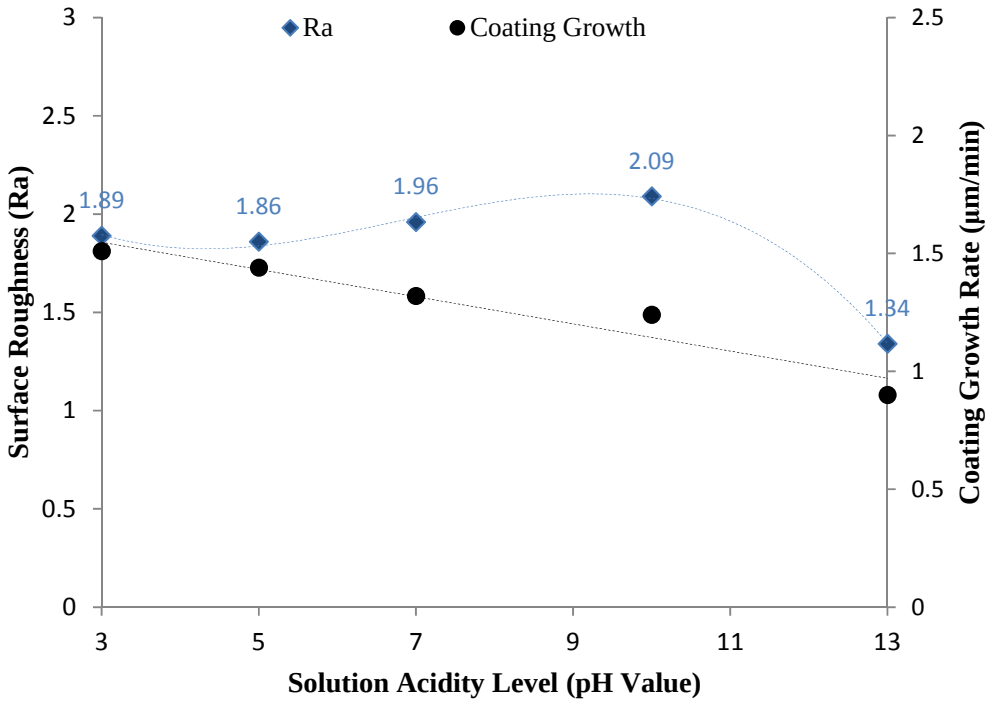

Figure 41. Effect of solution acidity level on surface roughness and coating growth rate.

Table 4. Test matrix for PEO coatings produced in acidity levels of (3 < pH <13).

Sample	Solution Composition (gr/lit)	pH	Treatment Time (min)	Output Voltage (v)	Average Vickers Hardness ($HV_{0.2}$)
P1	(6) Na_2SiO_4 + (2) KOH	13	5	441	345
P2	(6) Na_2SiO_4 + (2) KOH + (7) $C_6H_8O_7$	10	5	467	350
P3	(6) Na_2SiO_4 + (2) KOH + (10) $C_6H_8O_7$	7	5	472	375
P4	(6) Na_2SiO_4 + (2) KOH + (15) $C_6H_8O_7$	5	5	476	370
P5	(6) Na_2SiO_4 + (2) KOH + (23) $C_6H_8O_7$	3	5	492	245

P1- Coating produced in solution with acidity level of pH=13

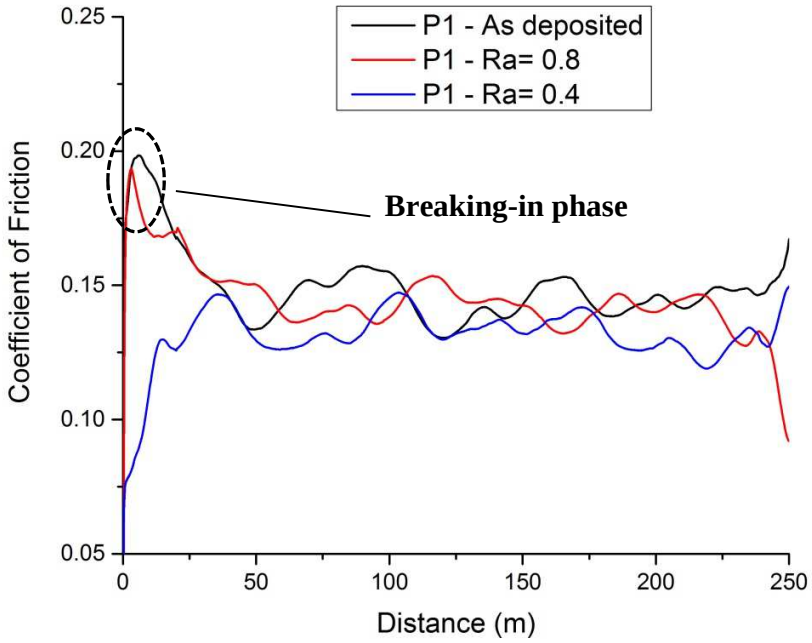

P2- Coating produced in solution with acidity level of pH=10

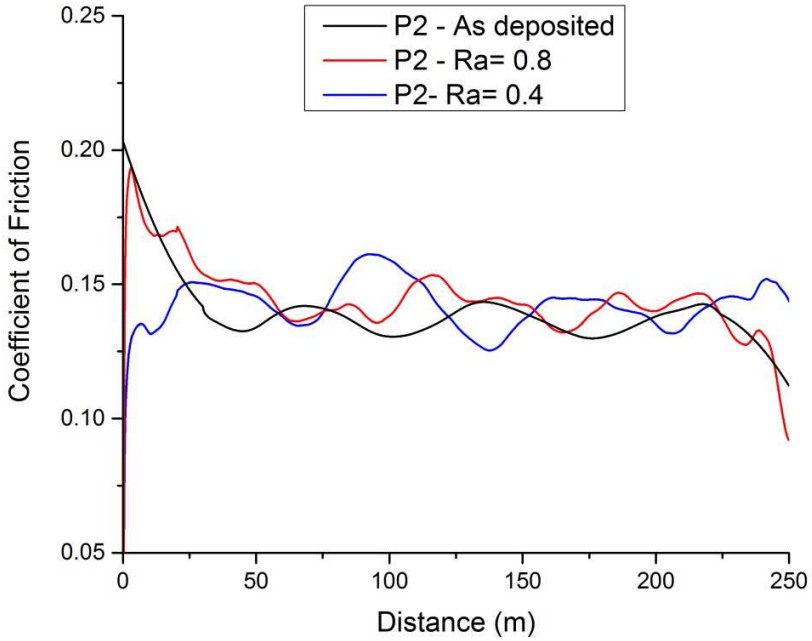

P3- Coating produced in solution with acidity level of pH=7

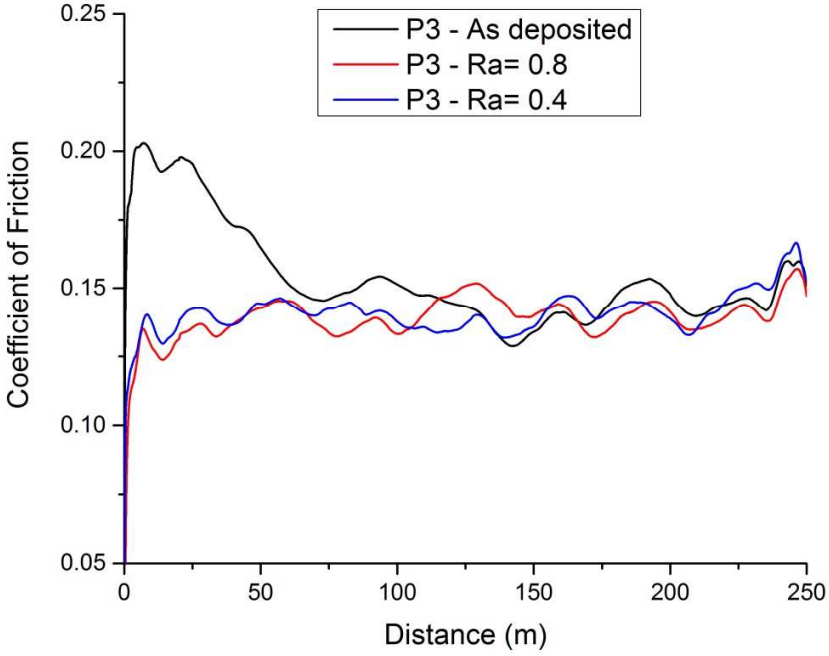

P4- Coating produced in solution with acidity level of pH=5

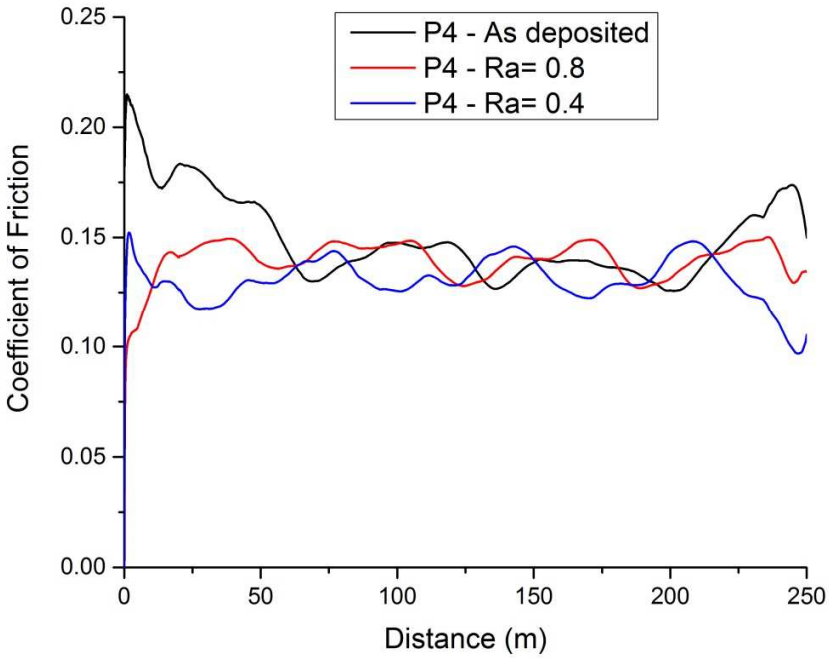

P5- Coating produced in solution with acidity level of pH=3

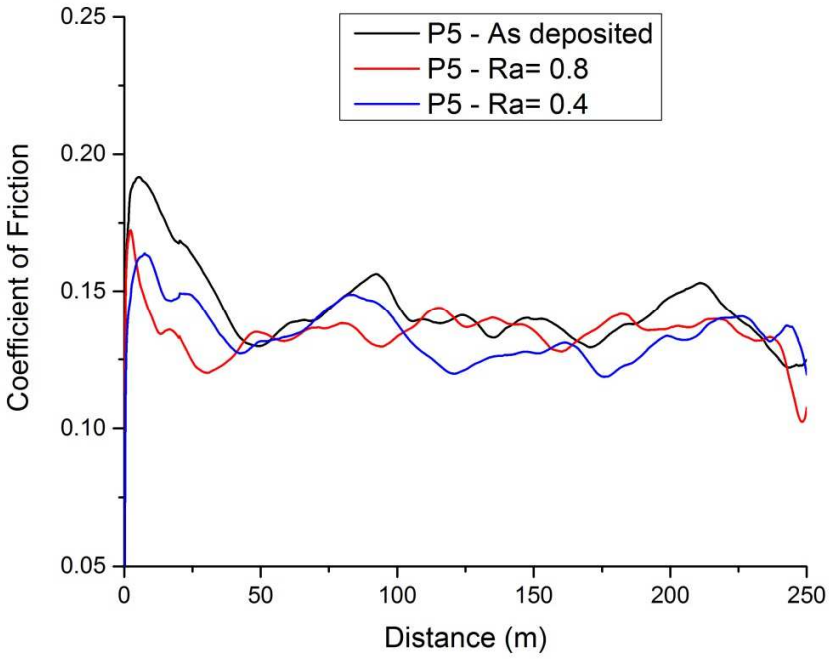

Figure 42. COF curves for the coatings produced in solutions with variety of pH levels at different roughness values. P1, P2, P3, P4 and P5 are coatings achieved in solutions with acidity levels of pH=13, 10, 7, 5 and 3 respectively.

As shown in Figures 42 for the as-deposited coatings and higher roughness values, there is a sharp increase and decrease at the start-up time of the tribo-test (as marked in Figure 42 – P1). This period is called the break-in phase. During this time, the tribo-set is settling-in which means the coating surface is being smoothed by the counterface on the spots that have high contact stress. Break-in phase usually prepares the surface for higher load bearings. Also in case of lubricated condition, the lubrication is seeping into the nicks and crannies of the surface and forms a boundary between two contacting surfaces. Sliding frequency is fixed during the tribo-test and was set to 4 Hz to keep the lubrication condition as “boundary lubrication”. This means that the lubricant film is thinner than the height of the asperities on the counter surface but not thinner than

the height of asperities on the coated surface. The boundary layer will protect the sliding parts of a tribo pair unless there is a change in load or roughness of the surface.

Roughness plays an important role in lubrication behavior of the sliding surfaces. At higher roughness values as shown in all P1 to P5 COF plots of Figure 42, for as-deposited curves, COF is higher and above the average value. This is due to the direct asperity contact between the surfaces. In tribology, this behavior can be quantified with a ratio called *Λ Ratio* [132] as reflected in Equation 17:

$$\Lambda = \frac{h}{\sigma} \qquad \textbf{Equation 17}$$

where h is the lubricant film thickness, and σ is the composite surface roughness of sliding distances described in Equation 18:

$$\sigma = \sqrt{\sigma_{PEO} + \sigma_{Counterface}} \qquad \textbf{Equation 18}$$

where σ_{PEO} is the composite surface roughness of the PEO coated surface and $\sigma_{Counterface}$ is the surface roughness of the counterface. If we assume that the composite surface roughness is the same as average surface roughness (Ra), Equation 19 can be reached:

$$Ra = \sqrt{Ra_{PEO} + Ra_{Counterface}}$$ **Equation 19**

and also if the thickness of the lubricant film is considered fixed due to the similar quantity of droplets of lubricant used for each test, it would be apparent that higher roughness values will bring lower Λ ratios which means more direct asperity contact between the sliding surfaces and eventually higher COF values. Figure 43 gathers coefficient of friction values of the mentioned samples that were tested over 1 km of sliding distance at three different roughness values (Ra= 1.2, 0.8 and 0.4).

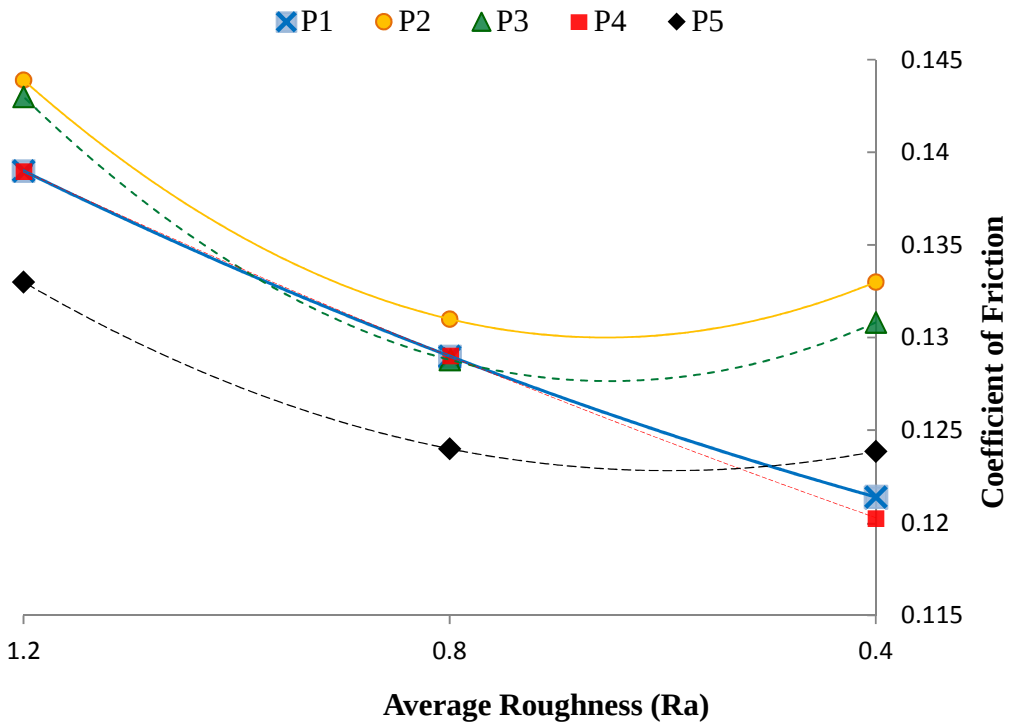

Figure 43. Coefficient of friction values against roughness values of samples P1 to P5. Samples were tested over 1 km of sliding distance at 4 Hz sliding speed (SD= ± [0.0008-0.0012]).

Coatings are influenced by the roughness values of the surface. Higher roughness (Ra=1.2) usually causes higher COF. As the roughness decreases, the COF decreases for P1 and P4 coatings which are produced in pH=13 and pH=5 respectively; the decrease of COF is sharp and has a linear trend. P2, P3 and P5 show a decreasing trend as the surface becomes smoother from Ra=1.2 to Ra=0.8 and show a slight increase from Ra=0.8 to Ra=0.4. A 2^{nd} order polynomial trendline is fitted to the data points for these coatings. P2 has the highest value of COF at Ra=1.2 and P5 has the lowest value of COF at the same roughness. P1 and P4 have the same trend and similar values of COF. By looking at the counter surface and its wear rate, it would be easier to understand which coating have the best tribological performance and is more adaptable to the counterface. Figure 44 shows the wear scar of the steel ball counterface against each of the coatings at different roughness values. As shown, coatings that are produced in a more acidic environment tend to have a larger scar on the counter surface. These images are taken using an LED illuminated microscope. Wear scars were then measured. Wear rate of the counter surface were calculated and plotted against roughness values in Figure 45.

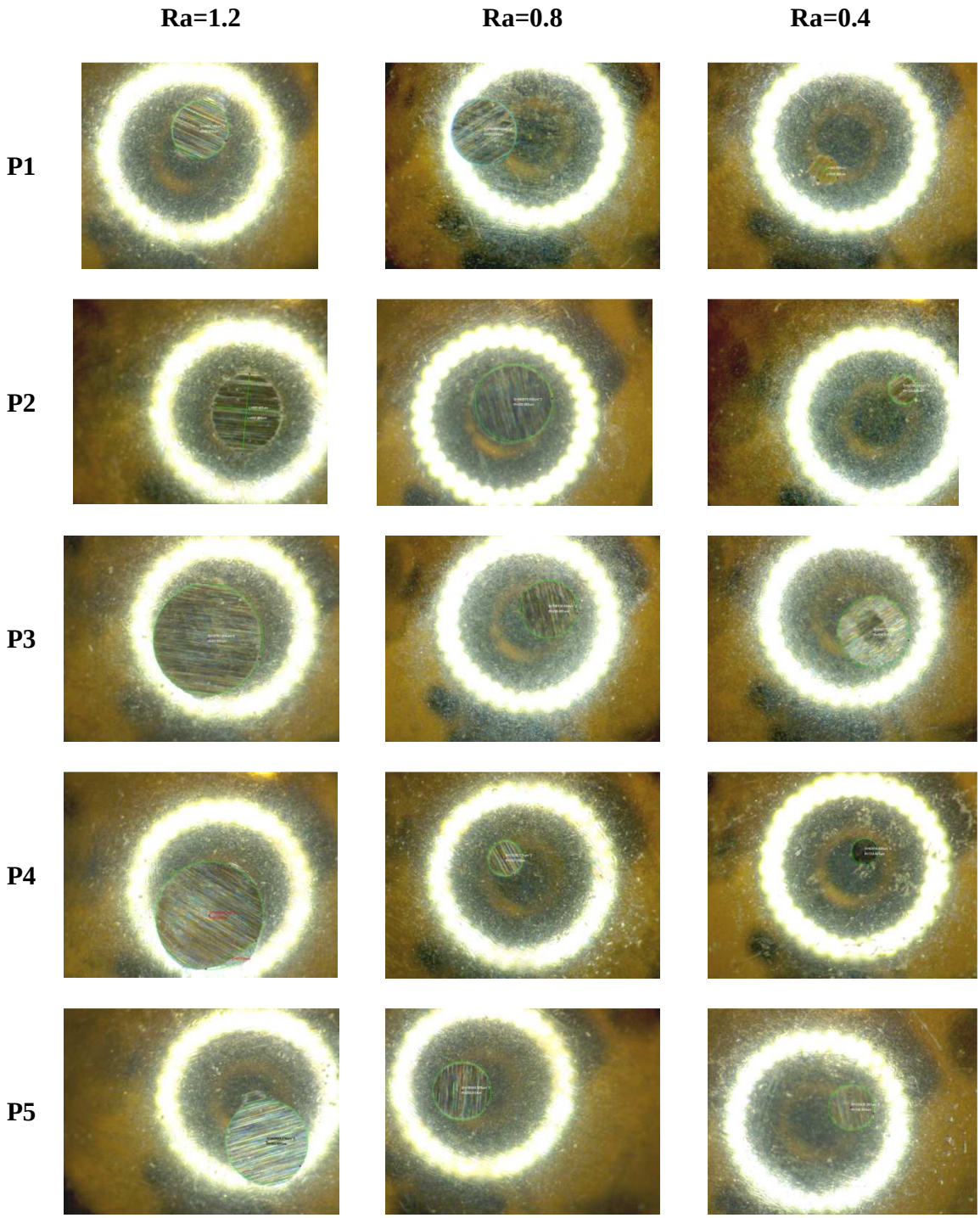

Figure 44. Wear scar on the counterface (steel ball) of P1 to P5 coatings with different surface roughness values observed under an LED illuminated microscope. All the images are taken at the same calibration scale.

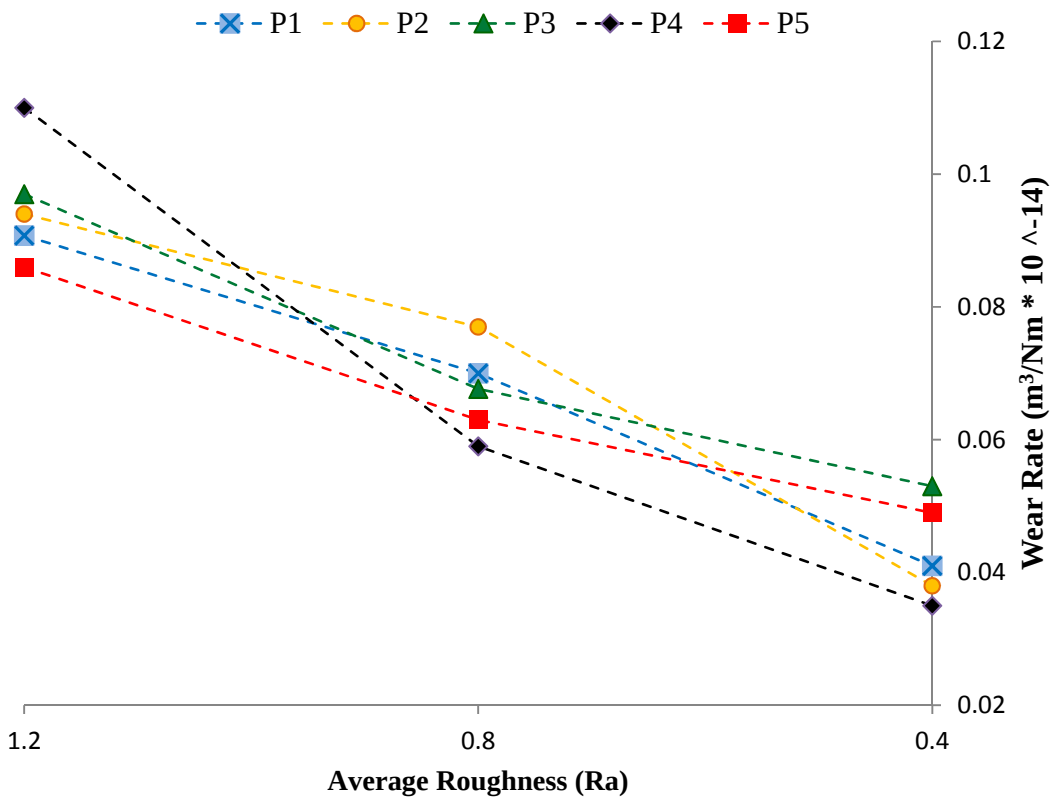

Figure 45. Wear rate of samples P1 to P5 at different average roughness values. (SD: ± 0001)

As a general rule, it is essential to consider surface roughness when studying the coefficient of friction. Coefficient of friction depends on the slope of the asperities and the engagement angle of theses asperities when in contact with the counter surface. Also once the deformation of the asperities starts due to friction and sliding motion; it can affect the angle of engagement and can change the coefficient of friction. During the break-in part, the higher values of coefficient of friction is because of the deformation of the materials at high angle of engagement which usually occurs at the beginning of the sliding and it decreases once the sliding surfaces engage at a lower angle of engagement. Since the material under study is a ceramic with relatively medium to high hardness levels (350 to 550) deformation in general is low.

4.5 Effect of Lubrication Mode on Tribological behavior of PEO

Lubrication condition is considered a sub-system of the tribo-system. Two different lubrication conditions with presence of 5W30 engine oil were defined and used during the tests. First condition is submerging the sample in a specific sample holder which guarantees that a thin layer of oil is over the surface at all time, which is called as *Lubricated (L)* condition and the second condition is dipping the samples in oil for five minutes and taking the samples out and let them drain off of the excessive oil overnight. A smear of oil residue on the surface was formed, this condition is called, *Starved (S)*. This condition is designed to mimic the start and stop system mode of the engine or when the engine is restarted after a period of rest. Figure 46 illustrates the two lubrication modes showing the sample condition in the sample holder of the tribo pair.

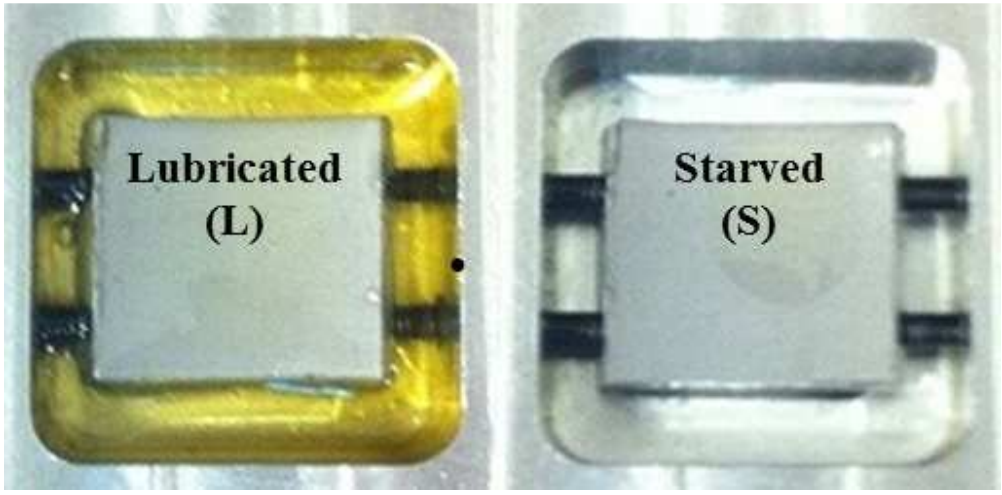

Figure 46.Lubrication modes of the tribo-tests.

As mentioned roughness structure and porosity network on the surface of the coatings can work as oil reservoirs for the sliding surfaces. In fact, automotive industry

use a surface texturing technique called *honing* in order to produce surface dimples to reserve the oil and help with keeping a smear of lubrication on the coatings even when the engine is not running otherwise gravity would drain all the oil from the surface and the tribo-pair will have a relevantly harsher contact at the start of the engine run. PEO coating does provide the same effect on the surface due to the existence of pores. In order to see the effectiveness of the oil reservoirs on keeping the coefficient of friction values low, four silicate samples of the same batch of PEO synthesis were chosen. Samples were polished to reach 0.53 (C1) and 0.3 (C2) average roughness values. Tribo-tests were conducted using dipped and starved condition at each roughness value. An uncoated Al319 substrate is also used for reference. Coefficient of friction curves are shown in Figure 47.

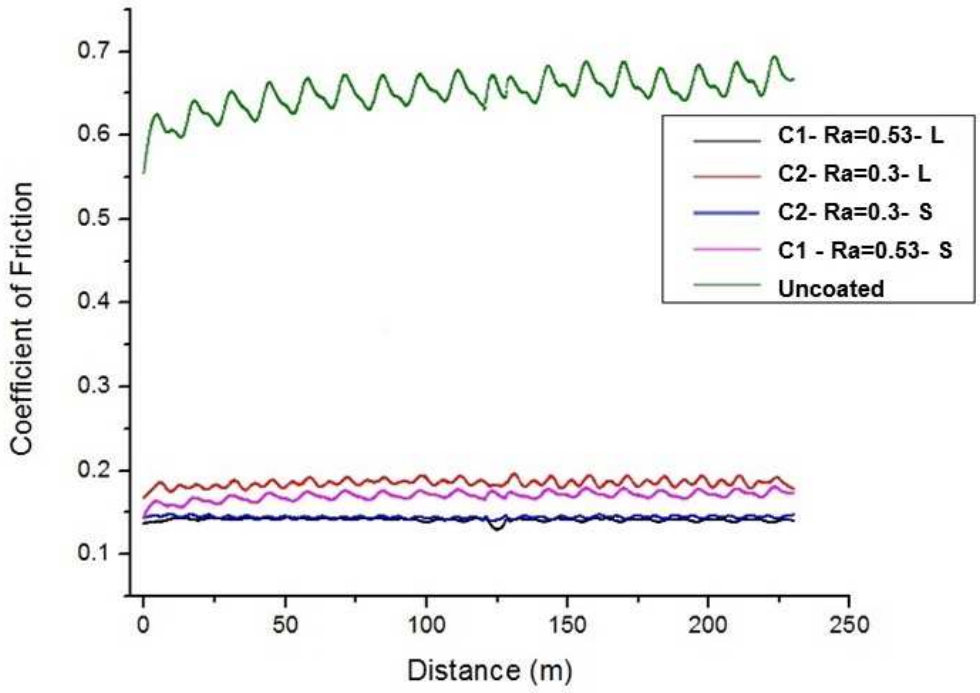

Figure 47. COF plots for sample at roughness values of 0.53 and 0.35 under dipped and starved lubrication modes.

At higher roughness values, the starved condition creates a higher friction force and shows a higher coefficient of friction. It is interesting to see that a rougher sample at dipped lubrication condition acts almost the same as a smoother surface at starved condition. This shows that the surface structure has helped with retaining the lubrication. Comparison of the two coatings with smoother surface at two lubrication modes shows that the dipped condition has a higher coefficient of friction than the starved condition. This is not a co-incident since this type of test was repeated twice more to ensure the repeatability of the results and the similar results were achieved. This can be due to the fact that the force that is needed to slide on the surface was used to move the extra lubricant on the surface and added to the value of coefficient of friction. Also it may be due to the liquid pressure upwards from the lubricants in the pores of the surface once the sliding distance glides above them. The upward fluid pressure can reduce the total friction force and decrease the coefficient of friction. Overall, this experiment showed the effect of lubrication mode on friction force and coefficient of friction trends.

4.6 Load Bearing of PEO coatings

Load bearing or load-carrying capacity of the surface can indicate the resistance of the thin film against wear and scuffing. There is a relation between load, lubrication mode and COF. As the load increases so the contact pressure on the asperities. However it is difficult to predict the behavior of the coating specifically under lubricated condition since the oil hydrodynamic pressure in the pores (oil reservoirs) is another indicating factor. Hydrodynamic pressure is influenced by surface roughness, waviness and

skewness of the surface. Hydrodynamic pressure can have different mostly beneficial effects on the behavior of the tribo system [132]:

1. *Hydrodynamic effect*: This effect occurs due to the projection of the asperities of the surface down into the lubricant which can create a step bearing. As the flow approaches the asperity, pressure increases around the contact points on the edge of a pore and decreases on the pore opening site and again increases at the other edge of the pore. However this decrease is not the anti-symmetrical value of the pressure increase that happens at the beginning of the process. This effect creates additional load carrying capacity.

2. *Secondary lubrication effect*: Another effect acts on the condition of mixed lubrication between the tribo pairs. The oil trapped in the valleys of the surface (oil reservoirs- pores and linear openings) can be considered as a secondary source of lubrication. As the tribo pair slide against each other, the relative movement creates pressure on the valleys and pushes the lubricant out. This secondary lubricant will permeate into the surrounding areas and reduces the friction between the tribo pairs.

One of the mentioned effects may be the cause for abnormal behavior of the dipped smoother surface versus the starved smoother surface in section 4.5. According to literature on friction and wear behavior of PEO coatings, loads equal and less than 2N are considered low [133] , [116] and loads below 40N are recognized as medium loads [134], [104]. There are studies on wear behavior of PEO coatings under heavy loads of 100N to 300N [133]. Coefficient of friction for tests under 300N on aluminum alloy (2A12) was

around 0.45 and led to 3 to 5 X 10^{-6} wear rate on the steel ball [135]. In order to understand the effect of load on the coefficient of friction of PEO coatings, samples P1, P3 and P5 of experiment matrix from section 4.4 were used. Samples were then tested under 2, 8 and 15 N of normal load under lubricated condition over 250 m of sliding distance. Figure 48 shows the effect of load on COF for P1, P3 and P5 samples. According to the plotted COF curves, coefficient of friction values are much less for P1 sample which is created in the typical pH range of basic solution. The effect of an extra 5N load is not much apparent and on the values of P1 under 2N and 8N. All the plots have one thing in common and that is the highest value of coefficient of friction at the highest load. Coefficient of friction values for sample P1 under all three load settings is in the acceptable range. However for P3 and P5 the values under 15N are high (around 0.22).

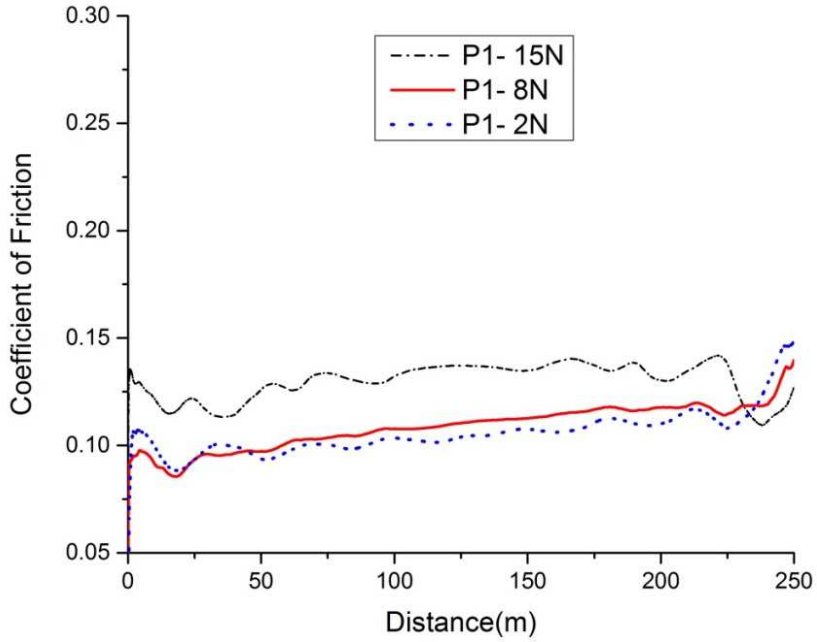

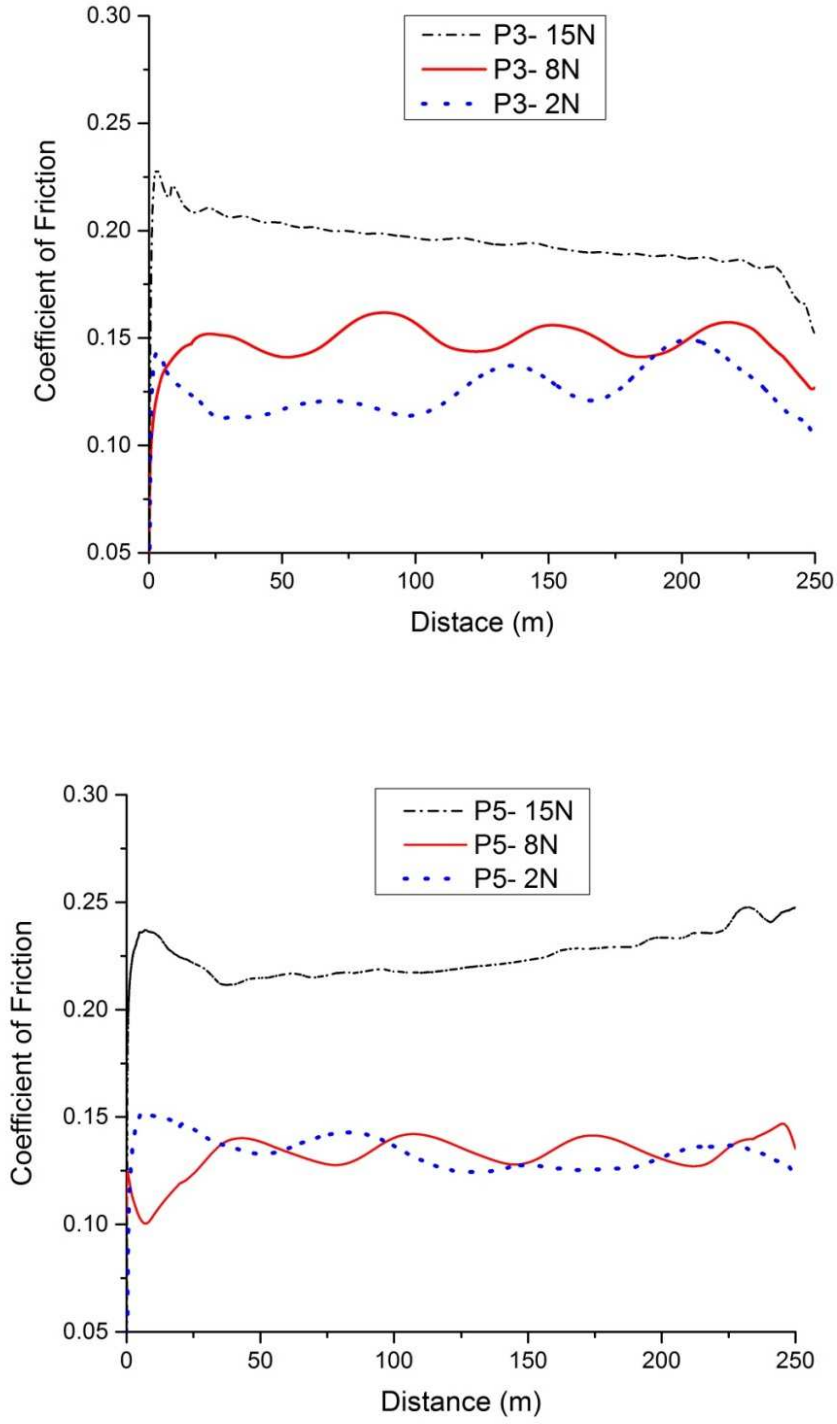

Figure 48. Coefficient of friction curves for three sets of loads 2N, 8N and 15N during the sliding distance of 250 m.

Figure 49 summarizes the COF curves and presents the average coefficient of friction values for under study samples at each applied load. At 15N load, P3 has the highest value for coefficient of friction. This can be due to the high hardness value of the coating compared to P1 and P5 samples. The load variation has less effect on coefficient of friction of P1 sample around 17%. For P3 and P5 samples, the effect of load variation on coefficient of friction is much more prominent. There is a 35% of increase in coefficient of friction for P5 sample with addition of extra 13N load. This value is around 40% for P3 sample. It can be concluded that samples produced in electrolyte solutions with pH value of 13 are more resistant to the increase of applied load. This resistance is what is known as "*load carrying capacity*" or "*load bearing properties*".

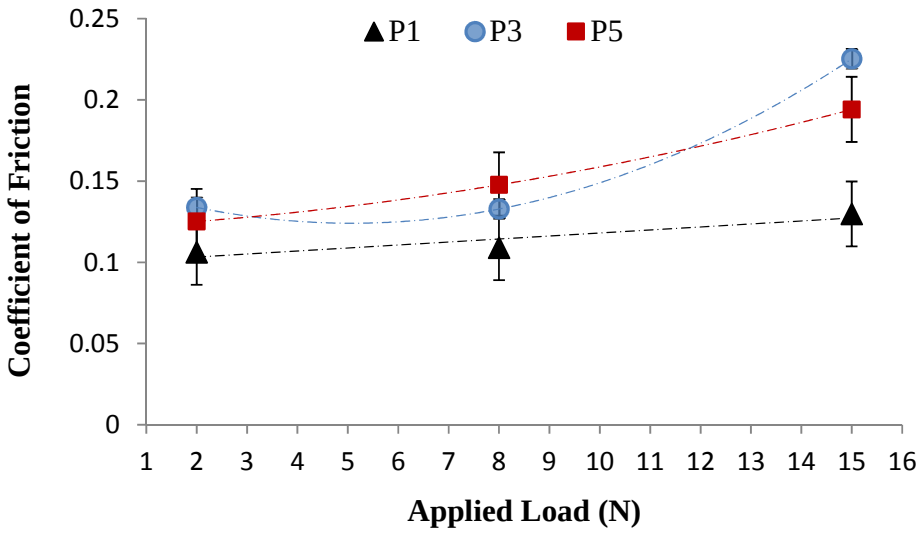

Figure 49. Coefficient of friction versus applied load for P1, P3 and P5.

Observation of wear tracks on the surface of the coatings can give a better understanding of the tribo-pair behavior. On sample P1, P3 and P5 no visible wear tracks can be detected under SEM after the 250 m of tribo test under 2N load. This is also true for P1 sample under 8N and 15N loads. Figure 50, shows the surface of the P1 coating after 250 m of sliding wear test under 15N load. Samples P3 and P5 were affected under both 8N and 15N load. Detected wear tracks for samples P3 and P5 can be found in Figure 51 and 53 for 8N applied load and Figure 52 and 54 for 15N applied load.

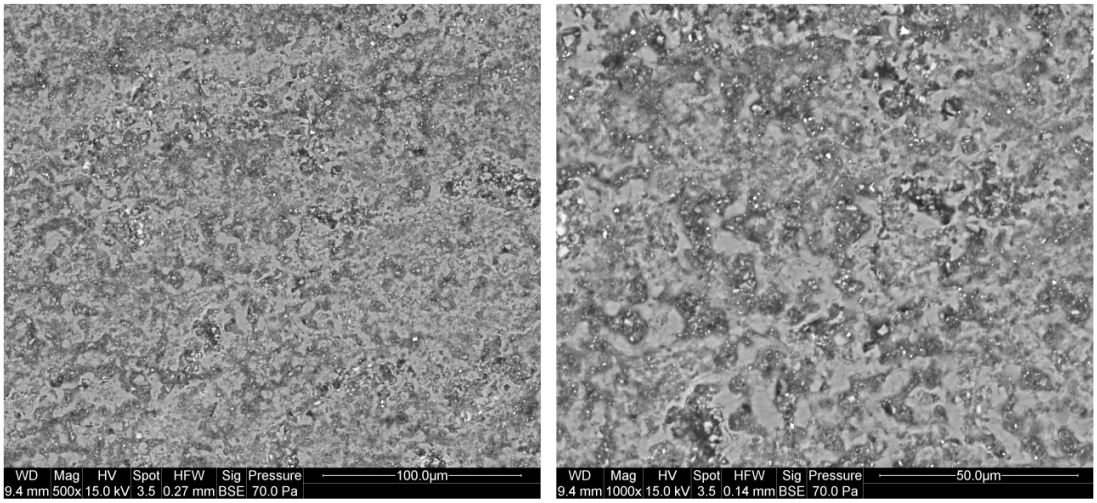

Figure 50. Surface of P1 sample after 250 m of wear test under 15N load with no detected wear tracks.

Based on the SEM observation of the coating surface, 15N load creates a wider wear track and it seems that the wear mechanism is abrasion due to hard particles. Adhesion can also be an influential factor in this kind of tribo system. A detailed study on the counter surface will be presented in Chapter 5.

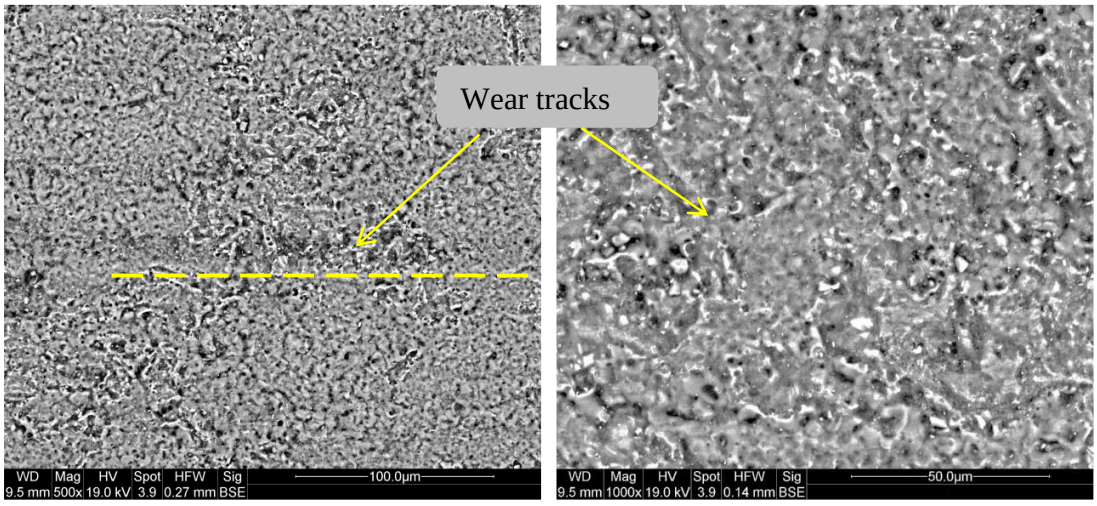

Figure 51. Wear tracks on the surface of P3 sample after 250 m of wear test under 8N load.

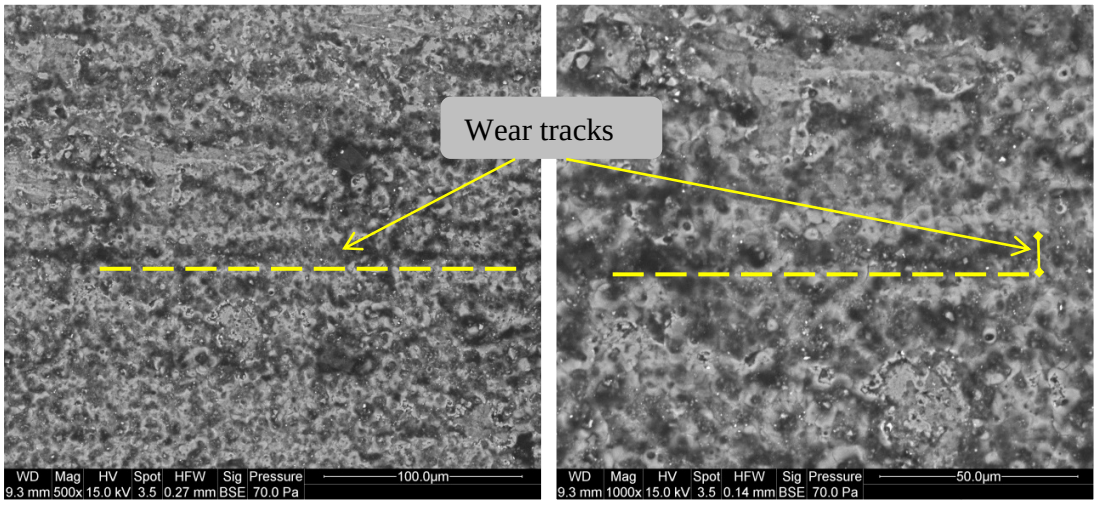

Figure 52. Wear tracks on the surface of P3 sample after 250 m of wear test under 15N load.

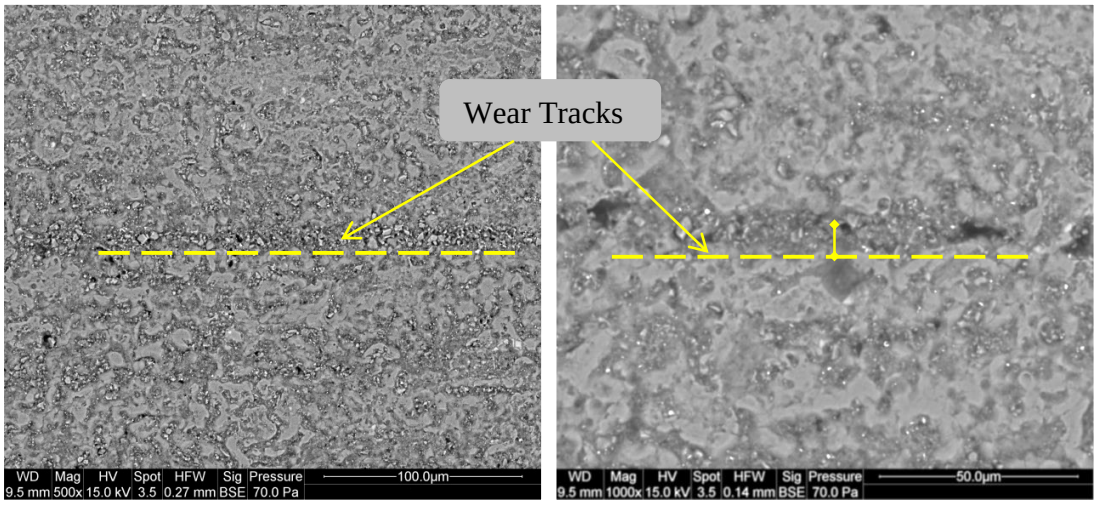

Figure 53. Wear tracks on the surface of P5 sample after 250 m of wear test under 8N load.

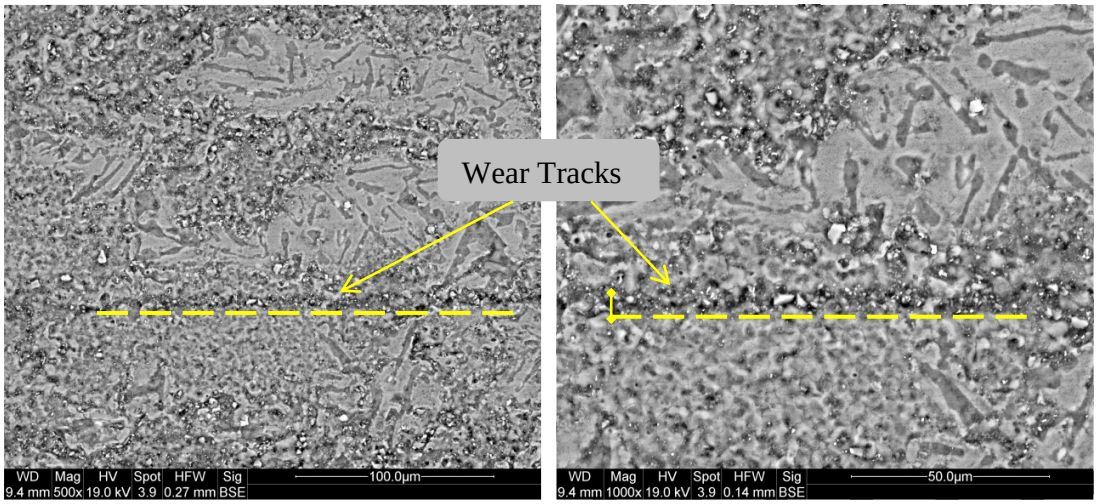

Figure 54. Wear tracks on the surface of P5 sample after 250 m of wear test under 15N load.

4.7 Effect of Dry Lubricant Additives on Tribological and Morphological Behavior of PEO Coatings

Additives can help reduce the coefficient of friction of the coatings if chosen correctly. One of the additives that is used in recent studies as dry solid lubricant is

molybdenum di-sulfide or molybdenite (MoS_2). However there is little study done on adding this lubricant to the electrolyte solution and researching the effects on improvement of tribo-pair dynamic. In this section, influence of MoS_2 addition to the electrolyte on COF and wear rate of the counter surface is investigated. Wear scars on the counter face and wear tracks on the coatings are examined.

Solid lubricants such as graphite and MoS_2 have been used since 1800s. These additives are composed of sheets in hexagonal arrays. Molybdenum atoms are packed between the sheets of sulfur. There is strong bonding force between atoms of molybdenum within a sheet and weak van der Waals bonding force between sulfide atoms of adjacent sheet. This results in low shear stress between the sheets and provides the lubricity properties of MoS_2. Figure 55 shows the crystal structure and coordination geometry of MoS_2.

https://online.ece.nus.edu.sg/cnng/research.html

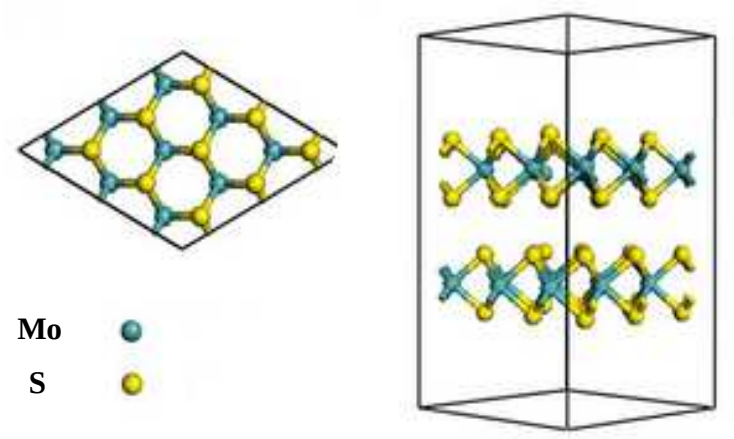

Figure 55. Hexagonal crystal structure and trigonal prismatic coordination geometry of molybdenum sulfide or molybdenite (MoS_2).

From 1950 to 1965, a wide range of powders, salts and oxides were investigated specifically by aerospace industry. It was found that some of these additives would not help solve any friction issues of the desired material due to the lack of chemical reaction between the pair. For instance, MoS_2 powder cannot lubricate glass or titanium but it can react with noble metals such as gold. Addition of MoS_2 to engine oils is common however if the amount exceeds the beneficial value, it can counteract and result in abrasion wear of the engine bearing surface. The goal of this part of the research was to impregnate the PEO coating with MoS_2 by introducing it to the electrolyte composition.

A series of specimens were produced in a solution with addition of MoS_2 as shown in Table 5. Samples were tested under tribo-test for

Table 5. Testing sample matrix for PEO coatings produced in a solution with addition of dry lubricant (MoS_2).

Sample	Solution Composition (gr/lit)	pH	Treatment Time (min)	Output Voltage (v)	Average Vickers Hardness ($HV_{0.2}$)
M1	(6) Na_2SiO_4 + (2) KOH + (10) MoS_2	13	5	480	345
M2	(6) Na_2SiO_4 + (2) KOH (10) MoS_2 + (10) $C_6H_8O_7$	7	5	503	350
M3	(6) Na_2SiO_4 + (2) KOH (10) MoS_2 + (30) $C_6H_8O_7$	3	5	513	325

For ease of blending, MoS_2 powder is dissolved in ethanol first and then added to the solution. Agitator (mixer) is set to high to ensure the uniform dispersion of MoS_2 particles into the electrolyte. Citric acid is also added to the solution at different stages of the treatment for further investigation of the effect of acidity on achieved coatings.

Figure 56 illustrates a comparison between samples' surface average roughness values with and without the use of dry lubricant. As seen, coatings with the MoS_2 have a lower value of average surface roughness compare to the ones without the use of MoS_2.

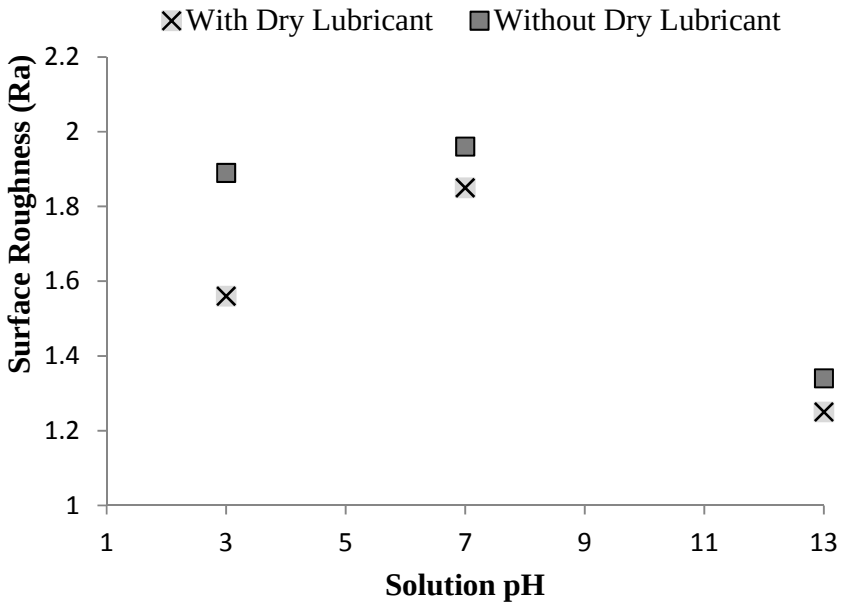

Figure 56. Surface roughness (Ra) values of coatings produced in solution with acidity levels of 3, 7 and 13 with and without the addition of MoS_2 powder to the electrolyte.

COF of these coatings with the added MoS_2 powder to the solution are smaller than the coatings achieved without the addition of MoS_2 powder (P samples). As shown in Figure 57, sample M2 which is created in a solution with pH=7 shows a higher COF (similar to P3) compared to M1 and M3.

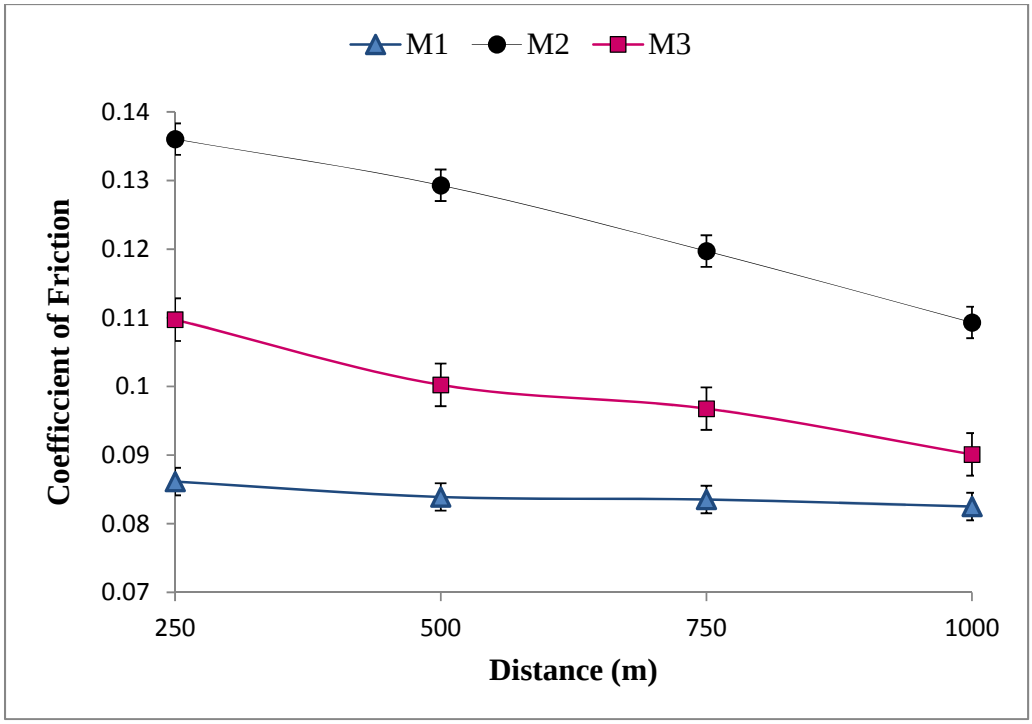

Figure 57. Coefficient of friction versus distance for M1, M2 and M3 samples.

Introducing low friction solid lubricant additive materials into the coating is an alternative way to modify the electrolyte and fabricate coatings with lower coefficient of frictions (COF). Since these additives are non-soluble in the electrolyte, a mechanical agitation or stirring method is needed to keep the solution in suspension mode. During the fabrication process, additives will be drawn onto the surface and then be embedded in to the oxide layer. The success of this approach depends on quantity and concentration of the additives, particle size and uniformity of particles' dispersion in the electrolyte. Addition of excessive amount of solid lubricants to the solution can influence the quality of the coatings for instance, addition of too much MoS_2 particles to the electrolyte resulted in higher roughness and poor adhesion to the substrate. Also too much solid lubricant particles can cause the embedding of excessive amount of lubricant into the

coating and could replace the ceramic composite components that are desirable for wear resistant properties of the coating and leads to failure of the coating under wear conditions. In order to optimize the uniform dispersion of the lubricants in the electrolyte, particles has to get wet beforehand and therefore a dispersant is used. In this study acetone and ethanol were used as dispersant to wet MoS_2 particles.

MoS_2 particles helped with reduction of the friction coefficient of the coating and also the volume loss during the sliding wear. The wear scars on the surface of the coating M1 and P1 were studied using AFM. As shown in Figure 58, the coating with the MoS2 showed a shallower wear scar and less abrasion wear on the surface.

Researchers have tried to incorporate solid lubricants such as graphite [101], [136] and PTFE [74] into the PEO ceramic coatings formed on aluminum alloys as friction reducing agents during wear. Graphite was successfully incorporated in the PEO treatment of 2024Al alloy in a sodium aluminate electrolyte [136] . Addition of 4 gr/L of graphite to the solution has helped to lower the coefficient of friction to 0.09 under a 1N load over a sliding distance of 18 Km. Also addition of Polytetrafluoroethylene (PTFE) nano-particles into the solution mix resulted in excellent self-lubricating property and, improved wear and corrosion resistance of the coatings. Addition of 3 vol.% of PTFE to Na_3PO_4 (10.0 gr/L) and KOH (1.0 gr/L) solution reduced the friction coefficient to less than 0.2 [74].

With MoS_2 **Without MoS_2**

M1 **P1**

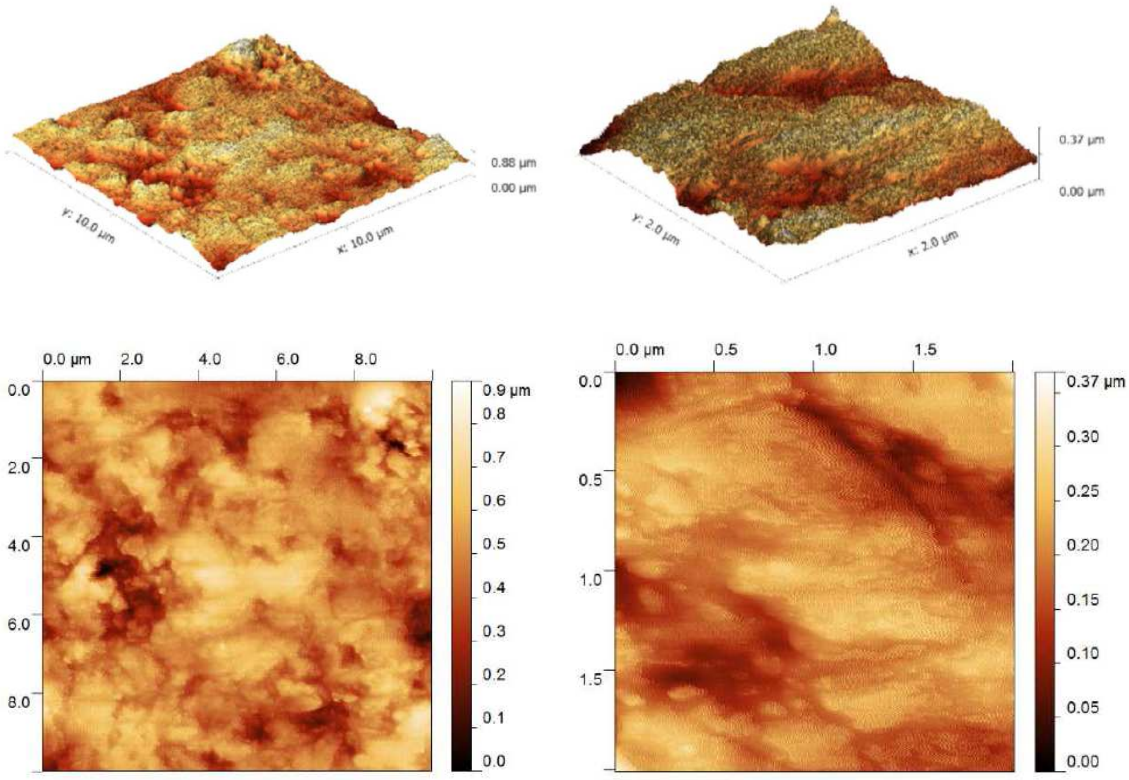

Figure 58. Comparison of AFM analysis of wear tracks on the surface of M1and P1. These two samples were tested under the same condition (lubricated, 1 km, 10mm sliding strokes under 2N load) and have the same roughness values before the running of tribo tester.

CHAPTER 5. ADAPTABILITY OF PEO COATINGS TO COUNTER SURFACE

All the wear tests performed during this research was to investigate the coefficient of friction along with the effect of wear on the coated surface and also to study the counter surface. As described in section 3.8, dependant on the type of counter surface, two types of reciprocating tribo-pairs were studied. A reciprocating ball-on-disk tribo-test machine was modified into a ring-on-disk tribo-test machine by adding a piston ring holder. Since the thermal effects on the wear behavior of the coatings is not a part of this research, sliding velocity was controlled to ensure the boundary lubrication condition and minimize the frictional heating. Considering PEO coatings as a ceramic-based material with poor thermal conductivity, the contact point heat is locked in at the surface of the thin film and does not dissipate easily without the help of the lubricant. At higher speed this may result in thermal fatigue and quenching effects at the point of contact. The ring-on-disk tribo-test involved low level of sliding distance with high rate of reciprocation. Higher rate of reciprocation at fixed low sliding speed can minimize the thermal cycle effect.

In order to find the effect of wear tests on the tribo-system, COF and wear rate are usually used. The changes in the wear track are monitored. Also the volume and mass loss on the counter surface is measured.

The tribo-system of ring-on-disk was used to emulate the piston ring interface with cylinder block wall. The piston ring-cylinder wall interface has been accounted for 20% of the total mechanical friction of engine [137]. Piston rings are usually a set of

three sliding seals (as shown in Figure 59) with the purpose of separating the combustion gases above the piston head from the crankcase environment. The first ring from the top is called the *compression ring* with the function of sealing the expanding combustion gases above the piston. The ring is sealed against the cylinder block wall through the pressure differential that happens during the combustion cycle. During the combustion cycle, pressure increases over the top ring and creates a tight seal pushing the ring outward to the cylinder wall and downward into the piston heads groove. Most of the compression rings are made of cast iron, ductile iron or nitride treated steel alloys. Premium top rings are plasma spray coated with plasma-molybdenum ("Moly" rings) or galvanically plated with chromium. Moly rings have more porosity and are softer compared to chromium rings. Although chromium rings are very durable but due to their high hardness and less oil-carrying capabilities, they can be hard on the cylinder walls [137]. Therefore in recent years, moly rings are replaced the chromium rings and have been used widely. The application of coatings/plating on the piston rings can change the performance expectancy from 50,000 km to almost double the amount and enhance the overall performance and life of the engine [138].

The second ring from the top is called the *wiper ring* and its function is to control the engine oil by wiping the excess oil from the cylinder walls. If the excess oil remains on the walls, it can reach the combustion chamber and creates major engine failure.

The third ring is called an *oil control ring* which removes the oil from the wall. Most of the oil control rings have multiple pieces, two oil ring rails or scrapers on top and bottom and an expander-spacer in the middle.

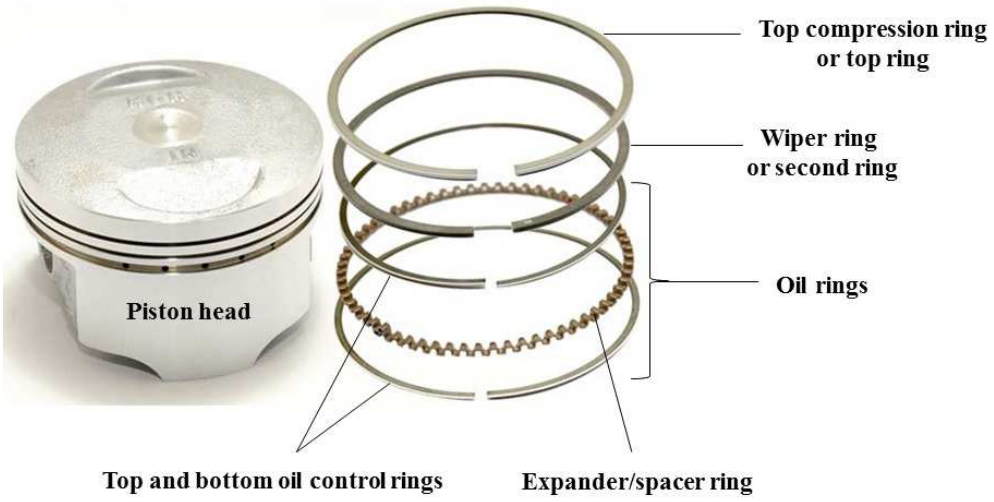

Figure 59. Piston head and piston rings.

Out of three rings mentioned, the top ring is subjected to the highest amount of tension (load) and is exposed to comparably harsher environment (heat). The second ring has shown very similar behavior to the E52100 steel balls. The types of rings tested in this study are moly plasma cast iron top ring and chromium stainless steel second ring.

The oil that was used to keep the wear tests in boundary condition was later analyzed. The oil was smeared on a strip of a copper tape and placed under an environmental SEM (ESEM) at low setting of chamber pressure to guarantee minimum to no oil evaporation. Shavings and residue of the wear of the tribo-pair can be seen in Figure 60. The major elements of the wear debris were determined using EDX analysis. Significant elements were aluminum, silicon, iron and chromium. Aluminum and silicon particles are revealed due to slight wear of PEO coating surface. Iron and chromium particles are detected due to mild wear of the counter surface. As seen in the EDX diagram in Figure 60, copper peaks are spotted since the copper tape was used as the

holder of the oil samples. Carbon and sulfur peaks are also representing the SAE 30 engine oil used in the tribo-tests.

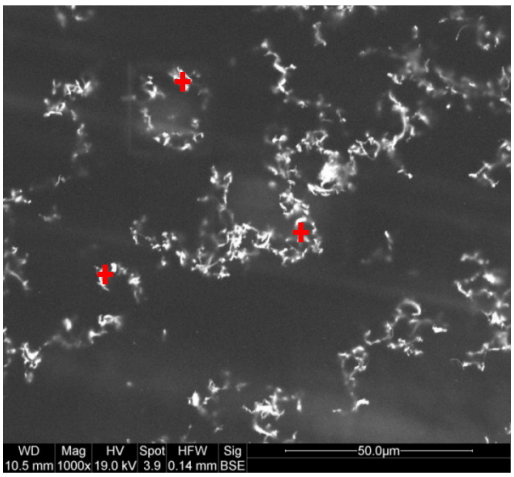

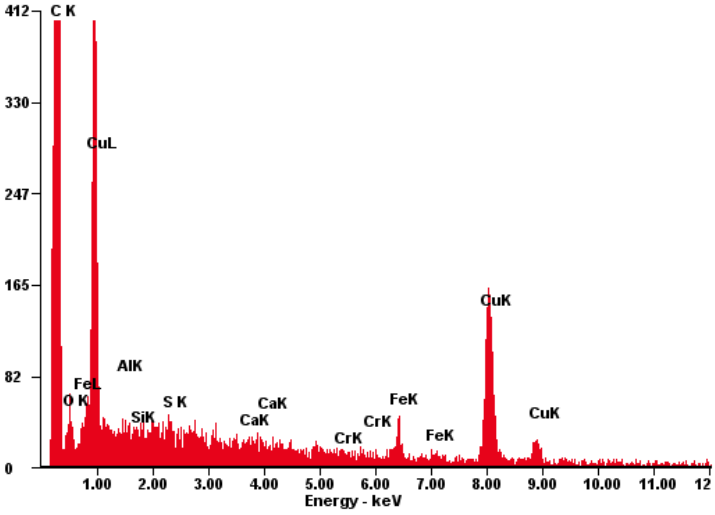

Elements	Wt%	At%
O	1.09	0.95
Al	0.11	0.06
Si	0.13	0.06
Cr	0.25	0.07
Fe	1.34	0.33

Figure 60. Wear debris in the oil under ESEM along with EDX analysis of the wear residue and weight percentage of detected elements.

5.1 Steel Ball as the Counter Surface

Observation on the counter surface for all three tribo-pairs was conducted. For the case of E52100 steel balls, LED illuminated microscope and SEM were used. The volume loss on the steel balls is then calculated using the radius of the wear scar on the counter surface and also the radius of the steel ball. The volume loss value (V_{loss}) is the same as calculating the spherical cap of a sphere (see Equation 20) with geometrical representation as shown in Figure 61.

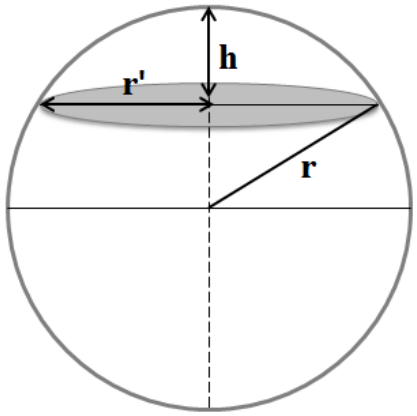

Figure 61. Geometrical representation of the steel ball wear loss volume.

$$\boldsymbol{V_{loss} = \frac{\pi}{6}\left(3\,r'^{2} + h^{2}\right)h} \qquad \textbf{Equation 20}$$

when *r* and *r'* are radius of the steel ball and circular plain radius of the wear scar respectively and *h* is the height of loss volume.

According to Figure 44, wear scars on the counter surface of tribo-pairs with smoother PEO coatings are significantly smaller than the rougher surfaces. Figure 62

shows the results of the volume loss on the counter surface of the E52100 steel balls at different roughness values. As shown there is a correlation between the volume loss on the counter surface and surface roughness of the PEO coated samples. Higher roughness means higher volume loss on the counter surface. However the volume loss variation on the counter surface for coatings with Ra=0.3 to Ra=0.7 is considerably small.

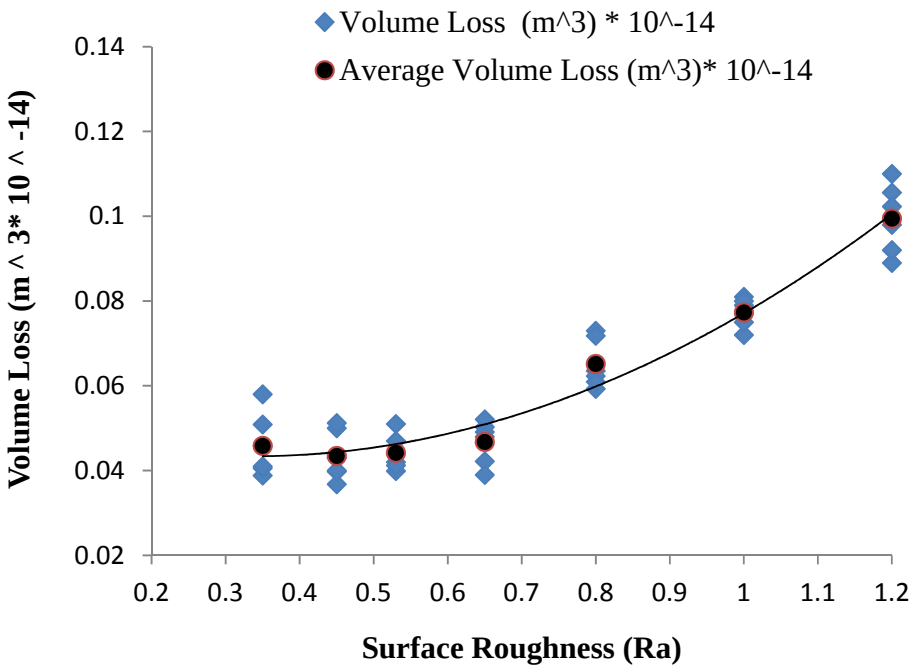

Figure 62. Volume loss on the counter surface versus average surface roughness of coatings.

Observation of the surface of the coatings and also the counter surface after each test helps to understand the wear behavior of the tribo-pair. So far, the wear tracks on the surface and wear scars on the counter surface of steel balls are analyzed under SEM and LED illuminated microscope respectively and were each plotted against coefficient of friction values. The overall performance of the tribo-pair depends on the adaptability of the sliding surfaces. Figure 63 is plotted to facilitate the objective. Wear track width of

the PEO coatings were measured with the metrology tools of SEM system. In a tribo system, a small wear track with minimum wear rate on the counter surface is desired. P1 shows a slight wear on the counterface and minimal wear tracks on the coating. This coating showed significant resistant against wear even at higher roughness values and has the lowest coefficient of friction values among other coatings. Counter surface used against P1 can be seen in Figure 64. Mild wear scars were seen on this coating with minimum of mass loss on the counter surface. Since the wear rates are very similar in value, the tribo-pair with less damage to the surface of the coating would be a potential candidate. P1 is the one in this case.

Looking at the wear rate of the counterface for P2 coating as well as the very high COF value, this coating showed abrasion wear with ploughing effects on the counterface and mild wear on the film surface. P3 exhibited minimal wear on the counterface with high values of COF which resulted in predominant wear tracks on the coating surface. P4 coating illustrated the highest value of wear rate on the counterface in comparison to other samples with mild wear of the surface. Both P3 and P4 samples are worst case scenarios due to their high wear rate of the counterface and wider wear track on the coating surface. Figure 65 shows P4 after 1 km of sliding distance. As shown the surface has wide planes of material removed. This type of wear could be a ploughing wear mechanism that happens due to plastic deformation and can cause a change in topography of the wear surface. Excess material that usually accumulates at the edges of the plough plane was polished off due to the abrasive wear. Also there are particles belonging to the PEO coating that are attached on to the surface and can create another mechanism of wear called adhesion wear. These coatings cannot be desirable due to the excessive mass

loss of the counterface. Figure 66 also shows the wear scar on the counter surface used against P5. The wear mechanism seems to be an abrasion wear with minimum of adhesion.

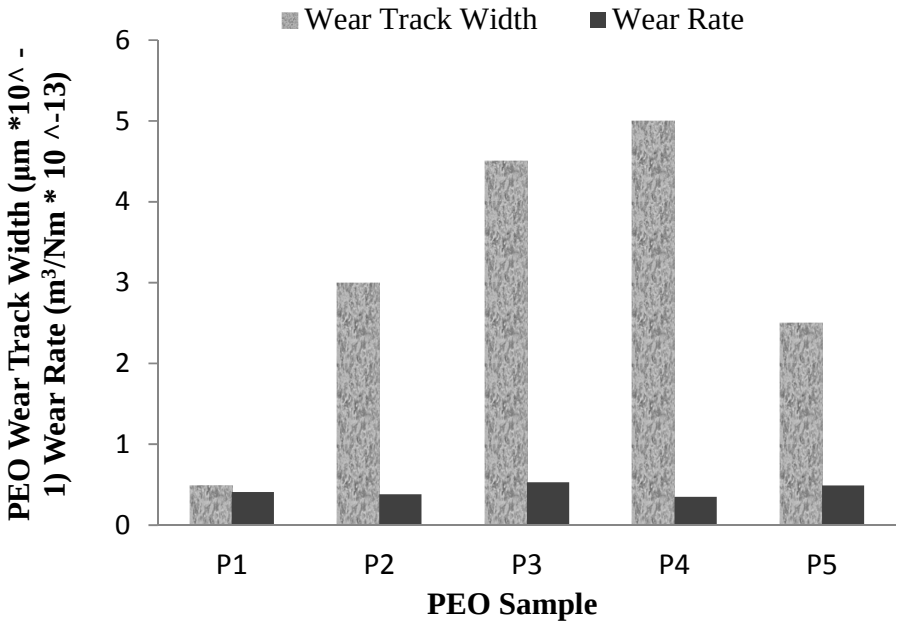

Figure 63. Effect of wear on the tribo-pair: wear track width on the surface and counter surface wear rate

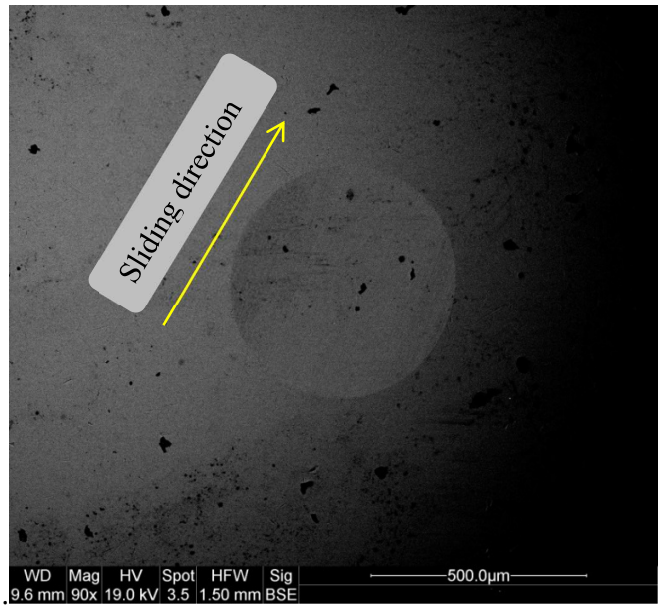

Figure 64.. Steel ball counter surface wear scar against P1 sample.

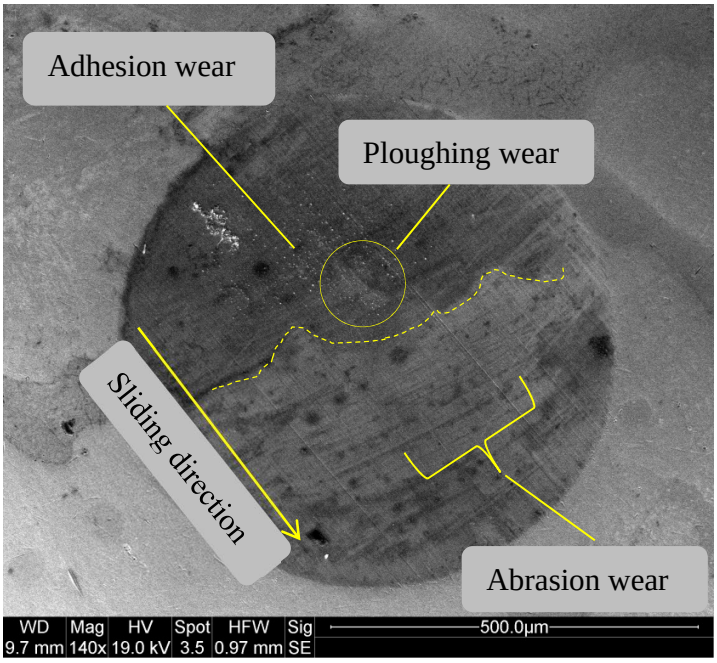

Figure 65. Steel ball counter face wear scar and wear mechanism effects against P4 sample.

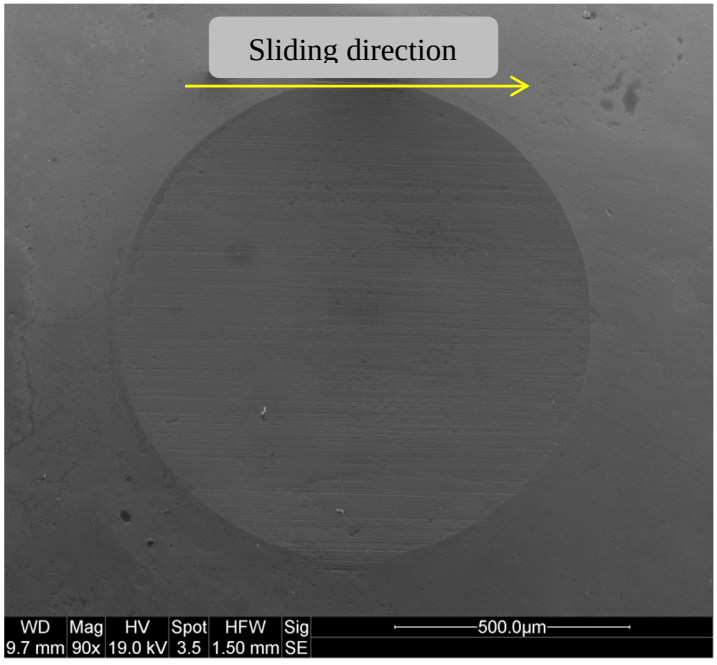

Figure 66. Steel ball Counter surface wear scar against P5 sample.

Figure 67 has the images of wear scars on the steel balls against P1, P3 and P5. The scouring marks on the steel balls are an indication of abrasive wear mechanism during the sliding. Darker regions on the wear scars can be the sign of oxidation of the steel and also particle transfer from the surface of the coating during the sliding wear. During the initial stages of sliding, the counter surface acts like a sander on the surface and flattens the peak points on the surface. The residue of the worn particles can cause further damage to the surface by abrasion wear mechanism and it might also adhere to the surface and acts like a cutting tool on the surface. Counter surface samples were also analyzed with EDX to identify any adhesion and wear residue transfer from the coating surface. These particles usually appear like spherical black particles as marked on the SEM image in Figure 68.

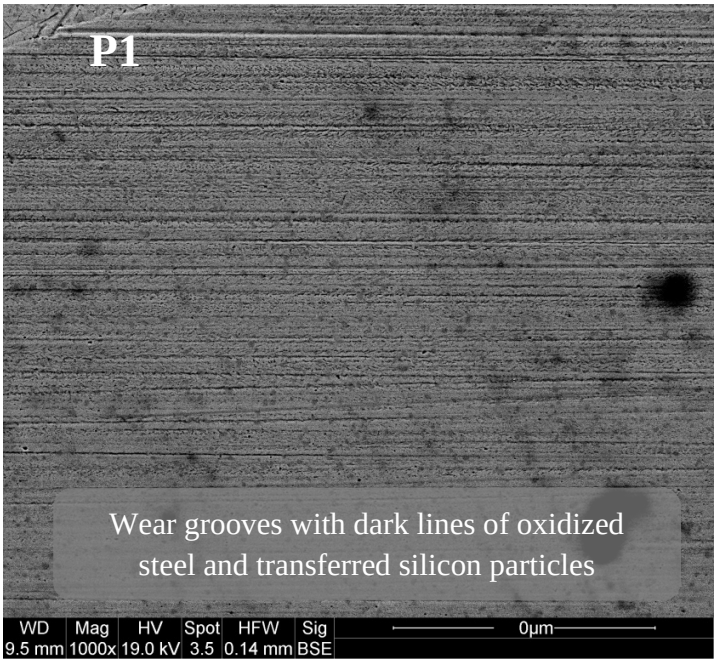

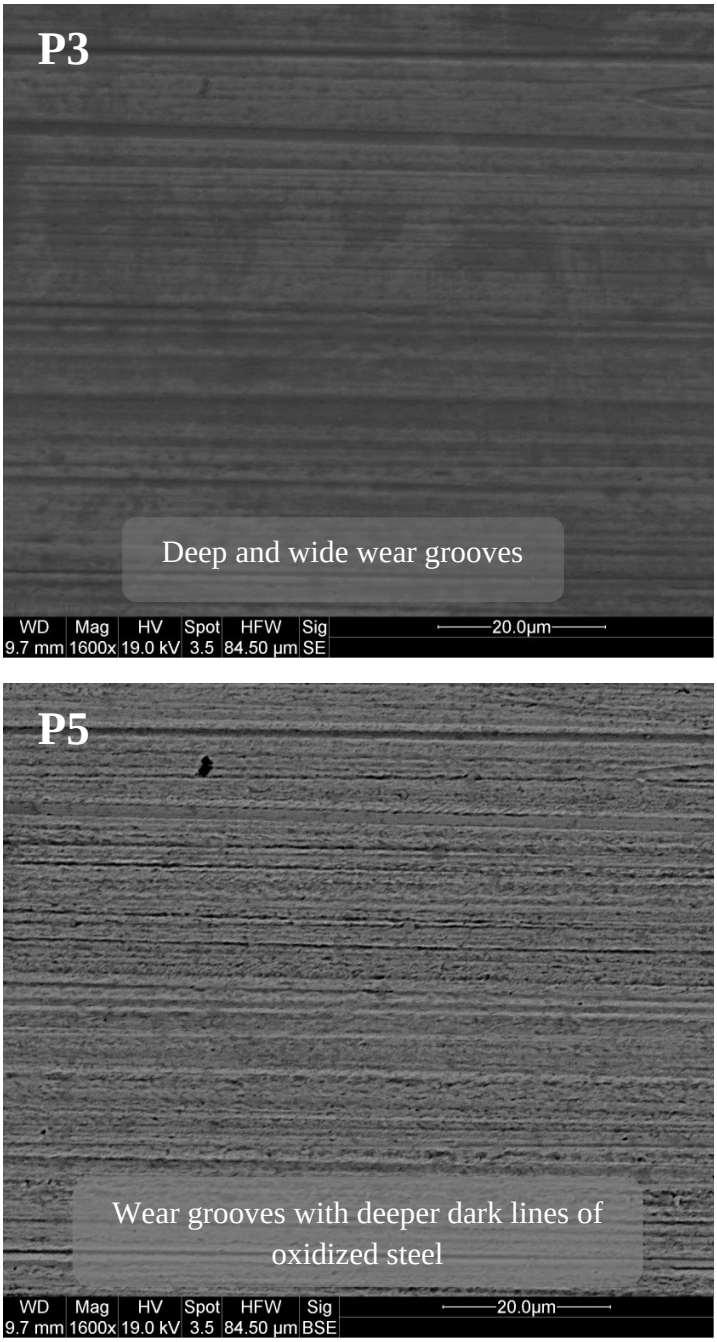

Figure 67. Wear scars on the surface of steel balls against P1, P3 and P5 coating.

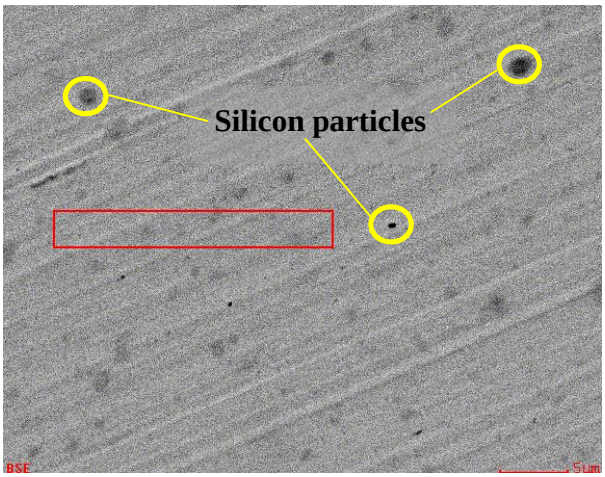

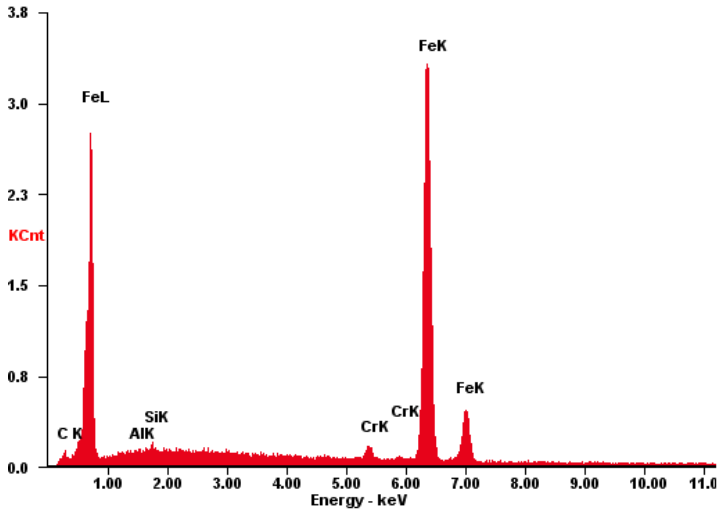

Elements	Wt%	At%
C	5.00	19.56
Al	0.05	0.09
Si	0.39	0.66
Cr	1.56	1.41
Fe	93.00	78.29

Figure 68. SEM images of the steel ball E52100 after 1 km of sliding distance under 2N load against PEO coating along with elemental analysis of the counter surface.

As two surfaces are sliding against each other, the contacting asperities deform elastically and later even plastically. This can create a partial welding effect of these asperities on the contact region. The shearing of this adhesive region produces wear particles and debris. This can cause the transfer of the material from one surface to another. If this transfer is severe, it is called scuffing. This form of wear is known as adhesive wear. As shown in Figure 67 black spots on the counter surface are the result of adhesive wear and according to the elemental analysis, it is a combination of aluminum and silicon and perhaps debris and oil contaminants that welded on to the counter surface during the sliding. The existence of oxygen in the elemental analysis for the steel ball and second ring is a sign of either alumina transfer or oxidation of steel which adds another problematic wear mechanism: oxidative wear mechanism. Oxidative wear mechanism can cause severe abrasive wear due to increasing of the hardness of the adhered particles. The harder the counter surface is, the more ridges and grooves on the wear track can be seen. On the surface of the coating, a wear track is apparent and it seems the higher asperities are flattened by the steel ball and this is another reason to the abrasion wear and damage of the counter surface.

5.2 Piston Rings as Counter Surface

Coefficient of friction was measured for the piston rings counter surfaces against coatings produced in three variable pH values of the electrolyte: acidic solution with pH=3, neutral solution with pH=7 and basic solution with pH=13. COF curves are plotted for all three counter surface materials for comparison study in Figure 69. For all three samples, the tribo-pair with the top ring as the counter surface which is a moly plasma

coated ring has a higher coefficient of friction compared to the 2nd ring which is a chromium plated stainless steel. Compared to steel balls, coefficient of friction against the 2nd piston ring showed lower coefficient of friction values.

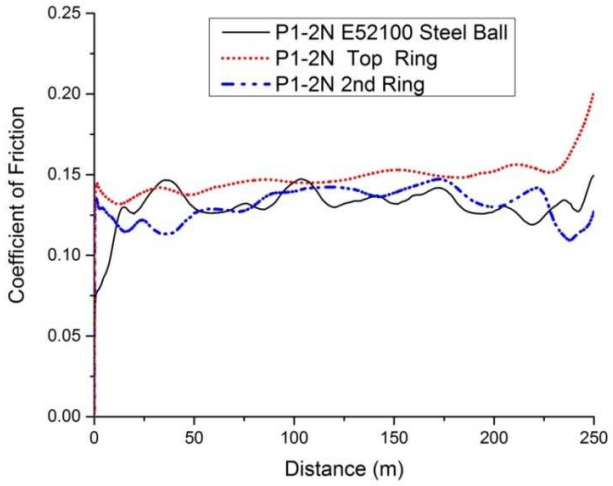

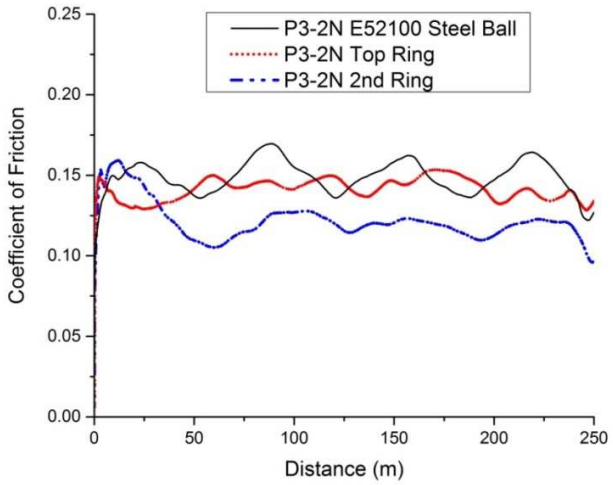

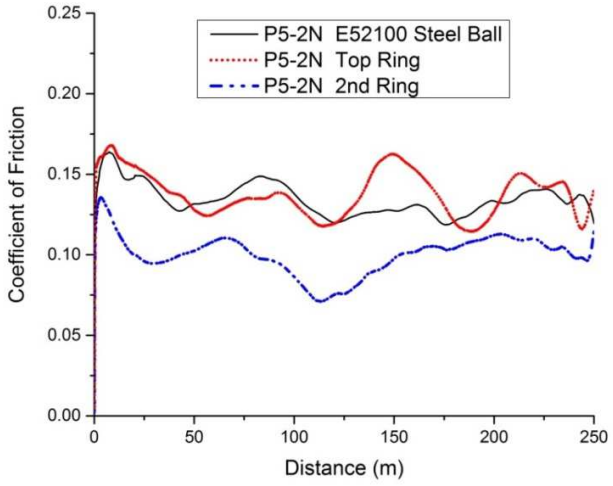

Figure 69. Coefficient of friction diagrams for coatings produced in three pH values of the electrolyte: Sample P5 produced in acidic solution with pH=3, sample P3 produced in neutral solution with pH=7 and sample P1 produced in basic solution with pH=13.

The average coefficient of friction is plotted for each counter surface in Figure 70. According to the results shown in Figure 67 and 70, P3 sample would be a less desirable choice since the wear rate is high, the wear track on the coating is wider than others and coefficient of friction is higher in comparison.

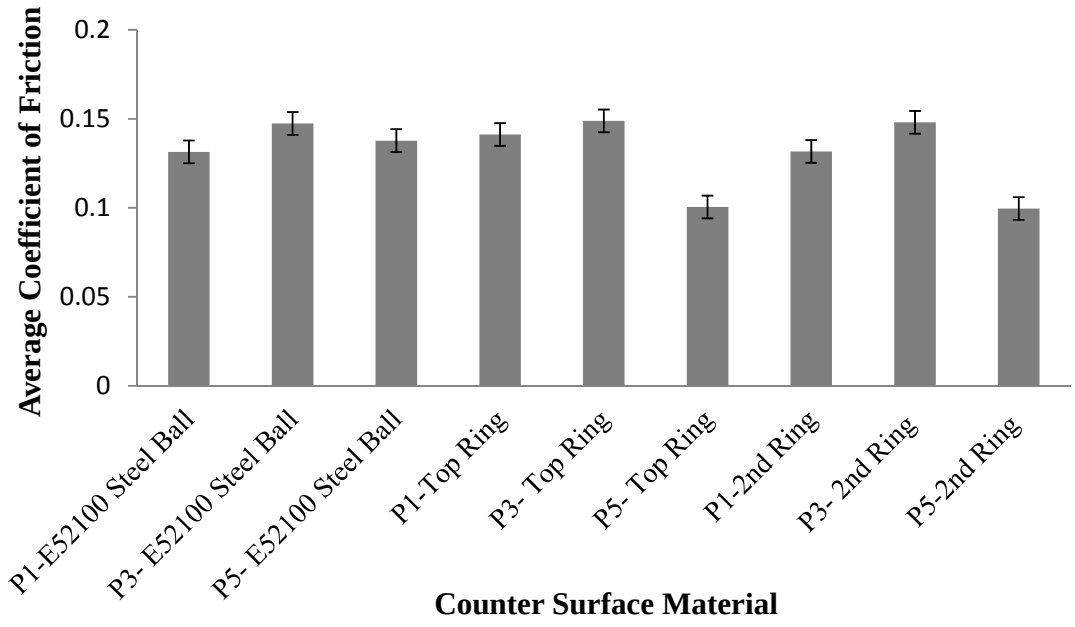

Figure 70. Average COF against different counter surface materials.

Based on the experimental tests done on this research, samples produced in electrolyte solutions with pH=7 (neutral) does not show a good adaptability to the counter surface. The average roughness of the treated samples are comparably high (around 1.96 μm) and needs further post treatment or post polishing or mild honing after the production. P1 and P5 are still good candidate for the cylinder wall application. P5 has shown lower coefficient of friction values specifically against the top and second ring. Wear scars on the top ring is presented in Figure 71. Moly ring paired with P1 has milder wear grooves with residue transition of the coating. The moly coating on the piston ring underwent mild abrasion wear. The elemental analysis of the top ring as shown in Figure 72, showed traces of PEO coating on the surface of the coating. For the case of P3, it is possible that the cracking or brittle fracture happened as well and the reason could be the

detachment of particle from the sliding surfaces that can create cutting effects on the surface or plough out particles. Stress concentration at the point of contact can increase due to the abrasive detached particles. Weak plastic deformation ability can cause removal of the larger piece from the surface and that is due to surface brittleness. These fractures usually start with micro cracks. Cracks will then propagate not only on the surface plane but also deeper into the thickness of the coating.

In case of the second piston ring, the wear grooves are apparent and some are deep. The almost mirror shine texture of the surface is due to the chromium element. This coating has shown many cracks on the surface almost like a broken mirror. This is an experimental error that happened due to faulty ring or brittle fracture on the surface of the coating when it was in contact with concentrated stress. An SEM image with the elemental analysis is represented in Figure 73. The elemental results are very similar to E52100 steel ball. Cross sectional study on the wear tracks of the PEO coatings also could help to understand the behavior of the tribo-pair. So far P1 has shown promising results, good coefficient of friction, milder wear grooves on both sides. Figure 74 has the cross sectional SEM of P1 after the tribotest against the moly ring.

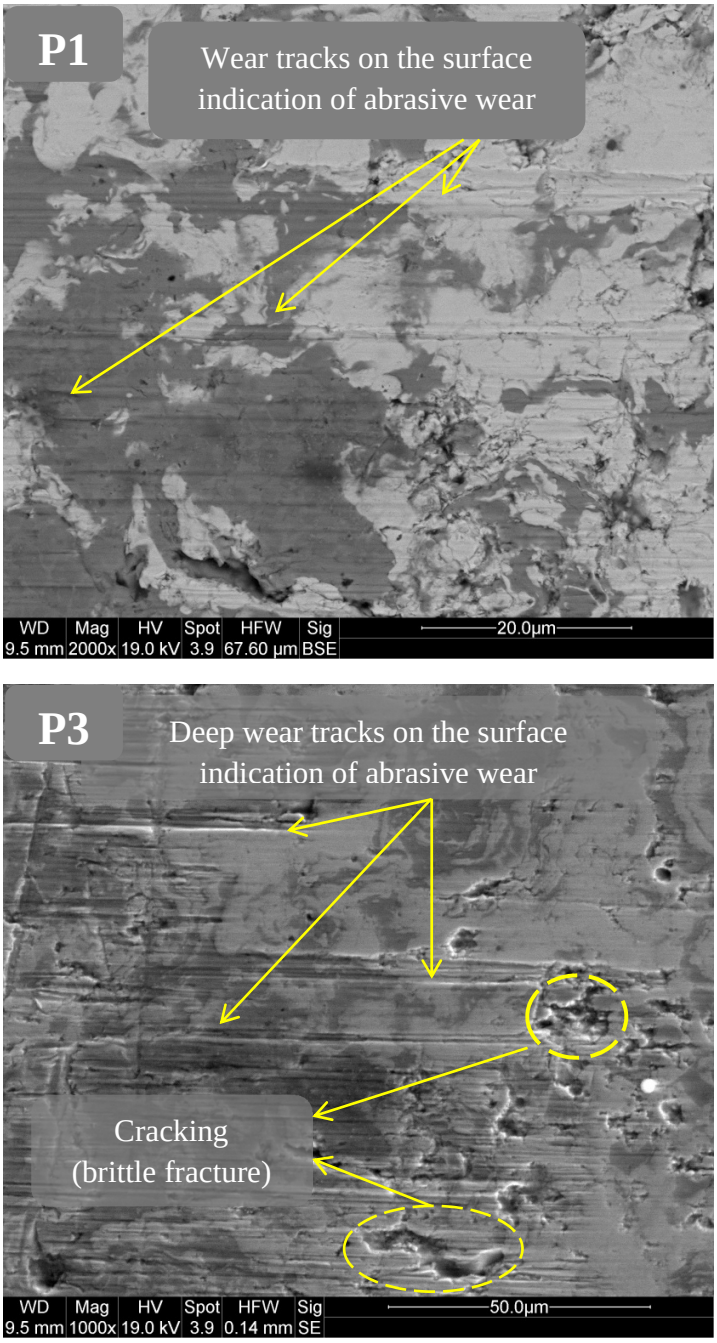

Figure 71. Wear scars on the surface of the top piston ring segments against P3 coating.

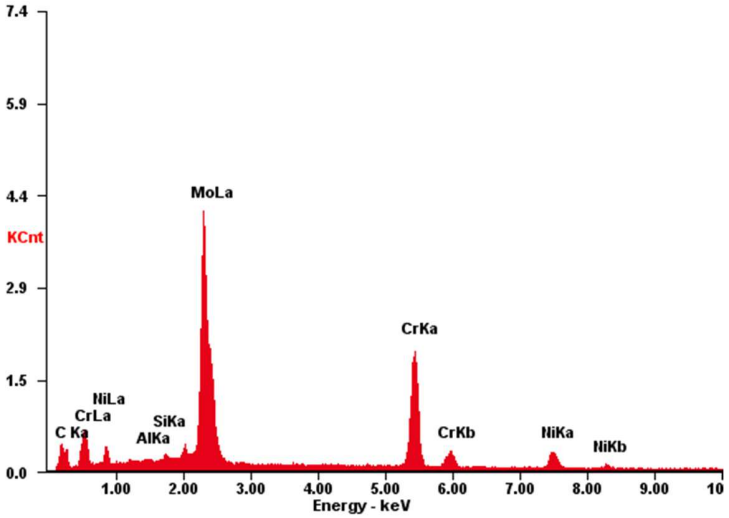

Elements	Wt%	At%
C	14.96	50.35
Al	0.17	0.26
Si	0.48	0.70
Mo	45.17	19.03
Cr	29.79	23.17
Ni	9.42	6.49

Figure 72. Elemental analysis of the moly ring after 1 km of sliding test against P3.

In order to compare the three tribo-pairs and understand the effect of counter surface material on the wear behavior of the coatings, specific wear rate percentage is used by weighing each counter surface before and after the tribo test with a high resolution scale. The main approach to measure the volume loss or mass loss of the segments of the piston rings is to weigh each segment before and after and consider the difference as the volume loss however the problem is the material transfer and the wear residues that can sit on top of the surface or inside the grooves or even welded on to the surface of the piston rings. The other approach would be to use atomic force microscopy (AFM) with the processing ability of measuring the wear scars. Figure 75 shows the wear

scars on the top ring against P1 sample after 1 km of siding under lubricated condition respectively.

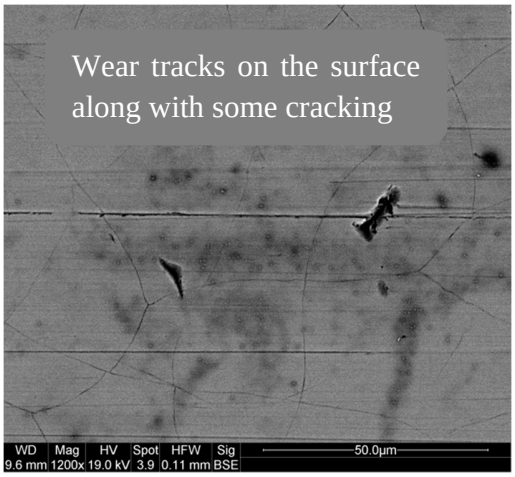

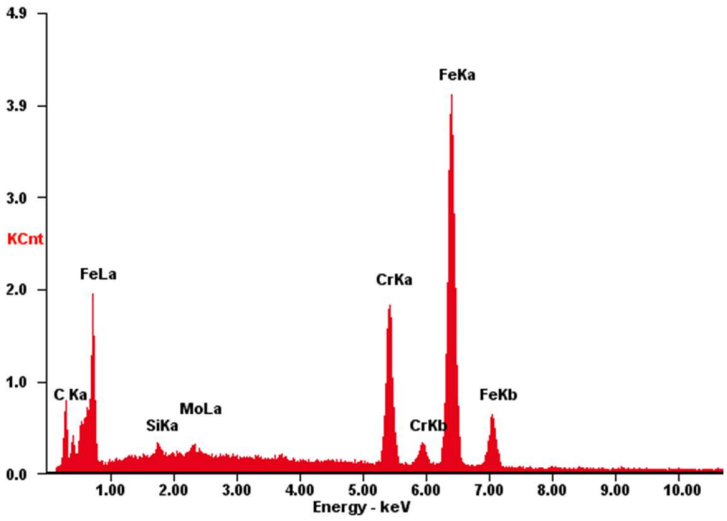

Elements	Wt%	At%
C	17.72	46.83
O	3.48	6.90
Si	2.62	2.96
Cr	0.26	0.16
Fe	75.92	43.15

Figure 73. Wear scars on the surface of the second piston ring segments against P1 coating. along with elemental analysis (EDX).

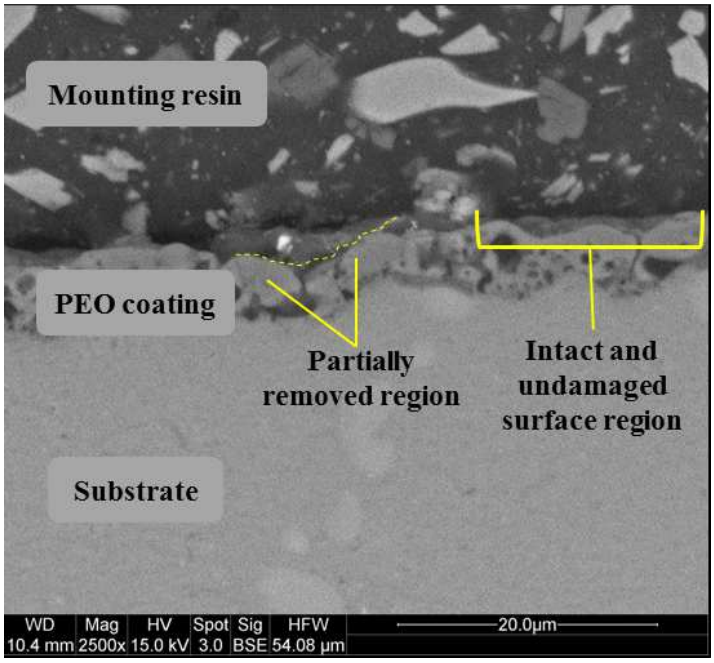

Figure 74. Cross sectional SEM image of wear track region on P3 surface against moly piston ring.

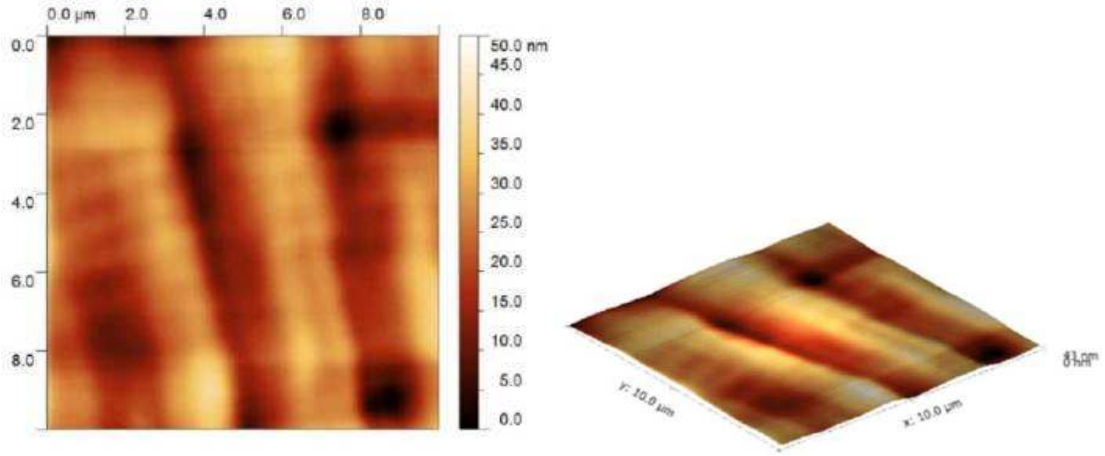

Figure 75. Top and side view of the wear scar on the top ring after sliding of 1 km against P1 sample observed using AFM.

CHAPTER 6. CONCLUSIONS, CONTRIBUTIONS AND PROPOSED FUTURE WORK

Plasma Electrolytic Oxidation process has shown promising results in terms of improving the wear resistance of the substrate, decreasing the wear rate and minimizing the volume loss of the counter surface.

6.1 Summary

Researchers and industry pioneers are still in search for a high quality coating with optimized wear resistant behavior that can reduce the total weight of the car, demonstrate good mechanical properties and provide longer wear life. PEO treatment has drawn enough attention to be a potential candidate for cylinder bore application. The goal of this research was to understand the effect of different factors on synthesis, morphology and wear behavior of these coatings.

Coating process configurations and solution composition are dictating factors for the coating morphology. The effect of electrical parameters, solution type and solution acidity on coating production, morphology structure and tribological behavior was studied in details. Surface metrology of the coatings was also conducted with more focus on average roughness and average slope of surface profiles. Surface properties such as oil retention and load carrying were studied on different samples. Adaptability of the optimized coatings to the counter surface was also investigated.

Electrical parameters such as current density or current polarity have a great impact on the characteristics of the achieved PEO coatings. Coatings achieved at unipolar

pulsed direct current (UPDC) are generally more homogenous with a uniform distribution of pores and micro cracks however denser coatings are achieved under bipolar pulsed direct current (BPDC) with less porosity. These coatings have shown better corrosion resistance in acidic environments compared to UPDC coatings. Using the right electrolyte composition along with the appropriate electrical parameters can guarantee a consistent coating formation on the substrate and may also improve the tribological behavior of PEO coatings. Therefore they are arrays of various recipes used in industry that are trademarked [119].

PEO coatings in general grow thicker with longer treatment time and faster with higher current densities however it is important to choose the right setting for current density and treatment time based on application. Higher current density caused rougher surface with higher percentage of porosity on the coatings used in this study. Also higher current density means higher growth rates. Coatings in silicate based solutions can grow with the rate of 30% per each increment of 0.2- 0.3 A/cm^2 increase in current density. Current polarity mode has also an effect on coating structure and performance. Bipolar coatings need up to 8% higher finishing voltage and that can be a concern for industrial application since the application should be financially and technically feasible. Other problems with bipolar coatings specifically in longer treatment times are the possibility of having more dominant surface defects and/or highly imperforated structure on the surface. Also the increase in hardness values in bipolar coatings, is much higher than the unipolar coatings and depend on the application, it might not be beneficial. Around 12% of increase in hardness values was seen comparing bipolar and unipolar coatings. All the electrical parameters involved such as current polarity and current density can change the

behavior of the coatings. In fact, the root cause of many surface defects such as non-homogeneity, loose depositions and excessive micro-cracks is due to the wrong settings of electrical parameters.

Surface roughness influences the coefficient of friction and the tribo-system behavior. It is important to know which roughness parameter can give a better prediction of the coating performance. Correlation coefficient of surface kurtosis, surface skewness, average roughness and average slope of the surface were found in this study. Average roughness has a positive correlation with coefficient of friction meaning the increase in one creates an increase in the other. This is not the case for surface kurtosis and skewness. The correlation was found to be weak and negatively related. Kurtosis values between 0 and 1.5 generally showed lower values of coefficient of friction. Negative kurtosis showed higher coefficient of friction. Same trend was observed for surface skewness. Surface skewness values below -0.5 created more friction between the sliding surfaces. Average slope showed a weak positive correlation with coefficient of friction. It is concluded that lower average slopes (around 0.5 and less) are desirable.

Solution composition in any electrolysis process is a dictating factor since it can play with the involved chemical reaction such as anodic oxidation and hydrogen evolution. Solution composition can have an influence on the structure of the coatings. Coatings defects such as non-homogeneity, excessive porosity and micro-crack propagations can be overcome by using the right type of electrolyte mixture or adjusting the concentration of each salt. Among many solutions and combinations used in this study, silicate based solutions has shown good adaptability to counter surface along with a more predictable performance. Acidity of the solutions has an impact on the coating

thickness and morphology of the oxide layer. More acidic solutions showed faster growth rate of 1.5 μ/min compared to 1 μ/min for a typical solution with pH=13. Coatings produced in more acidic solutions caused larger wear scars on the counter surface and this can be due to the increase of hardness values in more acidic solutions.

The comparison between two lubrication modes and their effect on coefficient of friction values showed that important role of surface reservoirs/pores in retention of lubricant. This is essential specifically when lubrication is not readily available on the surface like the start-stop mode of the engine or at the start of the engine when the oil on the surface is at its minimum amount. Therefore, surface texture can help to keep a smear of oil on the surface and prevent wear.

Load bearing capacity of the PEO coatings were tested under 2, 8 and 15 N of applied load and it was concluded that higher load can affect the coefficient of friction for the coatings produced in acidic solution. The load increase has less effect on coefficient of friction values of coatings produced in alkaline solutions than the acidic solution. No wear marks were detected on the surface of the coating produced in alkaline solutions up to 8N load. At 15N load shallow wear tracks were seen on the surface of the coating. Coatings produced in acidic solution showed wider and deeper wear tracks in comparison. The reason can be the hardness impact of the coatings on the tribo-pair behavior. Another reason can be the higher porosity of these coatings that has shown less load bearing capability. This might be due to the load distribution at the contact surface.

Solid lubricant can reduce friction force. MoS_2 powder was added to the solution to study the effect of solid lubricant on coefficient of friction. Up to 35% of improvement

was noticed on coefficient of friction values. It is however important to use an optimum concentration of MoS_2. By trial and error the amount of 10 gr/lit worked for this study. Addition of excessive amount to the solution can cause undesirable rough coatings with poor adhesion properties.

Counter surface wear rate and volume loss were also investigated for E52100 steel balls and piston rings. Top compression rings made of plasma sprayed Molybdenum also known as Moly ring along with second compression ring of typical chromium steel were used for this study. It is concluded that higher roughness cause more volume loss on the surface. Different types of wear were detected based on the material of the tribo-pair. Most wear grooves on the steel balls were mild. Deeper wear grooves showed traces of silicon and aluminum particles as a sign of adhesion wear. Both rings showed similar trends as steel balls. Abrasive wear was determined as the wear system for Moly rings. Brittle fracture and cracking was also detected but not the dominant wear system of the tribo-pairs. P1 (coating without the dry lubricant in the solution) and M1 (coating with the dry lubricant in the solution) samples showed very little wear on the counter surface and also mild wear on the surface of the coatings.

With the presented results, it can be concluded that PEO has the ability to resist wear and can be optimized further in order to be used on engine cylinder walls. Any failure in tribological behavior of the cylinder block can result into immediate failure of the engine or can cause excessive use of engine oil. Non-uniform formation of the coatings on the cylinder walls can cause wrong fitting of the piston rings in the cylinder and exposure of the coating materials, solution or the achieved oxide layer to any contamination during the process can also cause corrosion and pitting effects on the

cylinder walls. Further investigation is required to optimize the process and performance of the coatings for mass production of cylinder blocks. Table 6 summarizes the research objectives and achievement involved in this study.

Table 6. Research objectives and achievements.

Research Objectives	Research Achievements
Study the feasibility of PEO coatings for cylinder bore application	Coatings have demonstrated good wear resistance under 2N and 8N loads over 1 km of sliding distance.
Study the adaptability of PEO coatings to the existing piston rings	Most of the coatings did not show any signs of wear, delamination or ploughing effect. Additional load up to 15N did cause deeper wear grooves on the coatings. Wear scars on the counter surface were deeper in the absence of dry lubricant.
Conduct a comparison analysis between PTWA and PEO coatings in terms of application and cost	PEO coatings in comparison with PTWA are more cost efficient and are easier to implement.

6.2 Research Contribution

This research is conducted with the goal of studying the tribological behavior of the PEO coated Al319 aluminum alloy for engine applications. Based on the literature survey conducted for this research, following contributions are made to the field of study:

1- A series of electrolytes are used in development of PEO coated samples. Nowhere in the literature these electrolytes were compared and analysed in details for aluminum alloys.

2- The effect of current polarity on coating morphology and coefficient of friction is studied in details with three major groups of electrolytes (Aluminate, Silicate and Phosphate). There are studies done on the polarity effect on the synthesis of PEO coatings [73], [76], [89] and [90] using mainly the silicate and aluminate electrolytes. These studies are mainly done on thicker coatings and there is no evidence of comparison between solution compositions and polarity effects on thin coatings. The effect of the current polarity on wear behavior of thin PEO coatings mainly under 10 μm of thickness, produced in the major groups of electrolytes is hard to find.

3- Effect of MoS_2 dispersion in the electrolyte as a solid lubricant on tribological behavior of the coatings and counterface wear behavior are also studied. Use of this additive helps with enhancing the performance of the coatings.

4- PEO coatings are mainly produced in alkaline based electrolyte with pH values around 12 and 13. By addition of citric acid to the electrolyte mixture, the influence of pH values of the electrolyte on coatings' morphology and tribology was studied. It was concluded that more acidic environment facilitate faster transition of ions between the electrode and creates the sparks in a shorter period of time.

5- The study of adaptability of PEO coatings for engine application is also scarce. The use of piston rings as the counter surface for the tribo-pair, analysis of the coefficient of frictions and wear loss on the rings have not been attempted before.

6.3 Proposed Future Work

This research encountered some barriers to mimic the tribo-pair of cylinder wall and piston rings. For instance the effect of temperature raise inside the engine block on the tribological behavior of the tribo-pair was not studied due to the lack of proper testing instrument. The effect of substrate properties such strength or silicon weight percentage may also effect the tribological behavior of the coatings. This research could have benefited the study of nano-hardness of the coatings at different conditions in order to better compare the achieved coatings. Measurement of nano-hardness of the coatings was attempted however reliable data could not collected due to porosity. Nano-composition on the birth layer of the coating could also help with better understanding the influence of the doping elements on coating structure and phase analysis. The study of adhesive and adhesion forces between the substrate and the coatings can also investigate the PEO coating performance and its threshold to failure/delamination more precise.

Also with all the variable involved in this study and the results and relations presented, a comprehensive design of experiment can now be conducted which can investigate more specific correlations between the input, controlled and output variables.

6.4 Research Trends on PEO

PEO-treated lightweight metals have been studied widely however there are still shortcomings that could be addressed. The main concern would be to decrease the coefficient of friction values along with minimizing the wear loss on the counter surface. Many techniques are being considered but needs deeper research. Some of these techniques are gathered in this section:

1. Incorporating specific nanoparticles into the coating by adding them to the electrolyte: Monoclinic zirconia nanoparticles are considered as good candidates for improving the coatings produced n phosphate solution. This technique can improve the coating hardness and wear resistance. Matykina *et al.* [95] produced coatings on aluminum in a solution mixture of Na_2SiO_3, KOH and ZrO_2 particles. Hardness values were improved from 500 typical $HV_{0.05}$ to 1700 $HV_{0.05}$. However the effect of the addition of ZrO_2 on surface roughness and wear properties of the coating is unknown.
2. Using "*duplex coating*": This refers to two stages of PEO treatment either at different current settings or in different solutions that can enhance the coefficient of friction of the coatings. This is fairly a new horizon in optimization of PEO coatings and need further investigation.
3. Impregnation: Porosity of the coatings provides surface reservoirs that may be filled with small sized solid lubricant particles after the treatment. In this method, prepared PEO samples are immersed into an aqueous solid lubricant suspension and placed into a vacuum oven. Once the samples are heated, solid lubricant particles would set into micro pores and micro cracks. Under proper vacuum oven situation with adequate treatment time and temperature setting, a compact layer can be formed on top of the coatings that would improve the surface wear resistant quality [109]. PTFE (Polytetrafluoroethylene) has been used as a solid lubricant recently in many studies. PTFE has a very low COF against any solids ($0.1< COF_{PTFE} < 0.2$) [139]. In a study Wang et al [122] used vacuum impregnation of PTFE for coatings on LY12 aluminum alloy.

Using a vacuum oven with the pressure setting of less than 0.005 torr, samples were heated for 24 hours at 200 °C. Samples were tested over long periods of sliding test against steel balls. COF and wear rate of the coatings and counterface were improved remarkably. COF of PEO coatings changed to almost half the value (~ 0.13) compared to un-treated PEO coatings. PTFE powders need to be milled to a desirable size range. A size range of 100 to 170 nm for the PTFE powder particles was suggested. Further study is needed to investigate the effect of PTFE size on the COF and also the viability of using the impregnation method for engine block applications. One concern is the adhesion of PTFE particles to the coating and also the effect of loose PTFE particles in the oil mixture on performance of the engine.

4. Spraying a top layer on achieved PEO coatings: Spraying compared to impregnation is much simpler and lower in cost. Most of the studies on spray coating of PEO coatings have been conducted on titanium alloys (specifically Ti6Al4V) [140], [141]. Solid lubricants such as graphite and PTFE are sprayed over the PEO coated parts through a spraying gun with spraying pressure of 4 atmospheres followed by solidification treatment at 180 °C for 15 minutes. Tribo test results showed reduction of COF up to 20% of a typical PEO treated sample. Another study combined the PTFE method with an over spray of a solvent-based aerosol suspension [142]. PTFE over spray can reduce the COF from 0.8 to 0.2. Mentioned concerns about impregnation techniques exist for using this method for engine applications.

5. Integrating PVD and/or CVD treatment as a step to the PEO treatment: This method can improve the mechanical and tribological properties of aluminum alloys. PEO treatment was combined with arc ion plating technique (AIP) [143] on 2Al2 aluminum alloy. Thickness of alumina coating was roughly 40 μm with addition of 3-4 μm coating of TiN. Samples that were coated under 0.5 Pa pressure and at – 80 V exhibited high hardness and wear resistance with good load bearing properties.
6. Integrating Plasma immersion ion implantation to PEO treatment: Nie *et al.* [144] integrated PEO treatment with plasma immersion ion implantation (PI^3) technique for treatment of BS Al-6082 aluminum alloy. PI^3 is a surface treatment technique that implants the desired ion into the coating by exposing or immersing the substrate to/into the plasma. Thickness of alumina coating was 50-60 μm and the DLC layer achieved by PI^3 was around 2-3 μm. This study compared the results of tribotest on uncoated samples, PEO coated samples, DLC coated samples and DLC/PEO coated samples. The later has shown the lowest COF along with minimum wear rate of the coating.

It should be noted that all the modification treatment methods would add an extra step to the coating process which adds to the overall cost of the finished piece. What is apparent is that each application needs a specific set of parameters that could dictate the properties of the achieved coating and enhance the performance of the sliding distances.

REFERENCES

[1]. S. Chu and A. Majumdar, 'Opportunities and challenges for a sustainable energy future', Nature, vol. 488, no. 7411, pp. 294-303, 2012.

[2]. G. Maxwell and S. Drummond, Automotive Industry: Technical Challenges, Design Issues and Global Economic Crisis,. New York: Nova Science Publishers, 2010, pp. 22-58.

[3]. S. Beer, J. Klodt, H. Moding, B. Sommer, O. Vogt, H. Kohler, U. Bredenbreuker and J. Niehues, Aluminum Cylinder Blocks. Munich, Germany: Verlag Moderne Industrie, 2006, pp. 70-90.

[4]. H. Yamagata, The science and technology of materials in automotive engines. Cambridge: Woodhead Pub. and Maney Pub. on behalf of The Institute of Materials, Minerals & Mining, 2005.

[5]. S. Nixon, The Invention of the Automotive Industry (Karl Benz and Gottlieb Daimler). Country Life Ltd., 1936.

[6]. D. Hardcastle, The Rover V8 Engine, 2nd ed. Foulis Motoring, 1995.

[7]. A. Okada, Innovative materials for automotive industry. New York: Nova Science Publishers, 2010.

[8]. W. Crouse, Automotive engine design. New York: McGraw-Hill, 1970.

[9]. Kolbenshcmidt Pierburg Group, 'High-pressure Die Cast and Squeeze Cast Cylinder Blocks Made of Aluminum', KS Aluminum Technologies, Neckarsulm, Germany, 2007.

[10]. Cylinder components Properties, applications, materials. Berlin, Germany: MAHLE Group, 2010.

[11]. K. Bobzin, F. Ernst, K. Richardt, T. Schlaefer, C.Verpoort and G. Flores, 'Thermal spraying of cylinder bores with the Plasma Transferred Wire Arc process', Surface and Coatings Technology, vol. 202, no. 18, pp. 4438-4443, 2008.

[12]. D. Askeland and P. Phulee, Essentials of materials science and engineering. USA: Nelson- Thomson Canada Ltd., 2004.

[13]. J. Kaufman and E. Rooy, Aluminum alloy castings properties. Materials Park, OH: ASM International, 2004.

[14]. J. Hirsch, B. Skrotzki and G. Gottstein, Aluminum alloys. Weinheim: Wiley-VCH, 2008.

[15]. J. Jorstad, 'The Hypereutectic Al-Si Die Casting Alloy Used in the Vega Engine Block', Modern Casting, vol. 60, no. 4, pp. 59-64, 1971.

[16]. R. Green, 'Die Casting the Vega Engine Block', Cast Engineering, vol. 14, no. 5, pp. 12-26, 1970.

[17]. H. Kurita, H. Yamagata, H. Arai and T. Nakamura, 'Hypereutectic Al-20%Si Alloy Engine Block Using High-Pressure Die-Casting', SAE Technical Paper, 2004.

[18]. R. Zieris, G. Langner, L. Berger, S. Nowotny, E. Beyer and D. Dresden, 'Investigation of AlSi Coatings Prepared by Laser-assisted Atmospheric Plasma Spraying of Internal Surface of Tubes', 2004, pp. 651-654.

[19]. A. Macke, B. Schultz and P. Rohatgi, 'Metal matrix: Composites offer the automotive industry an opportunity to reduce vehicle weight, improve performance', Advanced materials & processes, vol. 170, no. 3, pp. 19 -23, 2012.

[20]. S. Prasad and R. Asthana, 'Aluminum Metal-Matrix Composites for Automotive Applications: Tribological Considerations', Tribology Letters, vol. 17, no. 3, pp. 445-453, 2004.

[21]. M. Ebisawa, T. Hara, T. Hayashi and H. Ushio, 'Production Process of Metal Matrix Composite (MMC) Engine Block', SAE Technical Paper, 1991.

[22]. T. Takami, M. Fujine, S. Kato, H. Nagai, A. Tsujino, Y. Masuda and M. Yamamoto, 'MMC All Aluminum Cylinder Block for High Power SI Engines', SAE Technical Paper, 2000.

[23]. J. Shackelford and R. Doremus, Ceramic and glass materials. New York: Springer, 2008.

[24]. K. Funtani and K. Kurosawa, 'Composite coatings improve engines', Advanced materials & processes, vol. 146, no. 6, pp. 27-29, 1994.

[25]. K. Funatani, L. Kurosawa, P. Fabiyi and M. Puz, 'Improved engine performance via use of nickel ceramic composite coatings (NCC coat)', SAE Technical Paper, 1994.

[26]. C. Liue, J. Wang and Y. Peng, 'Ni--SiC Composite Plating', MRL Bull. Res. Updated to MRS bulletin, vol. 4, no. 1, pp. 31-34, 1990.

[27]. D. Mattox, Handbook of physical vapor deposition (PVD) processing. Norwich, N.Y.: William Andrew, 2010.

[28]. P. Ernst and G. Barbezat, 'Thermal spray applications in powertrain contribute to the saving of energy and material resources', Surface and Coatings Technology, vol. 202, no. 18, pp. 4428-4431, 2008.

[29]. K. Bobzin, F. Ernst, J. Zwick, T. Schlaefer, D. Cook, K. Kowalsky, K. Bird, D. Gerke, R. Sharp, K. Raab and S. Lindon, 'Thermal spraying of cylinder bores with

the PTWA internal coating system', in Technical Conference of the ASME Internal Combustion Engine Division, 2008, pp. 4428-4431.

[30]. J. Vetter, G. Barbezat, J. Crummenauer and J. Avissar, 'Surface treatment selections for automotive applications', Surface and Coatings Technology, vol. 200, no. 5-6, pp. 1962-1968, 2005.

[31]. G. Barbezat, 'Thermal Spray Coatings for Tribological Applications in the Automotive Industry', Advanced Engineering Materials, vol. 8, no. 7, pp. 678-681, 2006.

[32]. K. Bobzin, F. Ernst, J. Zwick, T. Schlaefer, D. Cook, K. Nassenstein, A. Schwenk, F. Schreiber, T. Wenz, G. Flores and M. Hahn, 'Coating Bores of Light Metal Engine Blocks with a Nanocomposite Material using the Plasma Transferred Wire Arc Thermal Spray Process', Journal of Thermal Spray Technology, vol. 17, no. 3, pp. 344-351, 2008.

[33]. R. Hazen and R. Jeanloz, 'WÃ¼stite (Fe 1-x O): A review of its defect structure and physical properties', Rev. Geophys., vol. 22, no. 1, p. 37, 1984.

[34]. G. Barbezat, 'Low-Cost High-Performance Coatings Produced by Internal Plasma Spraying for the Production of High Efficiency Engines', in Thermal Spray 2003: Advancing the Science and Applying the Technology, 2003, pp. 139 - 142.

[35]. L. Rama Krishna, K. Somaraju and G. Sundararajan, 'The tribological performance of ultra-hard ceramic composite coatings obtained through microarc oxidation', Surface and Coatings Technology, vol. 163-164, pp. 484-490, 2003.

[36]. J. Feng Su, X. Nie, H. Hu and J. Tjong, 'Friction and counterface wear influenced by surface profiles of plasma electrolytic oxidation coatings on an aluminum A356

alloy', Journal of Vacuum Science & Technology A: Vacuum, Surfaces, and Films, vol. 30, no. 6, p. 061402, 2012.

[37]. Casting and Design Performance. ASM International, 2009.

[38]. A. Wilde, 'Ceramic-base surface treatment technology for light-metal alloys: a unique, innovative surface treatment technology provides an alternative to current traditional less environmentally friendly coating methods.(Ceramics & Refractories/Insulation)', Industrial Heating, 2005.

[39]. L. Rodriguez, P. Sundaram, E. Rosim-Fachini, A. Padovani and N. Diffoot-Carlo, 'Plasma electrolytic oxidation coatings on ɣTiAl alloy for potential biomedical applications', J. Biomed. Mater. Res., vol. 102, no. 5, pp. 988-1001, 2013.

[40]. N. Godja, W. Hansal, R. Mann, C. Kleber and S. Hansal, ' Pulsed plasma electrolytic oxidation processes for aeronautical applications and their technical application', Transactions of the IMF, vol. 91, no. 6, pp. 321-329, 2013.

[41]. S. Shrestha, 'Microstructural and thermo-optical properties of black Keronite PEO coating on aluminum alloy AA7075 for spacecraft materials applications', European Space Agency, 2006.

[42]. S. Shrestha, A. Merstallinger, D. Sickert and B. Dunn, 'Some preliminary evaluations of black coating on aluminum AA2219 alloy produced by plasma electrolytic oxidation (PEO) process for space applications', in Proceedings of the 9th International Symposium on Materials in a Space Environment, Noordwijk, Netherlands, 2003, pp. 57-65.

[43]. S. Suresh, K. Pavankumar, N. Rameshbabu and K. Venkateswarlu, 'Effect of plasma electrolytic surface treatment on the corrosion characteristics of the Ti-6Al-

4V in acidic, industrial and marine environments', in International Conference on Advances in Metallic Materials and Manufacturing Processes for Strategic Sectors, ICAMPS 2012, 2012, pp. 677-682.

[44]. R. Wood, 'Erosion-corrosion interactions and their effect on marine and offshore materials', Wear, vol. 261, no. 9, pp. 1012-1023, 2006.

[45]. D. Hendricks and T. Kolody, 'Treated structural components for a cooking appliance', WO2009062815 A2, 22-May-2009.

[46]. N. Sluginov and J. Russ. Phys. Chem. Soc., vol. 12, no. 1-2, p. 193, 1880.

[47]. L. Gruss and W. Mc Neil, 'Anodic spark reaction products in aluminate, tungstate and silicate solutions', Electrochem. Technol, vol. 1, no. 9, pp. 283-287, 1963.

[48]. G. Markov and G Markova, 'A method of forming anodes of electrolytic condensers', vol. 32, p. 63, 1976.

[49]. P. Kurze, W. Krysmann and H. Schneider, 'Application Fields of ANOF Layers and Composites', Cryst. Res. Technol., vol. 21, no. 12, pp. 1603-1609, 1986.

[50]. A Yerokhin, X. Nie, A. Leyland, A. Matthews and S. Dowey, 'Plasma electrolysis for surface engineering', Surface and Coatings Technology, vol. 122, no. 2-3, pp. 73-93, 1999.

[51]. J. Curran, S. Hutchins and S. Shrestha , 'Process for the enhanced corrosion protection of valve metals', WO2010112914 A1, 07-Oct-2010.

[52]. J. Bovee, 'Oxidizing electrolytic method for obtaining ceramic coating at surface of metal', CN 100482867 C, 02-Nov-2001.

[53]. E.L. Schmeling, B. Roschenbleck and M.H. Weidemann, Electro Chemical Engineering Gmbh, 'Anodic oxidation with borate, sulfate, phosphate, chloride and fluoride anions-low alkali bath', US4978432 A, 18-Dec-1990.

[54]. D.E. Bartak, B. E. Lemieux and E.R. Woolsey, Technology Applications Group, 'Hard anodic coating for magnesium alloys', US5470664 A, 28-Nov-1995.

[55]. J. Hyner and R.A. Michelson, Whyco Chromium Company Inc., 'Method of electrodepositing an alloy of tin, cobalt and a third metal and electrolyte therefor', US 3966564 A, 1976.

[56]. Micro-plasmic Corporation, 'Forming electrolyte bath; immersing bodies in bath; connecting bodies to electrode connected to phase of multiphase alternating current (ac) power supply; imposing potential between bodies and establishing micro-plasmic discharge', US 6197178 B1, 2001.

[57]. X. Nie and J. Zhang, 'Thin oxide coating and process', CA 2556869 C, 2015.

[58]. X. Nie and J. Zhang, 'Method of forming an oxide coating with dimples on its surface', US 20080248214 A1, 2008.

[59]. X. Shigang, 'Effect of current density on al alloy micro-plasma oxidation', J. Mater. Sci. Technol, vol. 17, no. 6, pp. 657-660, 2001.

[60]. F. Monfort, A. Berkani, E. Matykina, P. Skeldon, G. Thompson, H. Habazaki and K. Shimizu, 'A Tracer Study of Oxide Growth during Spark Anodizing of Aluminum', J. Electrochem. Soc., vol. 152, no. 6, p. C382, 2005.

[61]. P. Kurze, 'Coating by Anodic Oxidation with Spark Discharge', Metalloberflaeche vol. 40, no. 12, pp. 539-540, 1986.

[62]. X. Nie, A. Leyland, H. Song, A. Yerokhin, S. Dowey and A. Matthews, 'Thickness effects on the mechanical properties of micro-arc discharge oxide coatings on aluminum alloys', Surface and Coatings Technology, vol. 116-119, pp. 1055-1060, 1999.

[63]. E. Aver'yanov, 'Plasma processes in metal anodic oxidation', Elektron. Obrab. materialov, no. 1, pp. 60-63, 1994.

[64]. A. Rakoch, I. Bardin, V. Kovalev and T. Avanesyan, 'Microarc oxidation of light constructional alloys: Part 1. Main notions on the microarc oxidation of light constructional alloys', Russ. J. Non-ferrous Metals, vol. 54, no. 4, pp. 341-344, 2013.

[65]. C. Grubbs, 'Anodizing of aluminum', Metal Finishing, vol. 100, pp. 463-478, 2002.

[66]. D. Garcia-Alonso, N. Serres, C. Demian, S. Costil, C. Langlade and C. Coddet, 'Pre-/During-/Post-Laser Processes to Enhance the Adhesion and Mechanical Properties of Thermal-Sprayed Coatings with a Reduced Environmental Impact', Journal of Thermal Spray Technology, vol. 20, no. 4, pp. 719-735, 2011.

[67]. A. Tran, M. Hyland, T. Qiu, B. Withy and B. James, 'Effects of Surface Chemistry on Splat Formation During Plasma Spraying', Journal of Thermal Spray Technology, vol. 17, no. 5-6, pp. 637-645, 2008.

[68]. J. Abbott, 'Hardcoat Anodizing : Low-Cost Coating for Aluminum', Advanced Materials and Processes, vol. 146, no. 3, pp. 29-33, 1994.

[69]. Q. Li, J. Liang and Q. Wang, Plasma Electrolytic Oxidation Coatings on Lightweight Metals, 1st ed. Modern Surface Engineering Treatments, InTech, 2013, pp. 75-94.

[70]. F. Walsh, C. Low, R. Wood, K. Stevens, J. Archer, A. Poeton and A. Ryder, 'Plasma electrolytic oxidation (PEO) for production of anodized coatings on lightweight metal (Al, Mg, Ti) alloys', Trans. Inst. Met. Finish, vol. 87, no. 3, pp. 122-135, 2009.

[71]. L. Snizhko, A. Yerokhin, A. Pilkington, N. Gurevina, D. Misnyankin, A. Leyland and A. Matthews, 'Anodic processes in plasma electrolytic oxidation of aluminum in alkaline solutions', Electrochimica Acta, vol. 49, no. 13, pp. 2085-2095, 2004.

[72]. Wiscohitec Co., Ltd., 'Composition for plasma electrolytic oxidation (PEO) treatment of magnesium alloy products', US 8337689 B2, 2012.

[73]. G. Lv, H. Chen, W. Gu, L. Li, E. Niu, X. Zhang and S. Yang, 'Effects of current frequency on the structural characteristics and corrosion property of ceramic coatings formed on magnesium alloy by PEO technology', J. Mater. Process. Technol., vol. 208, no. 1, pp. 9-13, 2008.

[74]. J. Guo, L. Wang, S. Wang, J. Liang, Q. Xue and F. Yan, 'Preparation and performance of a novel multifunctional plasma electrolytic oxidation composite coating formed on magnesium alloy', Journal of Materials Science, vol. 44, no. 8, pp. 1998-2006, 2009.

[75]. J. Curran and T. Clyne, 'The thermal conductivity of plasma electrolytic oxide coatings on aluminum and magnesium', Surface and Coatings Technology, vol. 199, no. 2-3, pp. 177-183, 2005.

[76]. R. Hussein, P. Zhang, X. Nie, Y. Xia and D. Northwood, 'The effect of current mode and discharge type on the corrosion resistance of plasma electrolytic

oxidation (PEO) coated magnesium alloy AJ62', Surface and Coatings Technology, vol. 206, no. 7, pp. 1990-1997, 2011.

[77]. Y. Han, S. Hong and K. Xu, 'Porous nanocrystalline titania films by plasma electrolytic oxidation', Surface and Coatings Technology, vol. 154, no. 2-3, pp. 314-318, 2002.

[78]. H. Wu, X. Lu, B. Long, X. Wang, J. Wang and Z. Jin, 'The effects of cathodic and anodic voltages on the characteristics of porous nanocrystalline titania coatings fabricated by microarc oxidation', Materials Letters, vol. 59, no. 2-3, pp. 370-375, 2005.

[79]. Y. Li, B. Yao, B. Long, H. Tian and B. Wang, 'Preparation, characterization and mechanical properties of microarc oxidation coating formed on titanium in Al(OH)3 colloidal solution', Applied Surface Science, vol. 258, no. 13, pp. 5238-5243, 2012.

[80]. E. Matykina, P. Skeldon and G. Thompson, 'Fundamental and practical evaluations of PEO coatings of titanium', International Heat Treatment and Surface Engineering, vol. 3, no. 1-2, pp. 45-51, 2009.

[81]. W. Zhang, K. Du, C. Yan and F. Wang, 'Optimization of electrolyte for preparation of Si-Incorporated PEO film on pure titanium’, Corrosion Science and Protection Technology, vol. 21, no. 6, pp. 511-516, 2009.

[82]. W. Xue, Q. Zhu, Q. Jin and M. Hua, 'Characterization of ceramic coatings fabricated on zirconium alloy by plasma electrolytic oxidation in silicate electrolyte', Materials Chemistry and Physics, vol. 120, no. 2-3, pp. 656-660, 2010.

[83]. L. Wang, X. Hu and X. Nie, 'Deposition and properties of zirconia coatings on a zirconium alloy produced by pulsed DC plasma electrolytic oxidation', Surface and Coatings Technology, vol. 221, pp. 150-157, 2013.

[84]. S. Cengiz and Y. Gencer, 'The characterization of the oxide based coating synthesized on pure zirconium by plasma electrolytic oxidation', Surface and Coatings Technology, vol. 242, pp. 132-140, 2014.

[85]. Y. Cheng and F. Wu, 'Plasma electrolytic oxidation of zircaloy-4 alloy with DC regime and properties of coatings', Transactions of Nonferrous Metals Society of China, vol. 22, no. 7, pp. 1638-1646, 2012.

[86]. Y. Wang, Z. Jiang and Z. Yao, 'Formation of titania composite coatings on carbon steel by plasma electrolytic oxidation', Applied Surface Science, vol. 256, no. 20, pp. 5818-5823, 2010.

[87]. Y. Wang, Z. Jiang and Z. Yao, 'Preparation and properties of ceramic coating on Q235 carbon steel by plasma electrolytic oxidation', Current Applied Physics, vol. 9, no. 5, pp. 1067-1071, 2009.

[88]. Z. Wu, Y. Xia, G. Li and F. Xu, 'Structure and mechanical properties of ceramic coatings fabricated by plasma electrolytic oxidation on aluminized steel', Applied Surface Science, vol. 253, no. 20, pp. 8398-8403, 2007.

[89]. A. Yerokhin, A. Shatrov, V. Samsonov, P. Shashkov, A. Pilkington, A. Leyland and A. Matthews, 'Oxide ceramic coatings on aluminum alloys produced by a pulsed bipolar plasma electrolytic oxidation process', Surface and Coatings Technology, vol. 199, no. 2-3, pp. 150-157, 2005.

[90]. F. Jaspard-Mecuson, T. Czerwiec, G. Henrion, T. Belmonte, L. Dujardin, A. Viola and J. Beauvir, 'Tailored aluminum oxide layers by bipolar current adjustment in the Plasma Electrolytic Oxidation (PEO) process', Surface and Coatings Technology, vol. 201, no. 21, pp. 8677-8682, 2007.

[91]. C. Wei, X. Tian, S. Yang, X. Wang, R. Fu and P. Chu, 'Anode current effects in plasma electrolytic oxidation', Surface and Coatings Technology, vol. 201, no. 9-11, pp. 5021-5024, 2007.

[92]. J. Curran, H. Kalkancib, Y. Magurovac and T.W. Clynea, 'Mullite-rich plasma electrolytic oxide coatings for thermal barrier applications', Surface and Coatings Technology, vol. 201, no. 21, pp. 8683-8687, 2007.

[93]. R. Khan, A. Yerokhin, T. Pilkington, A. Leyland and A. Matthews, 'Residual stresses in plasma electrolytic oxidation coatings on Al alloy produced by pulsed unipolar current', Surface and Coatings Technology, vol. 200, no. 5-6, pp. 1580-1586, 2005.

[94]. S. Shrestha and B. Dunn, 'Advanced plasma electrolytic oxidation treatment for protection of lightweight materials and structures in a space environment', Advanced Surface Treatment, 2007.

[95]. E. Matykina, R. Arrabal, P. Skeldon and G. Thompson, 'Optimization of the plasma electrolytic oxidation process efficiency on aluminum', Surf. Interface Anal., vol. 42, no. 4, pp. 221-226, 2009.

[96]. E. Matykina, R. Arrabal, A. Mohamed, P. Skeldon and G. Thompson, 'Plasma electrolytic oxidation of pre-anodized aluminium', Corrosion Science, vol. 51, no. 12, pp. 2897-2905, 2009.

[97]. Y. Guan and Y. Xia, 'Correlation between discharging property and coatings microstructure during plasma electrolytic oxidation', Transactions of Nonferrous Metals Society of China, vol. 16, no. 5, pp. 1097-1102, 2006.

[98]. P. Zhang, X. Nie, H. Henry and J. Zhang, 'Preparation and tribological properties of thin oxide coatings on an Al383/SiO2 metallic matrix composite', Surface and Coatings Technology, vol. 205, no. 6, pp. 1689-1696, 2010.

[99]. L. Wang and X. Nie, 'Silicon effects on formation of EPO oxide coatings on aluminum alloys', Thin Solid Films, vol. 494, no. 1-2, pp. 211-218, 2006.

[100]. X. Nie, L. Wang, E. Konca and A. Alpas, 'Tribological behavior of oxide/graphite composite coatings deposited using electrolytic plasma process', Surface and Coatings Technology, vol. 188-189, pp. 207-213, 2004.

[101]. G. Lv, H. Chen, W. Gu, W. Feng, L. Li, E. Niu, X. Zhang and S. Yang, 'Effects of graphite additives in electrolytes on the microstructure and corrosion resistance of Alumina PEO coatings', Current Applied Physics, vol. 9, no. 2, pp. 324-328, 2009.

[102]. F. Jin, P. Chu, H. Tong and J. Zhao, 'Improvement of surface porosity and properties of alumina films by incorporation of Fe micrograins in micro-arc oxidation', Applied Surface Science, vol. 253, no. 2, pp. 863-868, 2006.

[103]. R. Hussein, X. Nie and D. Northwood, 'Influence of process parameters on electrolytic plasma discharging behavior and aluminum oxide coating microstructure', Surface and Coatings Technology, vol. 205, no. 6, pp. 1659-1667, 2010.

[104]. M. Treviño, N. F. Garza-Montes-de-Oca, A. Pérez, M. A. L. Hernández-Rodríguez, A. Juárez, and R. Colás, 'Wear of an aluminum alloy coated by plasma

electrolytic oxidation', Surface and Coatings Technology, vol. 206, no. 8-9, pp. 2213-2219, 2012.

[105]. H. Eiliat and X. Nie, 'Tribological behavior of plasma electrolyte oxidation coating on Al 319 aluminum alloy', SAE Tech. Pap., 2012.

[106]. R. Khan, A. Yerokhin, X. Li, H. Dong and A. Matthews, 'Surface characterization of DC plasma electrolytic oxidation treated 6082 aluminum alloy: Effect of current density and electrolyte concentration', Surface and Coatings Technology, vol. 205, no. 6, pp. 1679-1688, 2010.

[107]. W. Gu, G. Lv, H. Chen, G. Chen, W. Feng and S. Yang, 'Characterization of ceramic coatings produced by plasma electrolytic oxidation of aluminum alloy', Materials Science and Engineering: A, vol. 447, no. 1-2, pp. 158-162, 2007.

[108]. Y. Tang, X. Zhao, K. Jiang, J. Chen and Y. Zuo, 'The influences of duty cycle on the bonding strength of AZ31B magnesium alloy by microarc oxidation treatment', Surface and Coatings Technology, vol. 205, no. 6, pp. 1789-1792, 2010.

[109] J. Curran and T. Clyne, 'Porosity in plasma electrolytic oxide coatings', Acta Materialia, vol. 54, no. 7, pp. 1985-1993, 2006.

[110]. H. Giesche, 'Mercury Porosimetry: A General (Practical) Overview', Part. Part. Syst. Charact., vol. 23, no. 1, pp. 9-19, 2006.

[111]. I. McColm, Ceramic hardness. New York: Plenum Press, 1990.

[112]. H. Du, J. Shin and S. Lee, 'Study on Porosity of Plasma-Sprayed Coatings by Digital Image Analysis Method', Journal of Thermal Spray Technology, vol. 14, no. 4, pp. 453-461, 2005.

[113]. H. Eiliat, X. Nie, J. Tjong and J. Villafuerte, 'Outside-Engine Wear Study of Ceramic Coated Cylinder Wall Tribo-System', 2014.

[114]. K. Wang, B. Koo, C. Lee, Y. Kims, S. Lee and E. Byon, 'Effects of electrolytes variation on formation of oxide layers of 6061 Al alloys by plasma electrolytic oxidation', Transactions of Nonferrous Metals Society of China, vol. 19, no. 4, pp. 866-870, 2009.

[115]. M. Fink, J. Laimer and H. Stori, 'On the dynamics of unipolar and bipolar pulsed d.c. discharges used for plasma CVD', Vacuum, vol. 71, no. 1-2, pp. 219-223, 2003.

[116]. J. Liang, L. Hu and J. Hao, 'Characterization of microarc oxidation coatings formed on AM60B magnesium alloy in silicate and phosphate electrolytes', Applied Surface Science, vol. 253, no. 10, pp. 4490-4496, 2007.

[117]. G. Sundararajan and L. Rama Krishna, 'Mechanisms underlying the formation of thick alumina coatings through the MAO coating technology', Surface and Coatings Technology, vol. 167, no. 2-3, pp. 269-277, 2003.

[118]. A. Ghasemi, V. Raja, C. Blawert, W. Dietzel and K. Kainer, 'The role of anions in the formation and corrosion resistance of the plasma electrolytic oxidation coatings', Surface and Coatings Technology, vol. 204, no. 9-10, pp. 1469-1478, 2010.

[119]. T. King Country, C. Ronge, H. Tat, S. Yu, F. Yan and Z. Jinjie, 'Electrolyte for aluminum alloy micro-plasma electrolytic oxidation and treating process thereof', CN 103060877 A, 2013.

[120]. N. P. Suh, Tribophysics. Englewood Cliffs, N.J.: Prentice-Hall, 1986.

[121]. M. Koura and M. Omar, 'The effect of surface parameters on friction', Wear, vol. 73, no. 2, pp. 235-246, 1981.

[122]. A. Torrance, 'Using profilometry for the quantitative assessment of tribological function: PC-based software for friction and wear prediction', Wear, vol. 181-183, pp. 397-404, 1995.

[123]. M. Sedlacek, B. Podgornik and J. Vizintin, 'Correlation between standard roughness parameters skewness and kurtosis and tribological behavior of contact surfaces', Tribology International, vol. 48, pp. 102-112, 2012.

[124]. L. Chang and Y. Jeng, 'Effects of negative skewness of surface roughness on the contact and lubrication of nominally flat metallic surfaces', Proceedings of the Institution of Mechanical Engineers, Part J: Journal of Engineering Tribology, vol. 227, no. 6, pp. 559-569, 2012.

[125]. P. Menezes, K. Kailas and S. Kailas, 'Influence of roughness parameters on coefficient of friction under lubricated conditions', Sadhana, vol. 33, no. 3, pp. 181-190, 2008.

[126]. P. Menezes, K. Kailas and S. Kailas, 'Influence of surface texture and roughness parameters on friction and transfer layer formation during sliding of aluminium pin on steel plate', Wear, vol. 267, no. 9-10, pp. 1534-1549, 2009.

[127]. E. Gadelmawlaa, M. Kourab, T. Maksoudc, I. Elewaa and H. Solimand, 'Roughness parameters', Journal of Materials Processing Technology, vol. 123, no. 1, pp. 133-145, 2002.

[128]. A. Yerokhin, X. Nie, A. Leyland, A. Matthews and S. Dowey, 'Plasma electrolysis for surface engineering', Surface and Coatings Technology, vol. 122, no. 2-3, pp. 73-93, 1999.

[129]. M. Shokouhfar, C. Dehghanian, M. Montazeri and A. Baradaran, 'Preparation of ceramic coating on Ti substrate by plasma electrolytic oxidation in different electrolytes and evaluation of its corrosion resistance: Part II', Applied Surface Science, vol. 258, no. 7, pp. 2416-2423, 2012.

[130]. X. Shi-Gang, S. Li-Xin, Z. R. Gen and H. Xing-Fang, 'Properties of aluminum oxide coating on aluminum alloy produced by micro-arc oxidation', Surface and Coatings Technology, vol. 199, no. 2-3, pp. 184-188, 2005.

[131]. Y. Jiang, Y. Zhang, Y. Bao and K. Yang, 'Sliding wear behavior of plasma electrolytic oxidation coating on pure aluminum', Wear, vol. 271, no. 9-10, pp. 1667-1670, 2011.

[132]. K. Ludema, Friction, wear, lubrication: a textbook in tribology. CRC Press: Boca Raton, Fla., 2010.

[133]. C. Fei, Z. Hai, C. Chen and X. Yangjian, 'Study on the tribological performance of ceramic coatings on titanium alloy surfaces obtained through microarc oxidation', Progress in Organic Coatings, vol. 64, no. 2-3, pp. 264-267, 2009.

[134]. P. Srinivasan, C. Blawert and W. Dietzel, 'Dry sliding wear behavior of plasma electrolytic oxidation coated AZ91 cast magnesium alloy', Wear, vol. 266, no. 11-12, pp. 1241-1247, 2009.

[135]. J. Tian, Z. Luo, S. Qi and X. Sun, 'Structure and antiwear behavior of micro-arc oxidized coatings on aluminum alloy', Surface and Coatings Technology, vol. 154, no. 1, pp. 1-7, 2002.

[136]. X. Wu, W. Qin, Y. Guo and Z. Xie, 'Self-lubricative coating grown by micro-plasma oxidation on aluminum alloys in the solution of aluminate graphite', Applied Surface Science, vol. 254, no. 20, pp. 6395-6399, 2008.

[137]. E. Becker, 'Trends in tribological materials and engine technology', Tribology International, vol. 37, no. 7, pp. 569-575, 2004.

[138]. R. Van Basshuysen and F. Schalfer, Modern engine technology. Warrendale, SAE International, 2007.

[139]. S. Biswas and K. Vijayan, 'Friction and wear of PTFE: a review', Wear, vol. 158, no. 1-2, pp. 193-211, 1992.

[140]. Y. Wang, B. Jiang, L. Guo and T. Lei, 'Tribological behavior of microarc oxidation coatings formed on titanium alloys against steel in dry and solid lubrication sliding', Applied Surface Science, vol. 252, no. 8, pp. 2989-2998, 2006.

[141]. Y. Wang, B. Jiang, T. Lei and L. Guo, 'Microarc oxidation and spraying graphite duplex coating formed on titanium alloy for antifriction purpose', Applied Surface Science, vol. 246, no. 1-3, pp. 214-221, 2005.

[142]. C. Martini, L. Ceschini, F. Tarterini, J. Paillard and J. Curran, 'PEO layers obtained from mixed aluminate-phosphate baths on Ti-6Al-4V: Dry sliding behavior and influence of a PTFE topcoat', Wear, vol. 269, no. 11-12, pp. 747-756, 2010.

[143]. S. Awad and H. Qian, 'Deposition of duplex Al2O3/TiN coatings on aluminum alloys for tribological applications using a combined microplasma oxidation (MPO) and arc ion plating (AIP)', Wear, vol. 260, no. 1-2, pp. 215-222, 2006.

[144]. X. Nie, A. Wilson, A. Leyland and A. Matthews, 'Deposition of duplex Al2O3/DLC coatings on Al alloys for tribological applications using a combined micro-arc oxidation and plasma-immersion ion implantation technique', Surface and Coatings Technology, vol. 131, no. 1-3, pp. 506-513, 2000.

[145]. C. Zawde, Feasibility study. Newark, Del: Princeton Commercial Holdings, 2007.

[146]. The White House, 'President Obama Announces National Fuel Efficiency Policy', 2009.

[147]. M. Ducos and J. Durrand, 'Thermal coatings in Europe, business prospection', ASM Int. Mater. Thermal Spray 2001, vol., no. 1267-1270, 2001.

APPENDIX A. COPYRIGHT PERMISSIONS

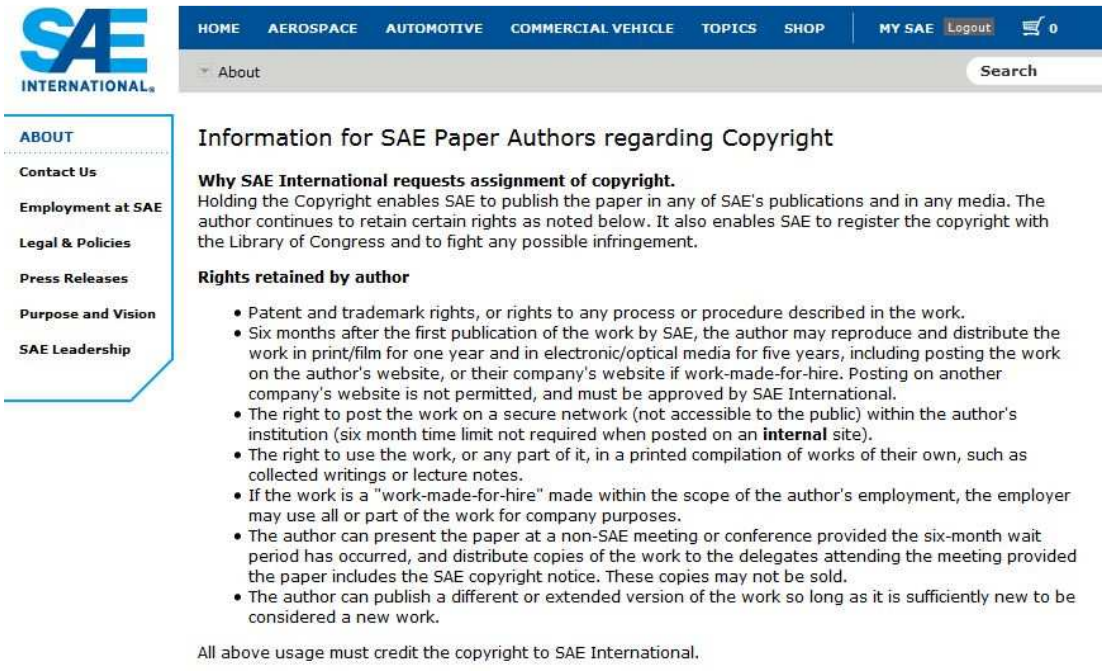

HOME AEROSPACE AUTOMOTIVE COMMERCIAL VEHICLE TOPICS SHOP MY SAE Logout 0

About Search

ABOUT

Contact Us

Employment at SAE

Legal & Policies

Press Releases

Purpose and Vision

SAE Leadership

Information for SAE Paper Authors regarding Copyright

Why SAE International requests assignment of copyright.
Holding the Copyright enables SAE to publish the paper in any of SAE's publications and in any media. The author continues to retain certain rights as noted below. It also enables SAE to register the copyright with the Library of Congress and to fight any possible infringement.

Rights retained by author

- Patent and trademark rights, or rights to any process or procedure described in the work.
- Six months after the first publication of the work by SAE, the author may reproduce and distribute the work in print/film for one year and in electronic/optical media for five years, including posting the work on the author's website, or their company's website if work-made-for-hire. Posting on another company's website is not permitted, and must be approved by SAE International.
- The right to post the work on a secure network (not accessible to the public) within the author's institution (six month time limit not required when posted on an **internal** site).
- The right to use the work, or any part of it, in a printed compilation of works of their own, such as collected writings or lecture notes.
- If the work is a "work-made-for-hire" made within the scope of the author's employment, the employer may use all or part of the work for company purposes.
- The author can present the paper at a non-SAE meeting or conference provided the six-month wait period has occurred, and distribute copies of the work to the delegates attending the meeting provided the paper includes the SAE copyright notice. These copies may not be sold.
- The author can publish a different or extended version of the work so long as it is sufficiently new to be considered a new work.

All above usage must credit the copyright to SAE International.

COPYRIGHT TRANSFER AND PERMISSION TO PUBLISH AUTHORIZATION FOR PAPERS SUBMITTED FOR PUBLICATION BY THE SOCIETIES LISTED ABOVE AS ORGANIZING THE MATERIALS SCIENCE & TECHNOLOGY 2013 CONFERENCE (HEREWITH REFERRED TO AS "MS&T'13 ORGANIZERS").

This form is to be completed, signed by the author or an authorized person, and returned with any paper submitted for publication (in conventional and electronic formats) by the MS&T'13 Organizers. If this form is not completed, signed, and returned with the paper for publication, the transfer of copyright from the author or an authorized person to the MS&T'13 Organizers, as well as permission to publish, will be implied in the act of submission of the paper for publication.

Title of publication: **Materials Science & Technology 2013 Conference Proceedings**

Title of paper: WEAR RESISTANT COATINGS FOR ENGINE APPLICATION

Author(s): Hoda Eiliat , Xueyuan Nie , Jimmy Tjong

PART A – COPYRIGHT TRANSFER

Copyright title, interest and all right in the paper named above is hereby transferred to the MS&T'13 Organizers, effective when the paper is submitted for publication. This assignment and transfer apply to any other publications produced by the MS&T'13 Organizers in addition to the designated publication.

I hereby transfer copyright, and all rights subsumed thereunder, to the paper named above to the MS&T'13 Organizers, under the terms outlined above and hereby certify that I am a self-employed author or authorized by my employer to transfer copyright, and that the paper has not been previously copyrighted, published, nor submitted for publication elsewhere.

Signature: Hoda Eiliat Date: May 1, 2013

Name (please print): Hoda Eilait

If this is a work made for hire:

Name of organization for whom the work was performed (please print): University of Windsor

Title of signer: PhD Candidate, Research Assistant

AUTHOR(S), OR EMPLOYER(S) IN THE CASE OF WORKS MADE FOR HIRE, RETAIN THE FOLLOWING RIGHTS:

1. All proprietary rights, other than copyright, such as patent rights.
2. The right to use all or portions of the paper cited above in oral presentations.
3. The right to make limited distribution of the paper, or portions thereof, prior to publication.
4. Royalty-free permission to reproduce the paper cited above for personal use or, in the case of a work made for hire, the employer's use, provided that a) the source and notice of the MS&T'13 Organizers' copyright are provided, b) the copies are not used in a way that implies endorsement by the MS&T'13 Organizers of a product or service, and c) the copies are not offered for sale.
5. In the case of work performed under U.S. Government contract, the MS&T'13 Organizers grant the U.S. Government royalty-free permission to reproduce all or portions of the paper, and to authorize others to do so for U.S. Government purposes.

PART B – U.S. GOVERNMENT EMPLOYEE CERTIFICATION

Note: If this work was performed under U.S. Government contract, but you are not a U.S. Government employee, you must sign part A of this form.

I hereby certify that all authors of the paper cited on this form are employees of the U.S. Government and performed this work as part of their employment, and that the paper is therefore not subject to the U.S. Copyright protection.

Signature: _____

Date: _____

Name (please print): _____

Name of U.S. Government organization: _____

Title of signer: _____

INFORMATION FOR AUTHORS

1. *Work made for hire*: If you are an employee and your paper was prepared as part of your job, the copyright to the paper belongs to your employer. If you as an author sign the copyright transfer form, you represent that you are authorized by your employer to do so and that your employer has consented to all of the terms and conditions of this form. If not, it must be signed by someone so authorized.

2. *Joint authorship*: For jointly authored papers, only one signature is required if all authors work for the same company; the paper thus is a work made for hire, the copyright rests with the employer rather than the individual authors, and anyone authorized by the employer may authorize the copyright transfer. When the authors work for different employers, a separate copyright transfer form must be signed by the authorized agent for each employer. When authors are self-employed, each must sign a separate copyright transfer form. Co-authors who are U.S. Government employees are not required to sign this form, but any co-authors outside the U.S. Government must sign Part A.

3. *Work performed under U.S. Government contract*: Authors whose work was performed under U.S. Government contract, but who are not employees of the U.S. Government, are required to sign Part A. Item 5 of Part A returns the reproduction rights to the U.S. Government when required for U.S. Government purposes, while retaining the MS&T'13 Organizers' copyright protection with respect to reuse of the material by the general public.

4. *MS&T'13 Organizers' policy on assignment of copyright*: As a convenience and courtesy to the technical community, the MS&T'13 Organizers will routinely grant permission upon request to authors to use in their papers, portions of works by other authors for which copyright has been transferred to the Organizers. The MS&T'13 Organizers reserve the right to use any parts or the entire paper in revised editions, derivative works, etc.

5. *The MS&T'13 Organizers' publishing policy on presentations accepted for conferences and symposia*: the MS&T'13 Organizers reserve the right to publish, reproduce and display presentations accepted for conferences and symposia prior to publication elsewhere. Permission to reprint presentations from the MS&T'13 Organizers' publications must be obtained prior to publication elsewhere.

PUBLISHER INDEMNITY

The author agrees that the article has not been previously submitted for publication or published elsewhere. Further, the author agrees that the article is original and that it contains no matter which is libelous, obscene, or infringes any existing right of privacy, copyright, trademark or any other statutory or common law proprietary or civil right and is not otherwise unlawful. The author agrees to indemnify, defend, and hold the MS&T'13 Organizers and their directors, officers, employees, and agents harmless against any claims to the contrary.

SUBMISSION OF FORM

Copyright transfer forms will be collected electronically on the ProgramMaster site when the article is uploaded.

APPENDIX B. COMPARASION ANALYSIS: PEO VERSUS PTWA

Since PEO coatings are being considered as an alternative surface treatment for liner-less cylinder engine blocks that are produced by PTWA technology, it would be beneficial to compare different aspects of the two methods.

PTWA as described in chapter 1 is a rotating thermal spray process which combines twin arc spray and atmosphere plasma spray processes. The process has a wire feeder with feeding speed of 1 m/min and can deposit 10 kg/h of molten material on the substrate. Achieved coating with PTWA has a 0.6 mm thickness and is honed as a post treatment technique to reach 150 μm of thickness. Mass addition to each cylinder bore after the treatment is about 100 gr. One of the drawbacks of the PTWA process is that the cylinder block can become overheated during the thermal spray process. Overheating can have negative effects such as block distortion which is usually happening in the bridge zones (the area between the aligned bores) and microstructure alteration of the aluminum. PEO on the other hand has much less of the temperature gradient due to the use of electrolyte. During the process the solution temperature stayed below 30 °C for 15 minutes of treatment.

In terms of treatment time, PTWA takes about 60 s to coat a V8 engine block. The spray head is controlled to move from one bore to another. PEO on the other hand, requires much longer treatment time. If one spray head is used per each bore at the same time, the process needs at least 5 to 8 minutes to complete. PEO process has an average of 1 μm/ min of deposition rate and effective treatment time range of 5 minutes according to the results shown in this research. Since the coatings are much thinner than PTWA

coatings (around 5 to 10 μm), the mass addition to the naked cylinder is almost negligible. PTWA shed 1 pound of weight per cylinder bore of a liner less engine block, this is about 8 pounds for a V8 engine. PEO technology helps to reduce the overall weight of the engine by another 800 gr (1.76 lb) for a V8 engine block.

In terms of energy consumption, PEO is on the front in comparison to PTWA. This is mainly due to the extreme high temperature needed to molten the twin wire on the surface and also heat up the compressed gas mixture of hydrogen and Argon to the plasma level. Particles with temperature of 2250 °C and speed of 135 m/s will be propelled towards the surface. At current densities under 0.10 A/cm^2, the output voltage is around 380 to 450 volts depends on the solution concentration and 0.40 to 0.46 kWh. There is a direct relationship between the current density and the electrical energy consumption. For current density of 0.2 A/ cm^2, the electrical energy consumption would be around 0.99 kWh.

B.1 Cost Benefit Analysis

Feasibility analysis is the process of determining if a technology can be utilized to reach the objective of the proposed process. The feasibility analysis has four main aspects: technical, economical, environmental and regulatory aspect [145]. The technical aspect of PEO technology is studied and analyzed throughout this dissertation. Results, discussion and potential benefits can be found in Chapter 4 and 5. Economical aspect of PEO application will be discussed in this section. Environmental aspect for this technology is assumed to be approved since the technology is eco-friendly with minimal by-product toxicity and ease of recyclability. Regulatory aspect is also aligned with increased government regulations to improve the fuel efficiency and decrease the

emission of greenhouse gases. In 2009, US government proposed a plan to cover 2012 to 2016 model year cars and ensure the average fuel economy of 35.5 miles per gallon (15 kg/lit) which is a 50% improvement compared to 2009 and previous model cars with average of 25 mpg (10.6 kg/lit) fuel economy. The proposed plan is said to save 1.8 billion barrels of oil along with omission of the greenhouse gas emissions by more than 900 million tons [146]. Automakers and automotive industries tried to tackle the issue mainly by two major approaches: improving the powertrain efficiency and reducing the rolling resistance. First approach can lead to success by reducing the friction loss and the second is by reducing the vehicle weight. PEO can deliver both.

However a new technology would not be desired by the automotive industry unless it passes a feasible financial analysis of the cash flows associated with the technology and shows a meaningful net gain. The key item is to analyze the costs of the implementation and of course determine the payback. Cost benefit analysis is chosen to determine the financial feasibility of using PEO as a method of surface modification for engine cylinder walls.

B.1.1 Benefit Measures

Benefits of implementing PEO technology for surface treatment of engine blocks for supplier companies can be categorized as below. Each of the benefits can be translated into monetary values. Also Return on Investment (ROI) determines if the desired net gain is achieved.

1. Reduced amount of reworking or faulty parts since PEO process is error proof once the right conditions are chosen for the treatment.

2. PEO coating has shown high wear resistance; also the ceramic nature of the alumina oxide layer is tolerant to corrosion which means reduced number of engine troubles, minimal after service repair work and higher customer satisfaction.

3. Reduction in production hazards such as toxic fumes, working with acidic solutions and difficulties of recyclability of the electrolytes which means simpler apparatus.

B.1.2 Costs

Aside from capital costs such as land, facility construction and …, implementation of PEO technology like any other coating technology has a great amount of details on initial investment. Following apparatus need to be collected, built and assembled:

1. Power supply, power control unit and pulse generator
2. Solution tank and circulating pump to keep the solution moving into the pipes and through the spray head
3. Spray heads (the number of spray heads depends on the type of engine and number of cylinder heads)
4. Cooling unit and heat exchanger to keep the temperature of the solution at an acceptable range
5. Solution filters to ensure the composition of the electrolyte is the same during the production

Other costs such as operating cost which includes the cost of materials and energy consumption and labor cost are to be considered. It is difficult to come up with a price range for the PEO treatment since there are many factors and variables involved. For instance the concentration and type of the salts or acids used in the solution have an influence on the discharge start time and growth rate which means it will dictate the electrical energy consumption level. Table 7 compares PTWA and PEO based on deposition rate, coating thickness, energy consumption and cost of raw materials.

Most of the aspects of PEO coating interpret to a less costly process. The main issue would be the completion time for each engine block. In general, PTWA process has a faster deposition rate (almost 10 times faster than the PEO growth rate). If the use of 8 rotating spray heads for a V8 engine block is assumed. An engine would take around 10 minutes to be finished this is almost 10 times more than the completion time using PTWA. In terms of energy consumption, the battle is between the treatment time and current density and considering the much less current density which is needed for PEO process and much longer treatment time, PEO consumes 32% less electrical energy in kWh. However according to a study on cost analysis of thermal spray processes [147], electricity is not one of the top three costly aspects of thermal spray since powder, gas, consumables (such as the electrode) and even labor have the highest percentage of influence on the total cost. Therefore, since the cost of raw material for the PEO (salts and water) is much less than PTWA raw materials (powder, wire, gas and electrode), it can be concluded that the overall cost of the PEO process is less than PTWA.

Table 7. Comparison between PTWA and PEO process.

Comparison Parameters	**Cylinder Wall Surface Treatment Technologies**	
	PTWA	PEO
Deposition Rate	106.6 gr/min 150 μm/min	10 gr/min 1-1.5 μm/min
Energy consumption (kWh)	200V x 15A x 0.017h 0.050	200V x 1A x 0.17h 0.034
Coating Thickness (μm)	150 (after honing) 200 (before honing)	10
Mass Addition per Cylinder (gr)	100	6
Raw Material Cost	Wire: $30/kg Electrode*: $6 Gas: $ 3.4/100 m3	Powder: $5-$10 Water: $1.5/ m^3

*: Electrodes should be replaced regularly.

This conclusion does not include the pre and post treatment of both technologies. However according to the same study [147] on thermal spray processes, 45% of the total cost is because of the coating treatment and 55% goes to Pre-treatment (machining, masking, degreasing, grit blasting and cleaning), post treatment (de-masking, honing, surface polishing, cleaning) and quality control. Honing is mainly done on PTWA coatings to create oil reservoirs and decrease the surface roughness of the coating. PEO

coatings on the other hand are porous by nature and do not need much of the post treatment except surface polishing and cleaning. This could also mean more cost savings.

VITA AUCTORIS

NAME:	Hoda Eiliat
PLACE OF BIRTH:	Tehran, Iran
YEAR OF BIRTH:	1983
EDUCATION:	University of Tehran, Bachelor of Science (B.Sc.) in Irrigation Engineering, Department of Hydraulics Engineering , Tehran, Iran, 2002
	University of Windsor, Master of Applied Science (MASc.), Mechanical Engineering, mechanical, Automotive and Materials Engineering Department, Windsor, Canada, 2009
	University of Windsor, Doctor of Philosophy (PhD) , Engineering Materials, Automotive and Materials Engineering Department, Windsor, Canada, 2015